INSTITUTO POTOSINO DE INVESTIGACIÓN CIENTÍFICA Y TECNOLÓGICA, A.C.

POSGRADO EN CIENCIAS APLICADAS

Anchorage of small cluster of manganese oxide, zinc oxide and silver on nitrogen doped and functionalized carbon nanotubes

Tesis que presenta

Edgar Eduardo Gracia Espino

Para obtener el grado de

Maestro en Ciencias Aplicadas

En la opción de

Nanociencias y Nanotecnología

Realizada bajo la codirección de:

Dr. Mauricio Terrones Maldonado

Dr. Humberto Terrones Maldonado

San Luis Potosí, S.L.P. México, Agosto de 2008

IPICYT

Certificate of Thesis Approval

The thesis "**Anchorage of small cluster of manganese oxide, zinc oxide and silver on nitrogen doped and functionalized carbon nanotubes**" submitted to obtain the degree of Master in Applied Science in the option of Nanoscience and Nanotechnology was developed by **Edgar Eduardo Gracia Espino** and approved on **August 20th of 2008** by the jury, assigned by the Professors Committee of the Advanced Material Division in the **Instituto Potosino de Investigación Científica y Tecnológica, A.C.**

Dr. Mauricio Terrones Maldonado
Thesis Co-supervisor

Dr. Humberto Terrones Maldonado
Thesis Co-supervisor

Dr. Fernando Jaime Rodríguez Macías
Committee member

Institutional Credits

This thesis was elaborated in the Nanostructures Laboratory of the Advanced Material Division at the Instituto Potosino de Investigación Científica y Tecnológica A.C., under the co-supervision of **Dr. Mauricio Terrones Maldonado** and **Dr. Humberto Terrones Maldonado**.

During the performance of this work, the author had a scholarship from the Consejo Nacional de Ciencia y Tecnología (Register number **204089**) and from the Instituto Potosino de Investigación Científica y Tecnológica A.C.

Instituto Potosino de Investigación Científica y Tecnológica, A.C.

Acta de Examen de Grado

El Secretario Académico del Instituto Potosino de Investigación Científica y Tecnológica, A.C., certifica que en el Acta 019 del Libro Primero de Actas de Exámenes de Grado del Programa de Maestría en Ciencias Aplicadas en la opción de Nanociencias y Nanotecnología está asentado lo siguiente:

En la ciudad de San Luis Potosí a los 26 días del mes de agosto del año 2008, se reunió a las 12:00 horas en las instalaciones del Instituto Potosino de Investigación Científica y Tecnológica, A.C., el Jurado integrado por:

Dr. Humberto Terrones Maldonado	**Presidente**	**IPICYT**
Dr. Mauricio Terrones Maldonado	**Secretario**	**IPICYT**
Dr. Emmanuel Haro Poniatowski	**Sinodal externo**	**UAM**
Dr. Fernando Jaime Rodríguez Macías	**Sinodal**	**IPICYT**

a fin de efectuar el examen, que para obtener el Grado de:

MAESTRO EN CIENCIAS APLICADAS
EN LA OPCIÓN DE NANOCIENCIAS Y NANOTECNOLOGÍA

sustentó el C.

Edgar Eduardo Gracia Espino

sobre la Tesis intitulada:

Anchorage of small clusters of manganese oxide, zinc oxide and silver on nitrogen-doped and functionalized carbon nanotubes

que se desarrolló bajo la dirección de

Dr. Humberto Terrones Maldonado
Dr. Mauricio Terrones Maldonado

El Jurado, después de deliberar, determinó

APROBARLO

Dándose por terminado el acto a las 13:40 horas, procediendo a la firma del Acta los integrantes del Jurado. Dando fé el Secretario Académico del Instituto.

A petición del interesado y para los fines que al mismo convengan, se extiende el presente documento en la ciudad de San Luis Potosí, S.L.P., México, a los 26 días del mes de agosto de 2008.

Dr. Marcial Bonilla Marín
Secretario Académico

INSTITUTO POTOSINO
DE INVESTIGACIÓN
CIENTÍFICA Y TECNOLÓGICA, A.C.
IPICYT
SECRETARIA ACADEMICA

L.C.C. Ivonne Lizette Cuevas Velez
Jefa del Departamento de Asuntos Escolares

Dedicado a:

Mi familia, mis padres, mi hermana y en especial
a mi sobrino, quienes siempre
me han apoyado.

Anchorage of small cluster of manganese oxide, zinc oxide and silver on nitrogen doped and functionalized carbon nanotubes

Edgar Eduardo Gracia Espino

Submitted for the degree of Master in Applied Sciences
August 2008

Abstract

Multi-walled carbon nanotubes (MWCNTs) exhibit outstanding mechanical and electronic properties. Due to their structure, the MWCNTs could also play an important role as substrates for the deposition of metal and metal oxide nanoparticles that allow the development of novel composite materials. These materials could be used as catalysts, gas sensors, ion-exchange materials, gas adsorbers, biomarkers, drugs delivery systems, etc.

The results obtained from the use of the MWCNTs as substrates for metal and metal oxide (e.g. ZnO, α-Mn_2O_3 and Ag) nanoparticles are presented in this work.

ZnO nanoparticles have been efficiently and homogeneously anchored on the surfaces of two types of carbon nanotubes. We use nitrogen-doped (CN_x-MWNTs) and functionalized carbon nanotubes with oxygen groups (CO_x-MWNTs) as substrate. The smallest particles were deposited on the CO_x-MWNTs with a mean size of 4.1 nm.

Furthermore, we developed a novel methodology that allows us to coat efficiently carbon nanotubes with α-Mn_2O_3 nanoparticles (particle size from 6 to 10 nm) without employing expensive and hazardous chemicals.

Finally, we developed a simple process able to anchor efficiently small Ag nanoparticles on different carbon nanotubes. This method is able to attach Ag

particles (ranging from 3 to 7 nm in size) without any external reducing agent. In this case, the CNTs could act as reducing agents for the silver ions.

KEY WORDS: CN_x-MWNTs | CO_x-MWNTs | Functionalized carbon nanotubes | N-doped carbon nanotubes | nanocomposites materials | metal oxide deposition | metal cluster deposition | zinc oxide (ZnO) | manganese oxides (MnO_x) |silver (Ag)|

Anchorage of small cluster of manganese oxide, zinc oxide and silver on nitrogen doped and functionalized carbon nanotubes

Edgar Eduardo Gracia Espino

Tesis presentada para obtener el grado de Maestro en Ciencias Aplicadas en la opción de Nanociencias y Nanotecnología

Resumen

Los nanotubos de carbono de pared múltiple (MWCNTs) exhiben excelentes propiedades mecánicas y electrónicas. Debido a su estructura y tamaño, los MWCNTs podrían ser utilizados como sustratos para la deposición de nanopartículas metálicas u óxidos metálicos que permitan el desarrollo de novedosos materiales compuestos.

Estos materiales podrían ser utilizados como catalizadores, adsorbedores de gases, intercambiadores de iones, sensores químicos, bio-marcadores, etc.

En este trabajo se presentan los resultados obtenidos al utilizar los MWCNTs como sustratos para el crecimiento de nanopartículas de óxido de zinc (ZnO), óxido de manganeso (III) (α-Mn_2O_3) y plata (Ag).

Nanopartículas de ZnO han sido eficiente y homogéneamente ancladas en dos tipos de nanotubos de carbono. Hemos utilizado como sustrato a nanotubos de carbono dopados con nitrógeno (CN_x-MWNTs) y nanotubos de carbono funcionalizados con grupos carbonilo e hidroxilo (CO_x-MWNTs). El tamaño de partícula más pequeño fue obtenido utilizando los CO_x-MWNTs con un diámetro medio de partícula de 4.1 nm.

Posteriormente, se desarrolló una novedosa metodología que nos permitió recubrir eficientemente a los MWCNTs con α-Mn_2O_3 (tamaño de partícula desde 6 a 10 nm), sin emplear reactivos costosos y/o peligrosos.

Finalmente, se diseñó un proceso sencillo para el anclaje de partículas de plata en diferentes tipos de nanotubos de carbono. Este método permite depositar nanopartículas de Ag (con un tamaño de partícula de 3 a 7 nm) sin el uso de agentes reductores externos, en este caso los MWCNTs podrían actuar como agentes reductores.

PALABRAS CLAVE: CN_x-MWNTs | CO_x-MWNTs | Nanotubos de carbono funcionalizados | Nanotubos de carbono dopados con nitrógeno | materiales nanocompuestos | deposición de óxidos metálicos | deposición de nanopartículas metálicas | Óxido de zinc (ZnO) | Óxidos de manganeso (MnO_x) | Plata (Ag)|

Acknowledgments

I would like to thank my advisors, Dr. Mauricio Terrones Maldonado and Dr. Humberto Terrones Maldonado for their guidance, comments, freedom and helpful suggestions during the development of this thesis. Equally, I am grateful to Dr. Fernando Jaime Rodriguez Macias and Dra. Yadira Itzel Vega Cantú for their suggestions and advices.

I also would like to recognize to Dra. María Magdalena Martínez Mondragón, Msc. Grisel Ramírez Manzanares and Ing. Daniel Ramírez González for their important help during samples characterization. Similarly, I want to thank Prof. M. Endo (Japan) for the TEM support and Prof. Saber Hussain (USA) for the biocompatibility studies.

I am thankful to all my laboratory colleagues, Claudia Guadalupe Espinosa González, Antonio Esaú del Río Castillo, Andrés Rafael Botello Méndez, Jessica Rosaura Campos Delgado, Abraham Guadalupe Cano Márquez, but in particular to Aarón Morelos Gómez for his friendship and his support in many aspects.

To my friends, Dra. Alicia Rodríguez Pulido, Dr. Hugo Martínez Gutiérrez and Dr. Ferdinando Tristán López, who helped me in diverse ways in the last months.

I am grateful to María de Luz Medina Llamas who always has supported me, her comments, help and pleasing company during many years have made a enjoyable period of my life.

Finally, I want to thank to CONACYT for the master's scholarship (204089) that allowed me finish my studies.

Eduardo Gracia

Contents

Chapter 5

Conclusions and Perspectives

List of Figures

List of Tables

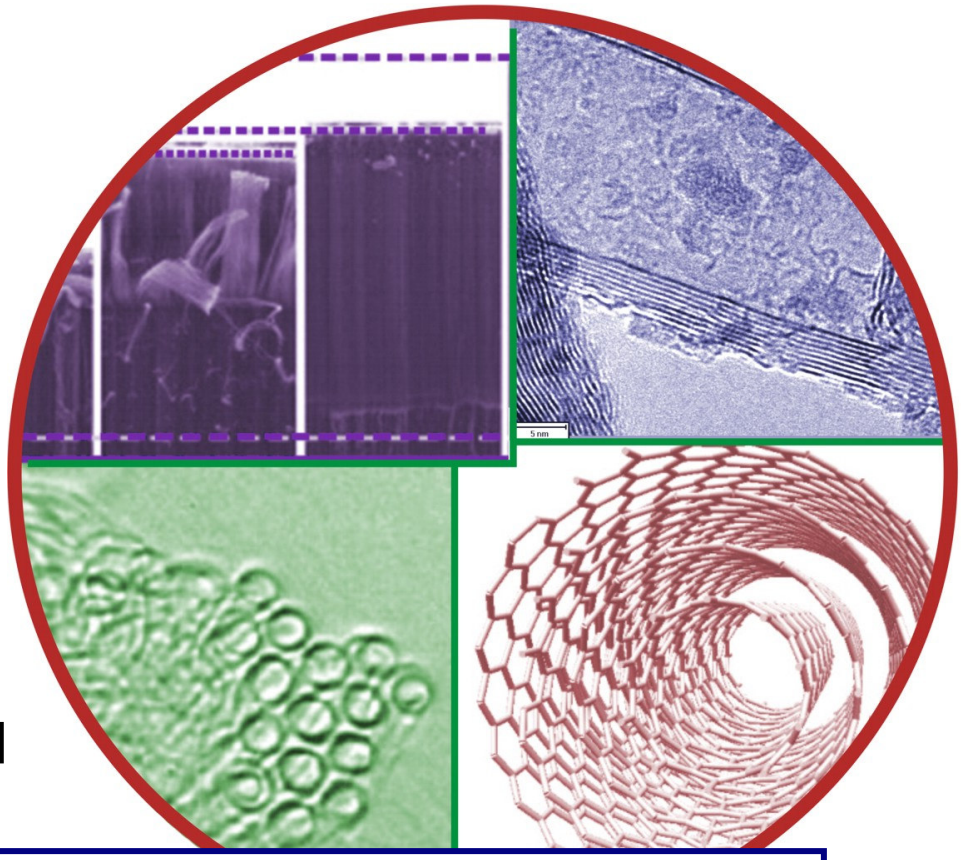

Chapter 1

Introduction: Carbon Nanostructures

Carbon is one of the most abundant elements in nature. It is essential to living organisms and it constitutes building blocks of a wide variety of compounds. Its chemical symbol is C and its atomic number is 6. It is able to form bonds with a wide variety of elements and it is also capable of forming multiple stable covalent bonds with such atoms. Carbon exhibits allotropic forms but before 1985 only know two of them were known, graphite and diamond, in the mid of the 80's the *Buckminsterfullerene*: C_{60} (the third allotrope of carbon) was discovery by H.W. Kroto *et al.*[1], since then, other carbon nanostructures were discovered and synthesized.

1.1 Fullerenes, graphitic onions and nanocones

Graphite exhibits a hexagonal crystalline structure, it consist of an array of stacked parallel flat layers, see Figure 1.1-(**a**); each atom has three nearest neighbors (within the layer) joined by a covalent bond of 1.415 Å with an sp^2 hybridization. The sheets of carbon are held together by Van der Waals forces with an "ABAB…" stacking (hexagonal graphite, space group $P6_3/mmc$) or "ABC…" (rhombohedral graphite, space group R3m); the interlayer distance corresponds to 3.35 Å. Each individual layer could be curled and curved to form different types of structures such as tubes, cages, fibers, cones and other complex structures. If the structures are small enough and belong to the nanometer scale (1 nm = $1x10^{-9}$ m) they are called *carbon nanostructures*.

The first know carbon nanostructures were fullerenes, discovered in 1985 by H.W. Kroto *et al.* [1] in the resulting soot from graphite vaporization with a powerful laser. These authors found a structure of sixty carbon atoms (C_{60}) and they proposed the shape of a truncated icosahedron, in which each vertex corresponds to a carbon atom, see Figure 1.1-(**c**). The C_{60} molecule has two bond lengths corresponding to the 6:6 ring bonds (between two hexagons) and the 6:5 bonds (between a hexagon and a pentagon); the first ones can be considered as "double bonds" and are shorter than the second ones. Following this discovery, the family of fullerenes increased, and other closed carbon cages molecules of C_{2n} with n = 12,13,14…, were synthesized and isolated (e.g. C_{70}, C_{76}, C_{84}). Figure 1.2 illustrates some higher fullerene structures, all of them are constructed with twelve pentagons. The nearly spherical cage C_{84}, Figure 1.2-(**b**), crystallizes in an *fcc* structure[2] in their crystalline form has a band gap smaller than the C_{60} probably induced by the lower molecular symmetry[3]. Other fullerenes could crystallize in *fcc* or *hcp* configurations depending on the isomeric form, such as $C_{70,}$ Figure 1.2-(**a**). The bulk production process of fullerenes is the arc discharge method and was development in 1990 by Krätschmer and Huffman[4]. With this process C_{60} and C_{70} could be predominantly produced but other higher fullerenes are present in smaller quantities.

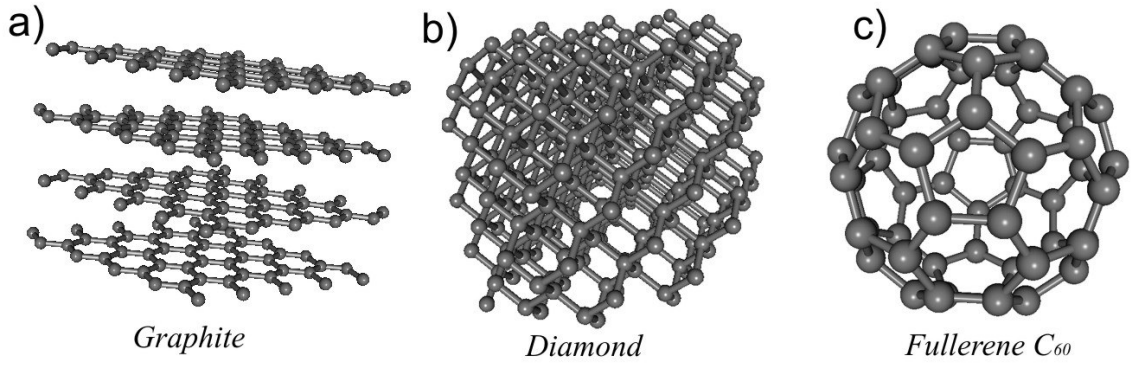

Figure 1-1.- Molecular models of carbon allotropes. Graphite (**a**) consisting of an array of parallel layers of graphene and is a semi-metallic material. In the Diamond structure (**b**), the carbon atoms possess a sp^3 hybridization and each atom has four nearest neighbors separated by a covalent bonds of 1.5445 Å with an angle of 109.5°, its space group is $Fd\bar{3}m$, the diamond is a hard and electrical insulator material. Fullerene (**c**) consisting of closed cage of sixty carbon atoms, adopting the structure of a truncated icosahedron [1].

Related structures to the fullerenes are the graphitic nano-onions (giant nested fullerenes). A simple method for producing them consist of a DC arc discharge across two graphite electrodes submerged in water [5]. Other fullerene-like structures could be produced from other materials, such as gold atoms [6]. Some applications of the carbon fullerenes include photosensitizers that can be an excellent bactericidal and fungicidal agents [7], other interesting applications could be as drugs delivery systems which could be used as a nanomedicine for cancer therapy, especially epithelially derived cancers [8].

Other interesting nanostructures are the carbon nanocones, the simplest nanocone is formed by substituting a hexagon from the graphitic layer by a pentagon, and this 5-membered ring introduces positive curvature in the carbon sheet. Ge and Sattler [9] originally discovered carbon nanocones in 1994, subsequently Krishnan A. et al [10] in 1997 developed a synthesis method by pyrolysis of hydrocarbons (heavy oils) in a carbon arc, they found different kind of turbostratic structures which have total disclinations (TD) of P60° (P from 0 to 5 pentagons), the cone angle θ is given by $\sin(\theta/2) = 1-(P/6)$, when P = 0 a flat disk is obtained.

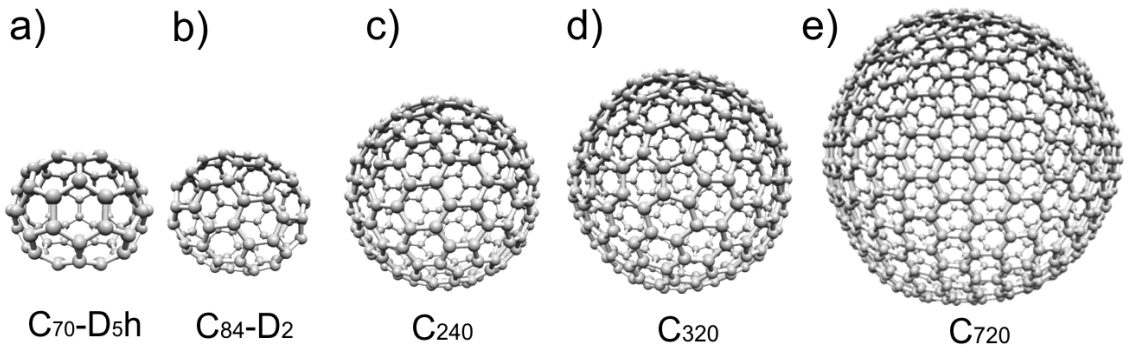

Figure 1-2.- Family of fullerenes. The C_{70} (**a**) has a space group D_5h. The C_{84} belong to different spaces groups, it depends on the array of atoms and in this case it shows the C_{84}- D_2 fullerene (**b**). In (**c**), (**d**) and (**e**) bigger fullerenes are shown, all these structures are made with only 12 pentagons in their structure. All the fullerene structures were downloaded from the fullerene library by M. Yoshida[11]

If we consider the symmetry of the graphene sheet and apply the Euler's rule, it can be shown that only five types of cones can be made from a continuous sheet, from P = 1 to 5. Figure 1.3-(**a-c**) illustrates how a graphene sheet can form a cone with one pentagon at the tip. In Figure 1.3-(**d**) a real carbon nanocone is observed, with the same characteristics as Figure 1.3-(**c**). If a cone contains six pentagons, it becomes a nanotube cap. The cones stacks in two ways: when they are of the same type and when the cones are different; the separation distance between two vertices of the cones depend in the stacking [12].

The graphitic cones have been object of study [13,14,15] due their predicted electronic[16] and mechanical properties generated by the pentagonal defects. An interesting property is that a graphene cone has two degenerate configurations, their original shape and its inverse, the inverted cone has exactly the same but opposite chirality [17]. The conical nanostructures can be produced from different materials such as nickel [18], boron nitride [19], silicon [20] and alumina [21]. These structures have attracted the attention of researcher because of their potential uses in field emission displays [16], nanoscaled manipulators, scanning probe microscopy [22] and near-field scanning optical microscopy probes, etc.

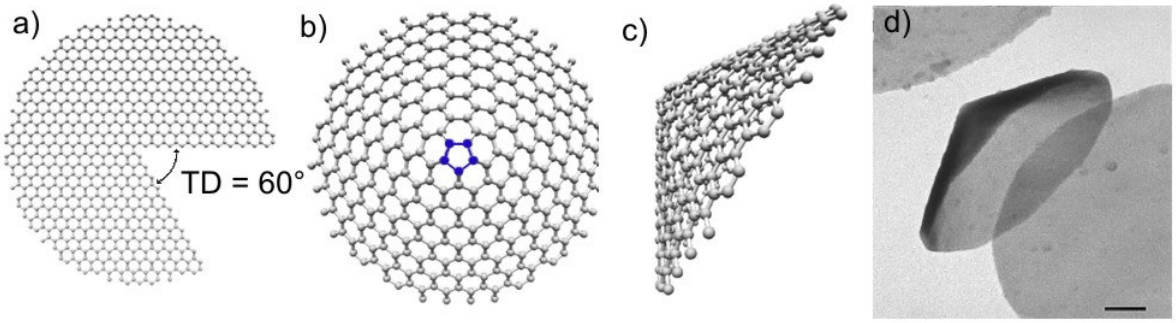

Figure 1-3.- Carbon nanocones. (**a**) A graphene disk with a total disclination equal to 60° ($P = 1$), when rolled become a cone (**b**) with a pentagon at the tip, (**c**) a side view of the cone. (**d**) A TEM image of a carbon nanocone[10] with an angle of $\theta = 112.9°$ (one pentagon in the graphitic layer), the same showed in (**b**) and (**c**); scale bar = 200 nm.

Other related structures are the nanohorns, which consist of stacked single-layered cones[23]. These structures show good field emission characteristics due to the sharp horn-like structure. Their synthesis method used intense CO_2 laser ablation on graphite[24]; nanohorns of uniform size distribution can be obtained. Due their efficient field emission characteristics, nanohorns could represent an alternative to field emission devices operating at low voltages [25]. Another application of carbon cones consist of generation of small metal clusters in the range of angstroms[26].

1.2 Carbon nanotubes

Carbon nanotubes are allotropes of carbon, produced and identified by Morinobu Endo[27] and Sumio Ijima[28] respectively. Nanotubes have been the most studied carbon nanostructures, they are members of the fullerene structural family, and they have a cylindrical shape and can be capped with a hemisphere consisting of a buckyball structure. The diameter of a nanotube is in the order of a few nanometers (e.g. 1 – 300 nm) while they can be up to several millimeters in length. There are two main types of carbon nanotubes: The tubes made from one rolled graphene layer, known as single-walled carbon nanotubes. The other type consists of two or more concentric graphitic layers. In general, carbon nanotubes may have many different applications due their outstanding electrical and mechanical properties.

1.2.1 Single-walled nanotubes (SWCNTs)

Single-walled carbon nanotubes (SWCNTs) can be constructed by wrapping a graphene layer into a cylinder made up of sp^2 hybridized carbon, and could be terminated by end-caps arising from the presence of twelve pentagons (six per end), thus introducing positive curvature (closing the structure). It is possible to arrange the hexagons within a cylinder when rolling up a hexagonal graphene sheet in different ways.

In order to construct a tube, one first selects the origin (0,0) in the hexagonal lattice, and then a lattice point in the graphene sheet given by (*m,n*), Figure 1.4 correspond to a graphene sheet marked with different index (*m,n*), by rolling up the sheet so that the chosen lattice point is superposed in the origin, the desired tube is generated, the indices *(m,n)* represent a particular nanotube structure and can be used to determine tube diameter, helicity (or chirality) and the electronic properties. The direction, in which the graphene layer is rolled, is represented by a *chiral vector* $\mathbf{C_n}$, composed by linear combinations of integer numbers, *m* and *n,* of the unit vectors $\mathbf{a}_1$ and $\mathbf{a}_2$.

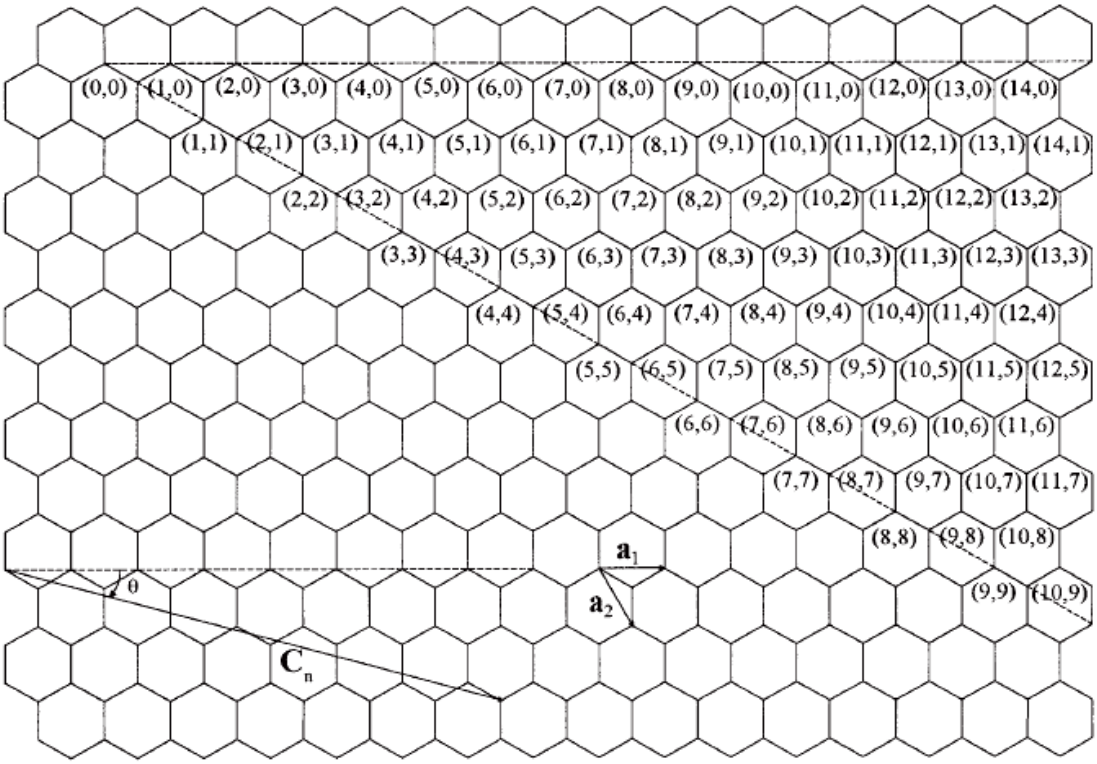

Figure 1-4.- A graphene sheet can be rolled in many ways. This vector convention is used to define each point on the lattice. Where $\mathbf{a_1}$ and $\mathbf{a_2}$ are the unitary vectors, $\mathbf{C_n}$ is the *chiral vector* that determines the rolling direction and θ is the *chiral angle,* Image taken from [29].

The vector $C_n = ma_1 + na_2$ determines the direction of rolling and therefore, the diameter can be expressed as [30]:

$$d = \frac{a\sqrt{m^2 + mn + n^2}}{\pi} \qquad \textbf{Equation 1-1}$$

where *a* is the length of the unit vectors $\mathbf{a_i}$, that is, the lattice parameter, in the case of graphene $|a_1| = |a_2|$ and their magnitude *a* takes the value of 2.46 Å. The generalized description of chiral tubes includes the range of orientations for C_n, a *zigzag* nanotube, in terms of (*m,n*) and the chiral angle, have the following conditions: $n = 0$, $\theta = 0$; an *armchair* nanotube meet: $m = n$, $\theta = \pm 30°$, and *chiral:* $0 < |\theta| < 30°$, $m \neq n$, In Figure 1.5 are illustrated three different types of nanotubes, armchair, zigzag and chiral, each one of them is identified by their own index

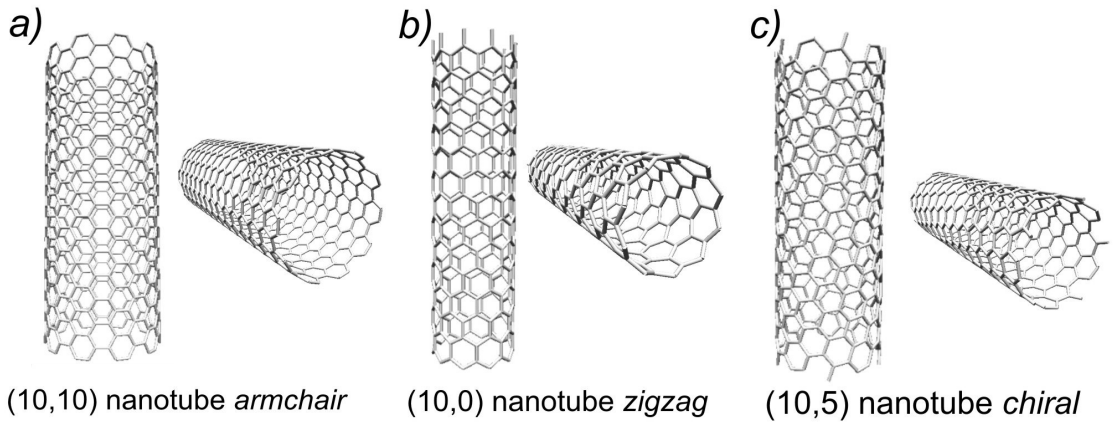

Figure 1-5.- Molecular models of single-walled carbon nanotubes of different helicities. (**a**) An *armchair* arrangement with $m = n$ *and* $\theta = \pm 30°$. (**b**) A *zigzag* configuration with $n = 0$, $\theta = 0$. (**c**) A *chiral* array with $m \neq n$, and in this case $\theta \sim -19.1°$.

(*m,n*), that define all their properties. The chiral angle θ (angle between $\mathbf{C_n}$ and the *zigzag* direction of the honeycomb lattice) is defined as[30]:

$$\theta = \arctan\left[-\frac{\sqrt{3}n}{2m+n}\right] \qquad \textbf{Equation 1-2}$$

Theoretical studies indicate that the electronic properties of single-walled nanotubes will vary as a function of its diameter and chirality, so the tube may behave as a semiconductor or metallic conductor. Theoretical studies indicate that all *armchair* tubes are metallic and the *zigzag* tubes when *m* is a multiple of three[30]. In general the metallic conductivity condition for these structures can be written as follow [30]:

$$\frac{(2m+n)}{3} = \text{integer} \qquad \textbf{Equation 1-3}$$

If Equation 1-3 is not satisfied, the tube will exhibit semiconducting properties. Therefore when nanotubes are formed with random values *n* and *m,* we would expect that one third of these tubes may be one-dimensional metals and the other two thirds one-dimensional semiconductors.

SWCNTs have other interesting properties, they can be joined by electron beam to form molecular junctions, via the creation and reconstruction of vacancies and interstitials [31]. In addition, It has been observed the coalescence of SWCNTs [32] into a larger nanotube, via a zipper like process [33]. Other materials can form SWNTs such as molybdenum disulfide, (MoS_2) [34], tungsten disulfide, (WS_2)[35], nanotubes with different composition of carbon, nitrogen and boron like $C_xB_yN_y$, C_2BN and C_3B.

1.2.2 Multiwalled carbon nanotubes (MWCNT)

A multiwalled carbon nanotube (MWCNT) consists of several graphite layers rolled up to form a series of coaxial tubes (see Figure 1.6-(**b-c**)). These tubes were structurally identified by Sumio Iijima in 1991 by electron diffraction and he found that the interlayer spacing within MWCNTs correspond to d(002) = 3.4 Å, slightly greater than graphite (d(002)=3.35 Å). This fact was ascribed to a combination of tubule curvature and Van der Waals force interactions between successive graphene cylinders. The X-ray diffraction pattern of MWCNTs is consistent with this spacing and provides information about crystallinity and structural dimensions in the bulk phase. MWCNTs contain several concentric graphene cylinders with interlayer spacing in the range of 0.34 and 0.39 nm. The intershell spacing within a MWCNT decreases as we move away from its principal axis, that is, as we increase the diameter of the coaxial graphene cylinder, the graphene layers tends to be closer (becoming closer to the value of graphite which has an interlayer spacing of 0.335 nm). Geometrical constraints in forming seamless graphene cylinders cause the layers to be uncorrelated with respect to one another. This contrasts to crystalline graphite, which could exhibit perfect “ABAB...” layer stacking.

Table 1-1.- Properties and advantage of carbon nanotubes[36]

Property	SWCNTs	Possible applications
Typical diameter	0.6 – 2.0 nm in	High resolution tips on AFM
Typical length	100 – 1000 nm	High aspect ratio, anisotropic properties
Density	1.33-1.4 g/cc	Light materials
Tensile strength	100 GPa, E = 1 TPa	Robust probes for STM
Resilience	Bent at large angles and re-straightened	Unbreakable tips
Current density	10^7 – 10^8 Amps/cm^2	Stable operation
Resistivity, 300 K	10^{-5}-10^{-3} Ω cm	
Intrinsic bandgap	0 eV/~0.5 eV (metallic/semiconductor)	CMOS, Nanoelectronics
Conductance quantization	(12.9 kΩ cm)$^{-1}$	Ballistic transport
Field Emission	Low turn on voltage (1-3V/μm)	High resolution display, X-rays sources
Field emission current density	10-1000 mA/cm^2	High resolution display, X-rays sources
High Thermal conductivity	20-3000 W/m.K	Excellent heat dissipation
Phonon mean free path	100 nm	Nanoelectronics
Temperature stability	~2800℃ in vacuum ~750℃ in air[37]	No probe contamination
Low tip surface	-	Minimum capacitance coupling
Contact independent of clamping force	-	Excellent nanoscale electrical contact
Chemical inertness	-	Biocompatibility
Hydrophobicity	-	Used in solutions

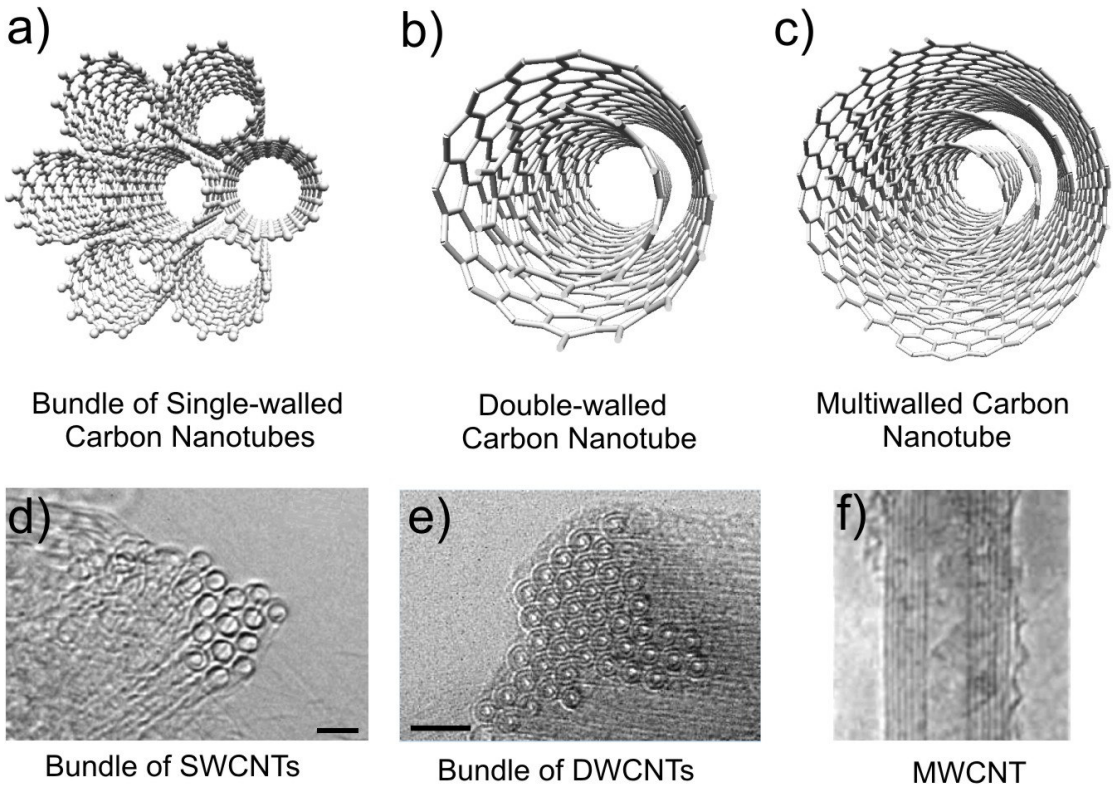

Figure 1-6.- Different types of carbon nanotubes. (**a**) A molecular representation of a bundle of SWCNT and (**d**) a HRTEM image of a group of SWCNTs [33], (scale bar = 2nm). (**b**) A representation of a DWCNT and (**e**) a HRTEM image of a bundle of DWCNT [38] (scale bar = 5 nm). (**c**) A representation of MWCNT and (**f**) an HRTEM of a seven-walled CNT with a hollow diameter of 2.2 nm[28].

Thus, MWCNTs tend to exhibit properties of turbostratic graphite, in which the layers are essentially uncorrelated and separated by distances larger than 0.335 nm. Therefore, every single carbon nanotube within a MWCNT is expected to have a different chirality. MWCNTs that exhibit large diameters experience low reactivity, because their surface is becoming close to that of planar graphite. There are other materials that can form MWNTs, such as $B_xC_yN_z$ [39] , CN_x[40], TiC[41], SIO_2[42].

1.2.3 Nitrogen-doped multiwalled carbon nanotubes (CN_x-MWNTs)

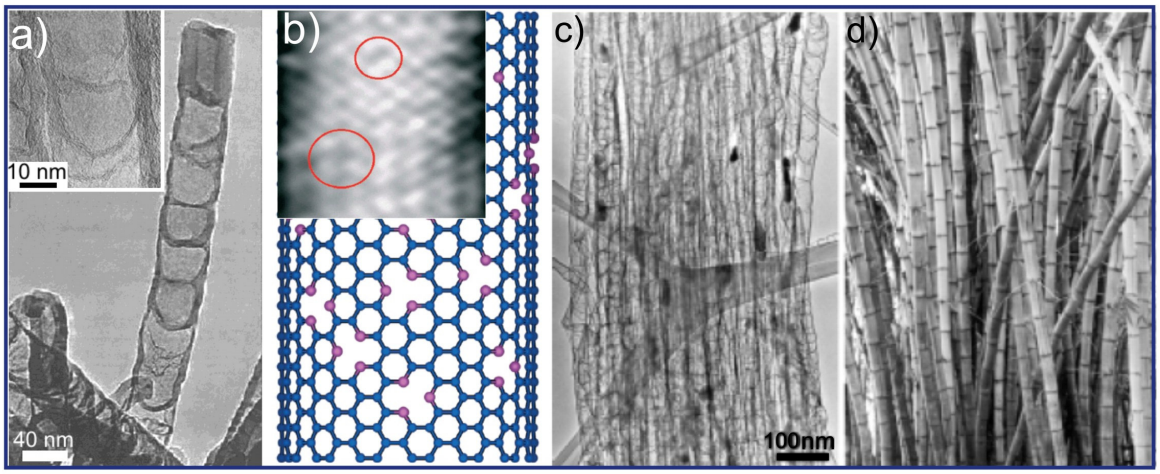

Figure 1-7.- Bamboo-like structure of the nitrogen-doped carbon nanotubes: (**a**) TEM image of a typical structure of N-doped carbon nanotubes, (inset) HRTEM of a aligned CN_x-nanotube exhibiting corrugation, interlinkage and compartments; (**b**) Molecular model of a CN_x-MWNT showing the pyridine-like nitrogen atoms replacing carbon atoms, (inset) Atomic resolution STM image of a 20 nm diameter N-doped carbon nanotube exhibiting distortion and holes (circles), possibly caused by the presence of a pyridine-like islands; (**c**) A TEM image of a typical region of aligned CN_x-MWNT and (**d**) where they show the bamboo-like structure. Images taken from references [44,45]

The carbon atoms in a nanotube could be replaced by other types of elements (such as nitrogen, boron, silicon, etc.). In this case, the doping is called subsitutional, thus leading to new nanomaterials with different properties, making possible the control of electronic, thermal and chemical properties by the addition of electron donors or acceptors into nanotubes. The nitrogen-doped carbon nanotubes (CN_x-MWNTs) exhibit interesting properties due to the incorporation of nitrogen atoms in the crystalline lattice. CN_x-MWNTs are more chemical reactive than the pure carbon MWCNTs due to the incorporation of nitrogen atoms in their structure. The nitrogen could be present in two different ways, *substitutional* (each N atom is bonded to 3 carbon atoms) or *pyridine-like* (where the nitrogen atom is just bonded to two carbon atoms).

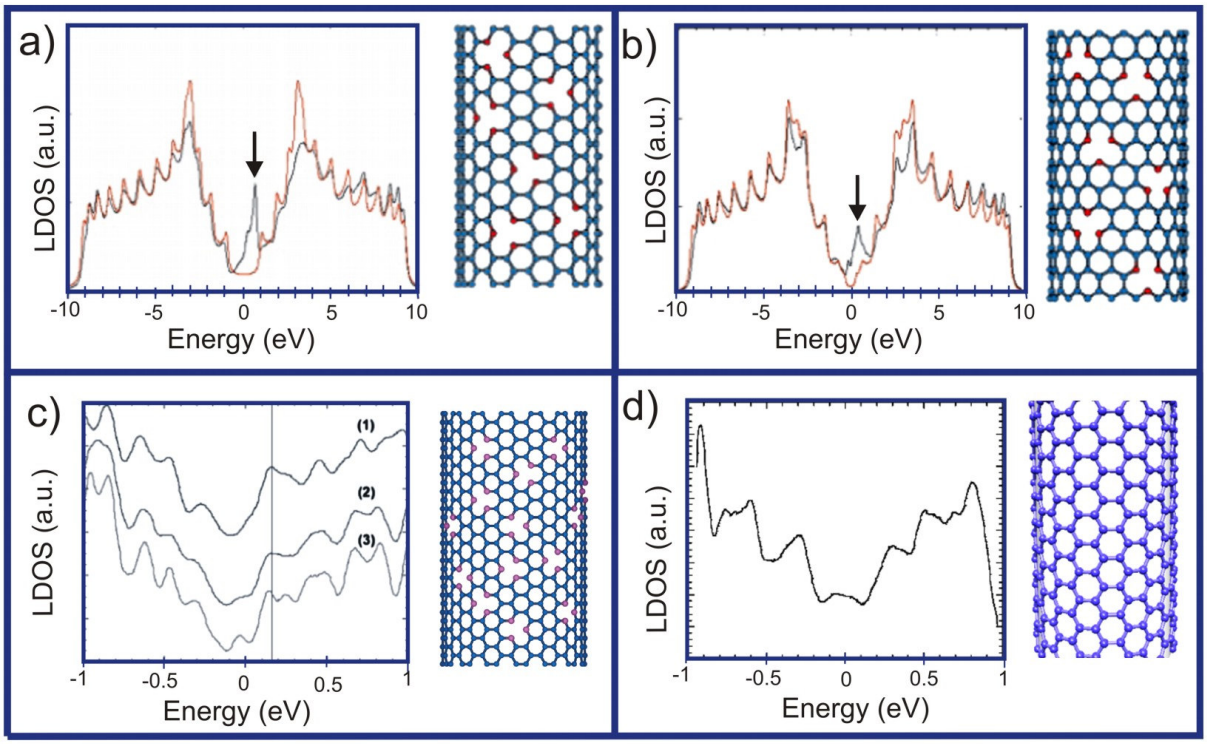

Figure 1-8.- Theoretical and experimental local density of states (LDOS) of a N-doped carbon nanotube and SWCNT. Theoretical LDOS associated with a pyridine like structure with N-doped carbon nanotubes corresponding to (**a**) armchair (10,10) and (**b**) to zigzag (17,0) configurations, (N*: red spheres,* C*: blue spheres*). In (**a**) and (**b**) the LDOS of N-doped (*black curve*) and undoped CNT (red curve) are shown, the pyridine-like structure of N atoms is responsible for the prominent donor-like features (*arrows* in the conduction band) just above the Fermi energy; (**c**) Tunneling spectra acquired on a straight section of a nonchiral N-doped carbon nanotube with an N content of ca. 3-4%. Note the peak at 0.18 eV in all spectra, and (**d**) Tunneling spectra along a pure MWNT of 20 nm. Images taken from [44,45]

Recently, it has been demonstrated that CN_x-MWNTs exhibit better biocompatibility when compared to SWCNTs and the MWCNTs[43]. Therefore, CN_x-MWNTs may have different uses in biological systems, such as delivery of drugs or infectious agents inhibitors.

CN_x-MWNTs could be metallic and exhibit strong electron donor states near the Fermi level[44]. It has been demonstrated that the substitutional or pyridine-like structures could be responsible for the metallic behavior and the prominent features near the Fermi level[45] (Figure 1.8-(**a-b**)). Prominent donor peaks just above the Fermi energy (at ca. 0.2 eV) have been theoretically predicted, which

are in good agreement with the experimental data obtained using scanning tunneling spectroscopy (STS), (see Figure 1.8-(**c**)). Thus, N-doping within carbon tubes, induces sharp localized states above the Fermi level due to the presence of additional electrons (shown by arrows of Figure 1.8-(**a-b**)). These doped tubes exhibit n-type conduction, and are more likely to strongly react with electron acceptor molecules. All these characteristics indicate that the CN_x-MWNTs are also more reactive than pure carbon MWNTs.

1.2.4 Functionalization of carbon nanotubes

There is presently great interest in the chemical functionalization of carbon nanotubes. In particular, in order to improve the solubility [46] and to enhance compatibility in composite materials surfaces nanotube functionalization is vital [47]. Both covalent and noncovalent sidewall functionalization has been explored, the most used technique is the surface modification of carbon nanotubes through covalent functionalization. This approach is vital for the development of high-performance composite materials, chemisensors, nanoelectronic devices, photovoltaic devices, as well as other biomedical components. Covalent functionalization of CNTs is most frequently initiated by introducing carboxylic acid groups using a nitric acid oxidation method. Thereafter, long alkyl chains, polymers [48], and sugars can be chemically attached to the CNT by esterification and amidation reactions through the carboxylic acid moieties.

Carboxylate groups have been introduced on to the surface of MWCNTs by reactions with strong oxidizing agents such as nitric (HNO_3) and sulfuric (H_2SO_4) acid [49], other covalent approaches include fluorination [50], alkanes [51], amines and hydrogen, usually the sidewall functionalization coverage is high, and result in a modification of the intrinsic SWCNT properties [52]. Noncovalent modifications of the CNT surface have been used to improve the wetting and solubility of CNTs. Moreover, the method could be used for diameter-selective CNT separation [53], useful in the fabrication of highly specific biosensors [54], protein immobilizers [55] and polymeric composites [56]. The noncovalent approach includes surfactant modification using ionic and non-ionic materials, such as sodium dodecyl sulfate

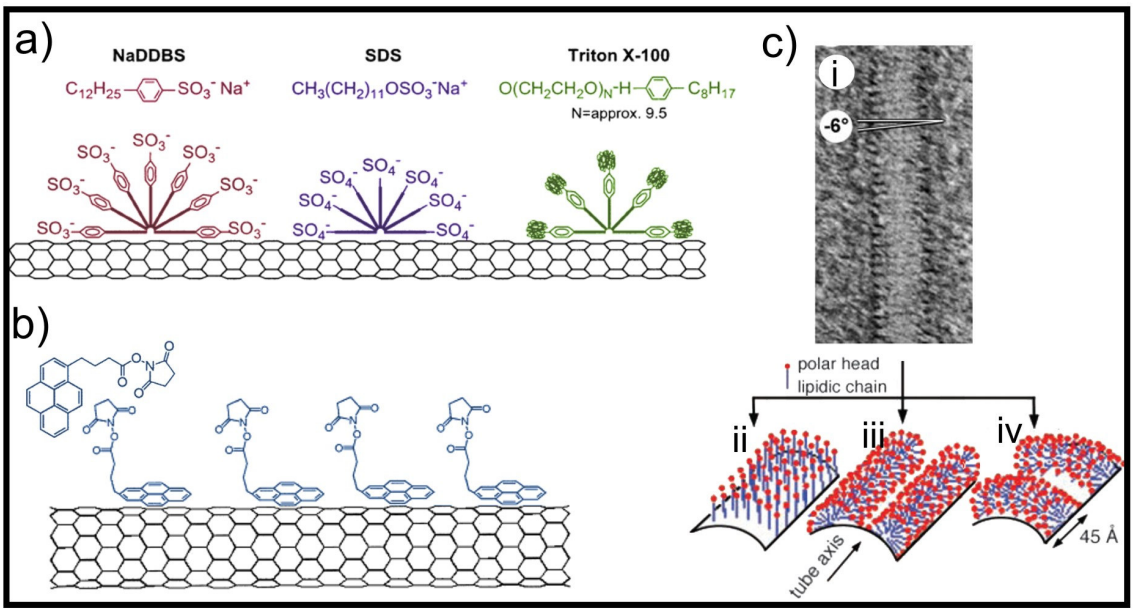

Figure 1-9.- Noncovalent functionalization of carbon nanotubes. (**a**) Different surfactant molecules interacting with CNTs. [57] (**b**) Interaction with aromatic molecules, the π orbital presented in both aromatic molecule and the CNT interact with each other. [55] (**c-i**) A CNT covered with SDS molecules, the SDS form a right helix tilted by –6° relative to the tube axis, (**c-ii-iv**) representation of different arrays of SDS molecules, the (**c-iv**) is the array obtained experimentally in (**c-i**). [59]

(SDS), Triton® X-100, octadecyl-trimethyl-ammonium bromide (OTAB) and sodium dodecyl-benzene sulfonate (NaDDBS) [57]. Some surfactants are able to enhance the stability of SWCNTs in water [57] but removing the surfactant afterwards is problematic. Other non-covalent approaches can be achieved using polymer wrapping, such as polystyrene sulfonate (PSS), poly(vinylpyrrolidone) (PVP) and polyethylene oxide-polybutylene oxide-polyethylene oxide (PEO-PBO-PEO) triblock polymer [58]. Many studies has been carried out in order to understand how these molecules aid to improve the interaction between the nanotubes and their surrounding media. Figure 1.9-(**a-b**) illustrates how some surfactants molecules can interact with a CNT, the molecules are self-assembled on the surfaces of the nanotubes, with their non-polar section near the CNT surfaces. In Figure 1.9-(**c**) an experimental result showing the organization of the SDS in a right helix tilted by –6° relative to the tube axis. In Figure 1.9-(**c-iv**) the supramolecular

organization is represented. This organization depends on the type, diameter and perhaps chirality of the nanotube [59].

The advantage of noncovalent attachment is that the structure of the CNT is not damaged and their mechanical properties remain intact. The main disadvantage is that the forces between the wrapping molecules and the CNT are weak, which means that the load may not be transferred efficiently from the matrix to the CNT filler. To avoid problems associated with the degradation of the mechanical properties of the CNTs, it would be desirable to find solvents capable of solvating the pristine tubes. To date, the best solvents reported for generating CNT dispersions are amides, particularly N,N-dimethylformamide (DMF) and N-methylpyrrolidone (NMP) [46].

1.2.5 Multiwalled carbon nanotubes with oxygen groups (CO_x-MWNT)

In order to increase the reactivity of MWCNTs, it is possible to modify their surface by introducing functional groups (such as carbonyl, carboxyl and hydroxyl groups). These groups improve the interaction with other materials. Usually these functional groups can be introduced by acidic treatments in HNO_3 or mixture of HNO_3 and H_2SO_4. These processes open the end-caps of the nanotubes containing pentagons and dissolve some catalytic particles (such as Fe, Ni, Co, etc). For this reason these processes are used to purify CNT samples, but if the chemical treatment is carried out for a long time, high temperatures or using an ultrasonic bath, the nanotubes could be segmented and damaged [49], thus altering their mechanical properties. Recently, the Terrones's group [60] demonstrated that the nanotubes can be functionalized during the synthesis process, avoiding additional procedures, and the use of chemicals such as acidic solutions. These authors add low ethanol concentrations during the chemical vapor deposition (CVD) synthesis allowing the introduction of carbonyl, hydroxyl and others oxygen functional groups on the nanotube surface. These nanotubes are called "multiwalled carbon nanotube with oxygen groups" (CO_x-MWNT).

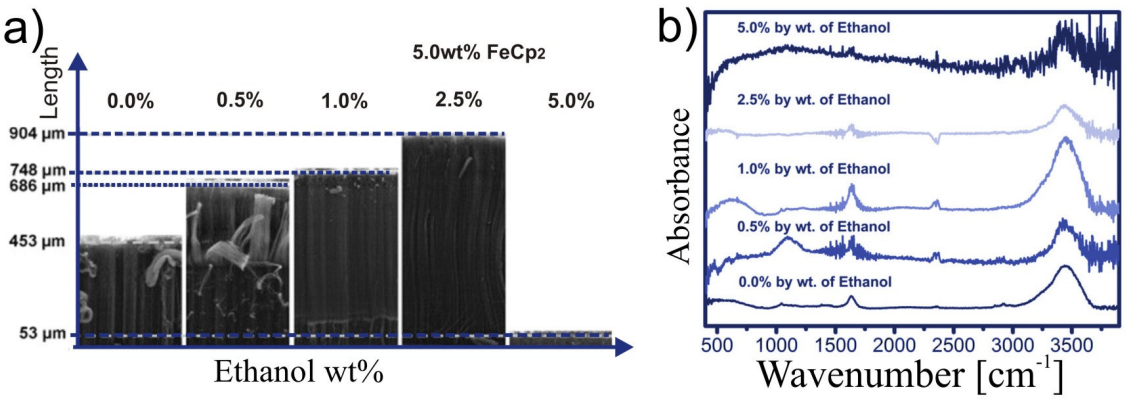

Figure 1-10.- Multiwalled carbon nanotubes produced with CO_x groups. (**a**) The length and crystallinity of the nanotube can be controlled by the addition of ethanol, when the ethanol is present in excess (more than 2.5wt%) acts as inhibitor agent of the CNT synthesis, and (**b**) The Fourier-Transform infrared (FTIR) spectra, the peaks correspond to carbonyl groups (1650 cm^{-1}) and hydroxyl groups (3450 cm^{-1}). Images taken from [60].

These types of nanotubes have different properties when compared to CN_x-MWNTs and pure carbon nanotubes (MWCNTs), the CO_x-MWNTs are more reactive than the MWCNT, but less than the CN_x-MWNTs. Some important advantages of using CO_x-MWNTs are that their length can be controlled (up to 5mm with 3 hours of synthesis) as well as their reactivity (varying the ethanol concentration). Usually CO_x-MWNTs are larger and exhibit higher crystallinity than CN_x-MWNTs with the same synthesis conditions. Moreover, we expect CO_x-MWNTs to display better mechanical properties than CN_x-MWNTs due the low amount of structural defects introduced in the graphitic network. The maximum introduction of functional groups take place when the nanotubes are synthesized using a solution with 1wt% of ethanol. In the Figure 1.9 (**b**), the peaks in the infrared spectra that correspond to carbonyl groups (1650 cm-1) and hydroxyl groups (3450 cm-1) are more intense.

1.3 References

[1] H. W. Kroto, J. R. Heath, S. C. O'Brien, R. F. Curl, R. E. Smalley. “C60: Buckminsterfullerene”, *Nature,* Vol. 318, 162-163 (1985)

[2] D. L. Dorset, J. R.Fryer, “Quantitative Electron Crystallographic Determinations of Higher Fullerenes in the Hexagonal Close Packed Polymorph”, *J. Phys. Chem. B.*, Vol. 105, 2356-2359 (2001)

[3] Kuzuo R., Terauchi M., Tanaka M., Saito Y., Shinohara H., “Electron-energy-loss spectra of crystalline C84”, *Phys. Rev. B*, Vol. 49, 5054-5057 (1994)

[4] W. Krätschmer, L. D. Lamb, K. Fostiropoulos, D. R. Huffman, “Solid C60: a new form of carbon” *Nature*, Vol. 347, 354-358 (1990)

[5] N. Sano, H. Wang, M. Chhowalla, I. Alexandrou, G.A.J. Amaratunga, “Nanotechnology: Synthesis of carbon 'onions' in water”, *Nature*, Vol. 414, 506-507 (2001)

[6] S. Bulusu., X. Li., L. Wang , X. C. Zeng. “Evidence of hollow golden cages”, *PNAS*, Vol. 103, 8326-8330 (2006)

[7] G. Tegos, T. Demidova, D. Arcila-Lopez, H. Lee, T. Wharton, H. Gali, M. Hamblin, “Cationic Fullerenes Are Effective and Selective Antimicrobial Photosensitizers”, *Chem. Biol.*, Vol. 12, 1127–1135 (2005)

[8] L. Ding, J. Stilwell, T. Zhang, O. Elboudwarej, H. Jiang,J.P. Selegue, P.A. Cooke, J.W. Gray, F.F. Chen, “Molecular Characterization of the Cytotoxic Mechanism of Multiwall Carbon Nanotubes and Nano-Onions on Human Skin Fibroblast”, *Nano lett.*, Vol. 5, 2448-2464 (2005)

[9] M. Ge, K. Sattler, “Observation of fullerene cones”, *Chem. Phys. Lett*. Vol. 220, 192-196 (1994)

[10] A. Krishnan, E. Dujardin, M. M. J. Treacy, J. Hugdahl, S. Lynum, T.W. Ebbesen, "Graphitic cones and the nucleation of curved carbon surfaces", *Nature*, Vol. 388, 451-454 (1997)

[11] M. Yoshida, The Fullerene Library, *http://www.cochem2.tutkie.tut.ac.jp/Fuller/Fuller.html*, May 30th (2006)

[12] D. Baowan, J. M. Hill, “Equilibrium locations for nested carbon nanocones”, *J. Math. Chem.* Vol. 43,1489-1504 (2008)

[13] K. Kobayashi, “Superstructure induced by a topological defect in graphitic cones”, *Phys. Rev. B*, Vol. 61, 8496-8500 (2000)

[14] R. Tamura, M. Tsukada, “Disclinations of monolayer graphite and their electronic states”, *Phys. Rev. B,* Vol. 49, 7697-7708 (1994)

[15] S. Garaj, L. Thien-Nga, R. Gaal, K.T. L. Forro, K. Takahashi, F. Kokai, M. Yudasaka, S. Iijima, “Electronic properties of carbon nanohorns studied by ESR”, Phys. Rev. B, Vol. 62, 17115-1719 (2000)

[16] X. Lu, Q. Yang, C. Xiao, A. Hirose, “Field electron emission of carbon-based nanocone films”, *Appl. Phys. A,* Vol. 82, 293–296 (2006)

[17] S.P. Jordan,V.H. Crespi, “Theory of Carbon Nanocones: Mechanical Chiral Inversion of a Micron-Scale Three-Dimensional Object”, *Phys. Rev. Lett.*, Vol. 93, 255504 (2004)

[18] T. Hang, H. Ling, Z. Xiu, M. Li, D. Mao, “Study on the Adhesion Between Epoxy Molding Compound and Nanocone-Arrayed Pd Preplated Leadframes”, *J. Electr. Mater,* Vol. 36, 1594-1598 (2007)

[19] M.P. Machado, P. Piquinia, R. Mota, “Energetics and electronic properties of BN nanocones with pentagonal rings at their apexes”, *Eur. Phys. J. D*, Vol. 23, 91–93 (2003)

[20] L. Cao,L. Laim,C. Ni, B. Nabet, J.E. Spanier, "Diamond-Hexagonal Semiconductor Nanocones with Controllable Apex Angle" *J. Am. Chem Soc.,* Vol. 127, 13782-13783 (2005)

[21] P.G. Li, X.L. Fu, L.M. Chen, H.Y. Zhang, L.H. Li, W.H. Tang, "Growth of alumina microcones by high-temperature oxidization", *Appl. Phys. A*, Vol. 81, 1269–1272 (2005)

[22] J. Charlier, G. Rignanese, “Electronic Structure of Carbon Nanocones”, *Phys. Rev. Lett.* Vol. 86, 5970- 5973 (2001).

[23] S. Berber, Y. Kwon, D. Tománek, “Electronic and structural properties of carbon nanohorns”, *Phys Rev B*, Vol. 62, R2291- R2294 (2000)

[24] S. Iijima, M. Yudasaka, R. Yamada, S. Bandow, K. Suenaga, F. Kokai, K. Takahashi, "Nano-aggregates of single-walled graphitic carbon nano-horns" *Chem. Phys. Lett.* Vol. 309, 165-170 (1999)

[25] J.-M. Bonard, R. Gaál, S. Garaj, L. Thien-Nga, L. Forró, K. Takahashi, F. Kokai, M. Yudasaka, S. Iijima, "Field emission properties of carbon nanohorn films", *J. Appl. Phys.,* Vol. 91, 10107 (2002)

[26] A. Hashimoto, H. Yorimitsu, K. Ajima, K. Suenaga, H. Isobe, J. Miyawaki, M. Yudasaka, S. Iijima, E. Nakamura, "Selective deposition of a gadolinium(III) cluster in a hole opening of single-wall carbon nanohorn", *PNAS,* Vol. 101, 8527-8530(2004)

[27] A. Oberlin, M. Endo, T. Koyama, "Filamentous growth of carbon through benzene decomposition", *J. Cryst. Growth*, Vol. 32, 335-349 (1976)

[28] S. Iijima, *Nature.* "Helical microtubules of graphitic carbon" Vol. 354, 56-58 (1991)

[29] M. Terrones, W. K. Hsu, H. W. Kroto, D. R.M. Walton, "Nanotubes: A Revolution in Materials Science and Electronics" Topics in Current Chemistry, Fullerenes and Related Structures, Vol. 199, 189-234, Ed. Springer (1999)

[30] M.S. Dresselhaus, G. Dresselhaus, R. Saito, "Physics of carbon nanotubes", *Carbon*, Vol. 33, 883-891(1995)

[31] M. Terrones, F. Banhart, N. Grobert, J.C. Charlier,H. Terrones, P. M. Ajayan, "Molecular Junctions by Joining Single-Walled Carbon Nanotubes", *Phys Rev Lett*, Vol. 89, 075505 (2002)

[32] P. Nikolaev, A. Thess, A. G. Rinzler, D. T. Colbert, R. E. Smalley, "Diameter doubling of single-wall nanotubes", *Chem. Phys. Lett.* Vol. 266, 422-426 (1997)

[33] M. Terrones, H. Terrones, F. Banhart, J. C. Charlier, P. M. Ajayan., "Coalescence of Single-Walled Carbon Nanotubes", *Science*, Vol. 288, 1226- 1229 (2000)

[34] M. Remskar, A. Mrzel, Z. Skraba, A. Jesih, M.Ceh, J.Demsar, P. Stadelmann, F. Lévy, D.Mihailovic, "Self-Assembly of Subnanometer-Diameter Single-Wall MoS_2 Nanotubes", *Science,* Vol 292, 479-481 (2001)

[35] I.Kaplan-Ashiri, S. R. Cohen, K. Gartsman, V. Ivanovskaya, T. Heine, G. Seifert, I. Wiesel, H. D. Wagner, R. Tenne, "On the mechanical behavior of WS_2 nanotubes under axial tension and compression", *PNAS*, Vol. 103, 523-528 (2006)

[36] A. Vaseashta, *Nanostructured materials based next generation devices and sensors, Nanostructured and Advanced Materials*, Ed. *Springer*, 1–30 (2005).

[37] T. W. Ebbesen, P. M. Ajayan, H. Hiura, K. Tanigaki, "Purification of nanotubes", *Nature*, Vol. 367, 519-519 (1994)

[38]M. Endo, H. Muramatsu, T. Hayashi, Y. A. Kim, M. Terrones, M. S. Dresselhaus, "Nanotechnology 'Buckypaper' from coaxial nanotubes" *Nature*, Vol. 433, 476 – 476 (2005)

[39] Z. Weng-Sieh, K. Cherrey, N.G. Chopra, X.blase, Y. Miyamoto, A.Rubio, M.L.Cohen, S. G. Louie, A. Zettl, R. Gronsky, "Synthesis of $B_xC_yN_z$ nanotubules", *Phys. Rev. B,* Vol. 51, 11229- 11232 (1995)

[40] M. Terrones, R. Kamalakaran, T. Seeger, M. Rühle, "Novel nanoscale gas containers: encapsulation of N_2 in CN_x nanotubes", *Chem. Comm.*, 2335–2336 (2000)

[41] E.W. Wong, B. W. Maynor, L. D. Burns, C. M. Lieber, "Growth of Metal Carbide Nanotubes and Nanorods", *Chem. Mater*, Vol. 8, 2041-2046 (1996)

[42] B. C. Satishkumar, A. Govindaraj, E. M. Vogl, L. Basumallick, C. N. R. Rao, "Oxide nanotubes prepared using carbon nanotubes as templates", *J. Mater. Res.*, Vol. 12, 604-606 (1997)

[43] J. C. Carrero-Sánchez, A.L. Elías, R. Mancilla, G. Arrellín, H. Terrones, J. P. Laclette, M. Terrones, "Biocompatibility and Toxicological Studies of Carbon Nanotubes Doped with Nitrogen", *Nano Lett.*, Vol. 6, 1609-1616 (2006)

[44] M. Terrones, P.M. Ajayan, F. Banhart, X. Blase, D.L.Carroll, J.C. Charlier, R. Czerw, B. Foley, N. Grobert, R. Kamalakaran, P. Kohler-Redlich, M. Rühle, T. Seeger, H. Terrones, "N-doping and coalescence of carbon nanotubes: synthesis and electronic properties", *Appl. Phys. A*, Vol. 74, 355–361 (2002)

[45] R. Czerw, M. Terrones, J.-C. Charlier, X. Blase, B. Foley, R. Kamalakaran, N. Grobert, H. Terrones, D. Tekleab, P. M. Ajayan, W. Blau, M. Rühle, D. L. Carroll,

"Identification of Electron Donor States in N-Doped Carbon Nanotubes", *Nano Lett*, Vol. 1, 457-460 (2001)

[46] K. D. Ausman, R. Piner, O. Lourie, R. S. Ruoff, "Organic Solvent Dispersions of Single-Walled Carbon Nanotubes: Toward Solutions of Pristine Nanotubes", *J. Phys. Chem. B,* Vol. 104, 8911-8915 (2000)

[47] S. Reich, C. Thomsen, P. Ordejón, "Electronic band structure of isolated and bundled carbon nanotubes", *Phys Rev B*, Vol. 65, 155411 (2002)

[48] G. X. Chen, H. S. Kim, B. H. Park,J. S. Yoon," Controlled Functionalization of Multiwalled Carbon Nanotubes with Various Molecular-Weight Poly(L-lactic acid)", *J. Phys. Chem. B*, Vol. 109, 22237-22243 (2005)

[49] J. Liu, A. G. Rinzler, H. Dai, J. H. Hafner, R. K. Bradley, P. J. Boul, A. Lu, T. Iverson, K. Shelimov, C.B. Huffman, F. Rodriguez-Macias, Y. S. Shon, T. R. Lee, D.T. Colbert, R. E. Smalley, "Fullerene Pipes", *Science,* Vol. 280, 1253-1256 (1998)

[50] E. T. Mickelson, I.W. Chiang, J.L. Zimmerman, P. J. Boul, J. Lozano, J. Liu, R. E. Smalley, R. H. Hauge, J.L. Margrave, "Solvation of Fluorinated Single-Wall Carbon Nanotubes in Alcohol Solvents" *J. Phys. Chem. B*, Vol 103, 4318-4322 (1999)

[51] P. J. Boul, J. Liu, E. T. Mickelson, C. B. Huffman, L. M. Ericson, I. W. Chiang, K. A. Smith, D. T. Colbert, R. H. Hauge, J. L. Margrave, R. E. Smalley, "Reversible sidewall functionalization of buckytubes", *Chem. Phys. Lett.*, Vol 310, 367-372 (1999)

[52] A. Garg, S. B. Sinnot, "Effect of chemical functionalization on the mechanical properties of carbon nanotubes", *Chem. Phys. Lett.*, Vol. 295, 273-278 (1998)

[53] R. M. Tromp, A. Afzali, M. Freitag, D. B. Mitzi, Zh. Chen, "Novel Strategy for Diameter-Selective Separation and Functionalization of Single-Wall Carbon Nanotubes ", *Nanolett,* Vol. 8, 469-472 (2008)

[54] R. J. Chen, S. Bangsaruntip, K. A. Drouvalakis, N. W. S. Kam, M. Shim, Y. Li, W. Kim, P. J. Utz, H. Dai, "Noncovalent functionalization of carbon nanotubes for highly specific electronic biosensors" *PNAS,* Vol. 100, 4984-4989 (2003)

[55] R. J. Chen, Y. Zhang, D. Wang, H. Dai, "Noncovalent Sidewall Functionalization of Single-Walled Carbon Nanotubes for Protein Immobilization", *J. Am. Chem. Soc.*, Vol. *123,* 3838-3839 (2001)

[56] X. Gong, J. Liu, S.Baskaran, R.D.Voise, J.S. Young., "Surfactant-Assisted Processing of Carbon Nanotube/Polymer Composites" *Chem. Mater*., Vol. 12, 1049-1052 (2000)

[57] M. F. Islam, E. Rojas, D. M. Bergey, A. T. Johnson, A. G. Yodh, High Weight, "Fraction Surfactant Solubilization of Single-Wall Carbon Nanotubes in Water" *Nanolett*, Vol. 3, 269-273 (2003)

[58] V. C. Moore, M. S. Strano, E. H. Haroz, R. H. Hauge, R. E. Smalley, "Individually Suspended Single-Walled Carbon Nanotubes in Various Surfactants", *Nanolett*., Vol. 3, 1379-1382 (2003)

[59]C. Richard, F. Balavoine,P. Schultz,T. W. Ebbesen, C. Mioskowski, "Supramolecular Self-Assembly of Lipid Derivatives on Carbon Nanotubes", *Science*, Vol. 300, 775-778 (2003)

[60] A. Botello-Méndez, J. R. Campos, A. Morelos-Gómez, J. M. Romo-Herrera, A. G. Rodríguez, H. Navarro, M. A. Vidal, H. Terrones, M. Terrones, "Controlling the dimensions, reactivity and crystallinity of multiwalled carbon nanotubes using low ethanol concentrations", *Chem. Phys. Lett*. Vol. 453, 55–61(2008)

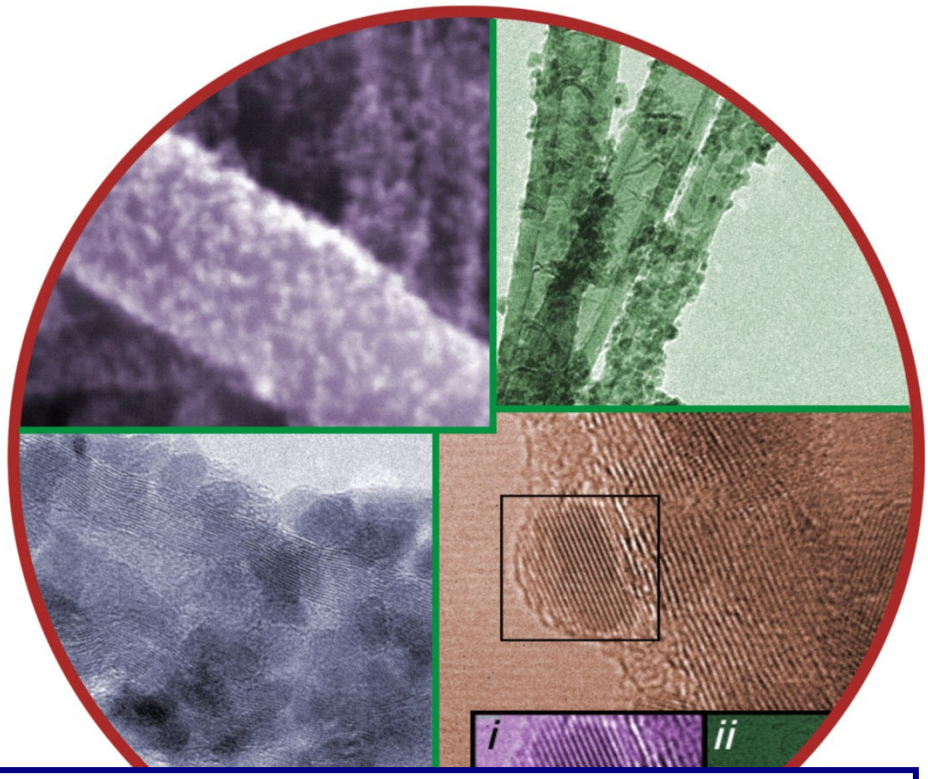

Chapter 2

Zinc Oxide Cluster Deposition on Nitrogen-Doped (CN_x-MWNTs) and Functionalized Multiwalled Carbon Nanotubes (CO_x-MWNTs)

ZnO nanoparticles have been efficiently and homogeneously anchored on the surfaces of nitrogen-doped multiwalled carbon nanotubes (CN_x-MWNTs) and multiwalled carbon nanotubes with oxygen groups (CO_x-MWNTs). These two types of nanotubes exhibit different reactivity and properties. During the coating process, thiophene was added to stabilize the nanoparticles and improve the attachment to the nanotube; the smallest particles were deposited on the CO_x-MWNTs with a mean size of 4.1 nm. The results show that addition of thiophene into the system controls the average particle size, decreases the size distribution and improves the homogeneity and the spatial density of the anchored ZnO particles on the nanotube walls.

2.1 Introduction

Zinc oxide (ZnO) is a unique material with very attractive engineering properties such as the large exciton binding energy (60 meV), photoluminescence, and piezoelectricity. While ZnO could be easily synthesized in a plethora of different morphologies in single-crystal form, nanostructured ZnO has become one of the most studied semiconductor nanomaterials in the beginning of the 21st century.

2.1.1 Nanostructured zinc oxide

ZnO is a functional material, it displays unique properties in the near-UV[1] emission, outstanding piezoelectric properties, ZnO has also been used widely in catalysis, and in the fabrication of electric, optoelectronic and photochemical devices[2]. ZnO has demonstrated being a promising material in the field of semiconductor solar cells [3], due its band gap (3.37 eV), as a good field-emission material[4], which could also be used as gas and force sensors[5], cantilevers scanning probe microscopy[6], etc.

Among several types of ZnO nanostructures with different morphologies[7], we could mention, nanowires[8,9], nanobelts[10], nanotubes[11], nanocables, as well as nanorods[12,13], tetrapods[14], swords, flowers[15], nanonails[16], nanobridges [16], nanohelices[17], and other complex structures[18]. Even heterostructures of ZnO-Zn coaxial nanowires[19] and nanotubes has been recently obtained.

These unique nanostructures demonstrate that ZnO is probably the richest family of nanostructures among all materials, with a vast range of possible applications. Since ZnO exhibits both semiconducting and piezoelectric properties, it could be used to form the basis of electromechanically coupled sensors and transducers. In addition, it is relatively biosafe and biocompatible, with important implications in biomedical science.

In Figure 2.1 we can observe the wide diversity of ZnO nanostructures, all these structures could be produced with almost 100% purity. Some techniques used to produce these structures are laser assisted methods, vapor liquid solid processes and thermal evaporation.

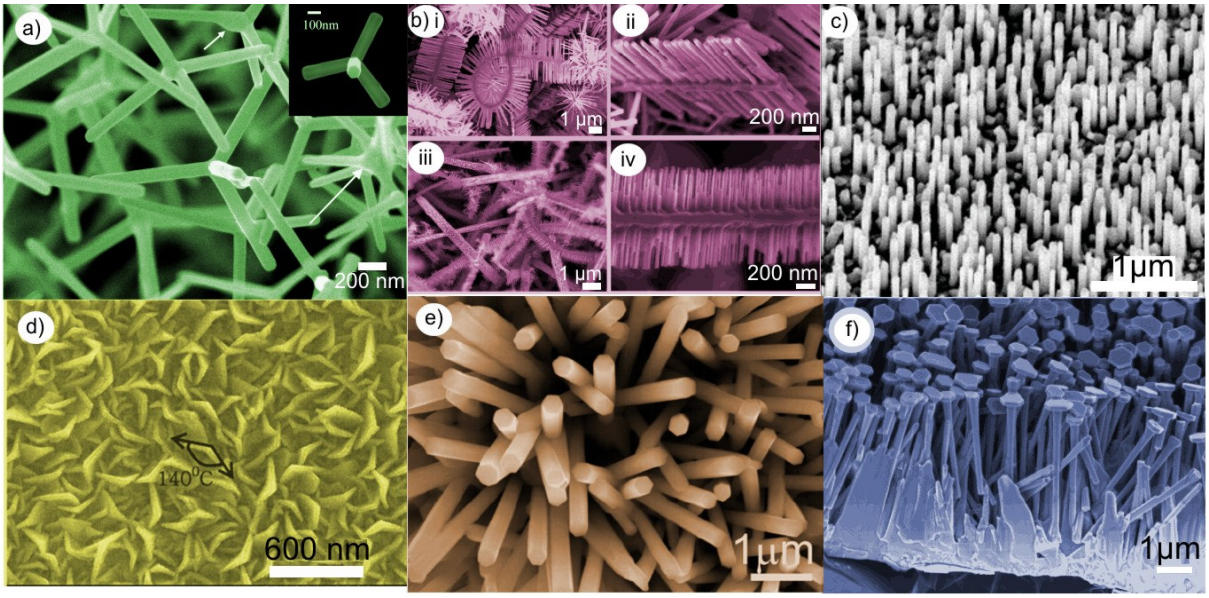

Figure 2-1.- Zinc oxide nanostructures. (**a**) Tetrapod-like ZnO nanocrystals [14]; (**b**) 2-fold nanostructures [20]; (**c**) ZnO aligned nanowires [21]; (**d**) Nanoflowers [22] (**e**) Nanorods [34], and (**f**) Nanonails [16]. All these structures exhibit interesting electrical and optical properties, which could be used in a wide range of applications.

These structures present interesting properties could have numerous potential applications in a variety of fields such as field emission, photovoltaics, transparent EMI shielding, supercapacitors, fuel cells, high strength and multifunctional nanocomposites, gas adsorption devices, etc. The zinc precursors generally used to generate ZnO nanostructures via wet chemical methods are zinc nitrate ($Zn(NO_3)_2$), zinc acetate ($Zn(C_2H_3O_2)_2$) and zinc carbonate ($ZnCO_3$) due their low thermal decomposition and their wide solubility in different types of solvents.

2.1.2 Carbon nanotubes-zinc oxide functional composites

Nanoparticles integrated with one-dimensional (1D) nanostructures are novel composite materials that have attracted intensive interest because they exhibit novel optical and electrical properties. The outstanding properties of ZnO nanoparticles could be efficiently transferred to other materials when interacting with other surfaces such as cotton fabrics [23] for the protection of the body against solar radiation. Over the last years, CNTs have been used as templates to obtain ZnO nanostructures. The resulting materials display enhanced properties in comparison with the individual materials. Actually, researchers have synthesized rods, wires, thin films and quantum dots of ZnO on the outer wall of carbon nanotubes[24].

Various groups have also reported different coating methods to obtain ZnO nanoparticles on MWCNTs. These composites have demonstrated to be an efficient field emitter with increased lifetimes [25] at a low electric field [26]. These composites material could be used as a cathode material for field emission flat panel displays [27]. However, agglomeration of nanoparticles is still a problem in which these unique properties are diminished. In order to enhance the interfacial adhesion between nanoparticles and CNTs, many groups have modified chemically the surface of the CNTs. Generally, they use a sonochemical (sonication with strong acid solutions) or thermal oxidation process to generate surface functional groups, but unfortunately these processes alter significantly the properties of the nanotubes.

Some other methods to synthesize MWCNTs/ZnO nanoparticles composites such as CVD or plasma enhanced chemical vapor deposition (PECVD) [28] require high temperatures and sophisticated equipment. Other versatile methods allow the production of quantum dots and nanowires using high temperatures but offer low control on particle size within the nanoparticles [23]. Other authors have reported the use of water-in-oil microemulsions that require several types of surfactants to produce ZnO nanoparticles, however the process is only able to generate very small amount of products [29].

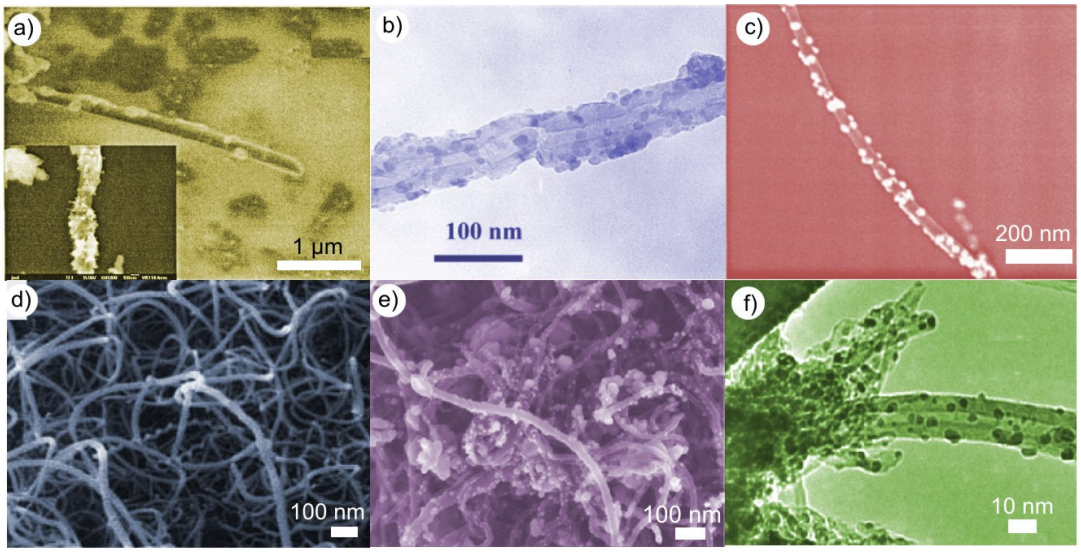

Figure 2-2.- Carbon nanotubes/ZnO composites. (**a**) MWCNTs with different nanostructures of ZnO [24], (**b**) MWCNTs/ZnO composite prepared by water-in-oil microemulsions [29]**,** (**c**) MWCNTs composite prepared by atomic layer deposition[25], (**d**) Composite material with a continuous coating of ZnO particles (size from 11 to 48 nm) [30], (**e**) MWCNTs/ZnO material exhibit small ZnO particle size (~10 nm) but large size distribution[31] and (**f**) Composite prepared by PECVD at high temperatures [28].

Others research groups have been reported some simple methodologies to produce nanocomposites, usually obtaining large particle size distribution due the very low control and low load of nanoparticles[31].

Other groups employs an *atomic layer deposition* (ALD) method at high temperatures (900℃), and discovered that the field emission properties of ZnO/MWCNTs and ZnO/SWCNTs composites were enhanced dramatically when compared to uncoated MWCNTs and ZnO nanowires [24,32]. Other production techniques include filtered cathodic vacuum arc (FCVA) to deposit ZnO particles on aligned MWCNTs in order to obtain a super-hydrophobic surface [33].

It is important to emphasized that all the researchers have focused just on pure carbon nanotubes (MWCNTs or SWCNTs), and it is likely that other nanotubes exhibiting different properties may offer better chemical reactivity that enhances the interaction between the ZnO and nanotubes. Here we propose the use of N-doped carbon nanotubes (CN_x-MWNT) and functionalized nanotubes with oxygen groups (CO_x-MWNT) as a substrate to attach efficiently ZnO particles.

2.2 Zinc oxide cluster deposition on carbon nanotubes; Experimental section

2.2.1 Reagents

The ferrocene ($FeCp_2$) and $Zn(acac)_2$ used in the experiments were from Aldrich®, benzylamine (99%), N,N-dimethylformamide (99%) and thiophene (99%) were from Sigma-Aldrich®, ethanol and toluene were reactive grade from CTR scientific®. All the chemicals were used as a received.

2.2.2 Carbon nanotube synthesis

The nanotubes were synthesized by a chemical vapor deposition (CVD) technique using two tubular furnaces. The experimental setup is illustrated in Figure 2.3. The two furnaces were kept at the same temperature. When the nebulizer containing the solution of ferrocene, and benzylamine was turned on, it forms a mist that is carried by the argon flow into a quartz tube used as a substrate. After the reaction time was completed, the nebulizer was turned off and the system was maintained at 825℃ for 10 additional minutes. Subsequently, the system was cooled down to room temperature with an argon flow of 0.5 l/min. In particular, the nitrogen-doped carbon nanotubes (CN_x-MWNTs) were prepared using a solution of ferrocene (2.5 wt%) and benzylamine pyrolyzed at 825℃ during 30 minutes under an argon atmosphere (Ar flow = 2.5 l/min). The nanotubes with oxygen groups (CO_x-MWNTs) were produced using a solution of ferrocene (2.5 wt%), ethanol (1 wt%) and toluene under the same conditions. The nanotube material was recovered by scraping it from the quartz tube. The two types of nanotubes were used without further treatment or chemical modification.

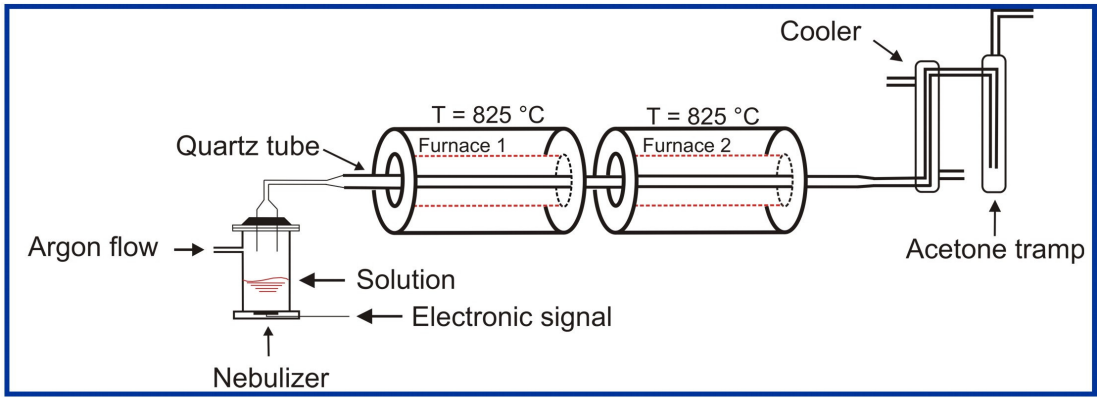

Figure 2-3.- Experimental setup for the CVD synthesis of MWCNTs. When the temperature is reached (825℃), the nebulizer is turned on for 30 minutes, an argon flow carries the solution into the furnaces, and the carbon nanotubes grown on the quartz tube and they are subsequently recovered by scrapping.

2.2.3 Zinc oxide deposition process

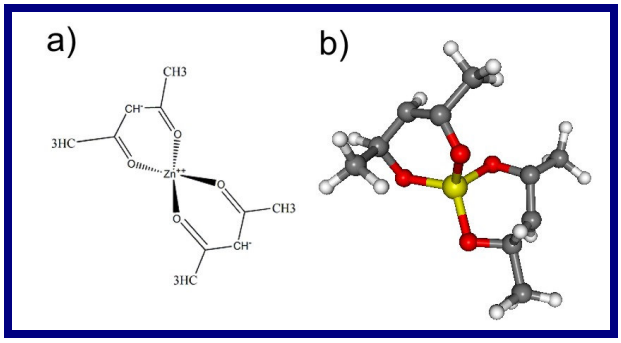

Figure 2-4.- Molecular structure of zinc acetylacetonate. (**a**) Molecular representation of Zinc acetylacetonate, $Zn(acac)_2$. (**b**) A 3D view of $Zn(acac)_2$.

We chose the zinc acetylacetonate molecule, $Zn(acac)_2$ as a source of Zn, for its low decomposition temperature, easy use, nontoxicity, wide availability and wide solubility in various solvents. $Zn(acac)_2$ has been used in the synthesis of ZnO nanowires, nanotubes[12] rods and particles[34]. This molecule is usually hydrated, it contains a resonant bond between zinc and oxygen atoms, and it is a white crystalline powder with a melting point of ~135℃.

Anchoring method

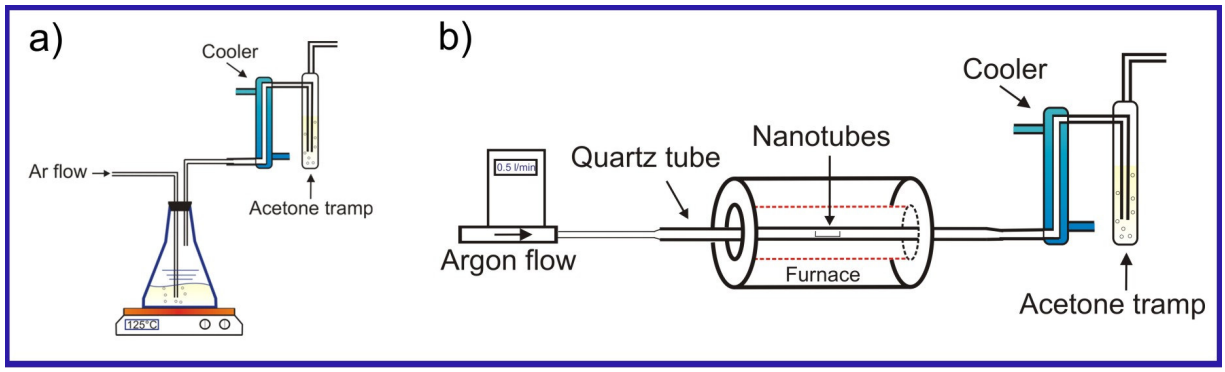

Figure 2-5.- Experimental setup for ZnO deposition. (**a**) The nanotube suspension is placed in a flask at 125℃ under magnetic stirring; an argon flow is maintained during the entire coating process. (**b**) Thermal treatment of the ZnO/CNTs composite is carried out at 400℃ under an argon atmosphere. The composite is placed in the middle zone of the furnace; the temperature is maintained for 15 minutes.

The general procedure consisted of adding 5 mg of nanotubes to a solution containing 10 ml N,N-dimethylformamide (DMF), Zinc acetylcetonate, ($Zn(acac)_2$) and Thiophene (from a molar ratio of thiophene:Zn 0:1 to 80:1) in a flask, the molar ratio of carbon (from the MWCNTs) and Zinc was kept at 10. Subsequently, the suspension was dispersed ultrasonically for 30 minutes. The flask was kept under an argon atmosphere (Ar flow of 0.3 l/min) and then it was placed in a glycerin bath in order to increase the temperature up to 125℃; the temperature was maintained for 40 minutes or until the solution was totally evaporated, see Figure 2.5-(**a**). Once the MWCNTs/ZnO composite is obtained a residual material was also observed, the final step consisted of a thermal treatment at 400 ℃ under an argon atmosphere (Ar flow = 0.5 l/min); the composite was placed in an alumina boat in the middle zone of the furnace, and the temperature was maintained for 15 minutes. Subsequently, the system was cooled down to room temperature; the experimental setup is illustrated in Figure 2.5-(**b**).

2.3 Results and discussions

2.3.1 Characterization of nitrogen-doped (CN_x-MWNTs) and functionalized carbon nanotubes (CO_x-MWNTs)

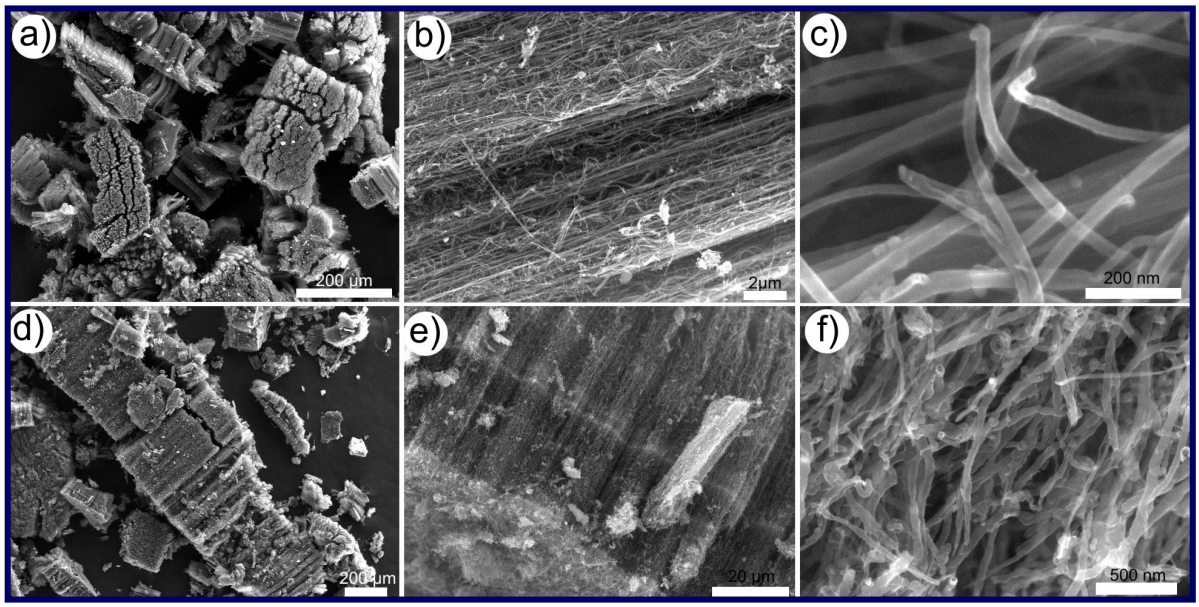

Figure 2-6.- SEM images of carbon nanotubes. (**a**)-(**c**) SEM micrographs of CN_x-MWNTs; (**d**)-(**f**) show CO_x-MWNTs at different magnifications. The CO_x-MWNTs exhibit larger diameters and lengths when compared the CN_x-MWNTs.

The samples were characterized by scanning electron microscopy, (SEM FEI XL30 SFEG at 15 kV), X-ray diffraction powder patterns were obtained using XRD D8 Advance–Bruker Axs, with Cu K_α radiation (λ = 1.54060 Å) operated at 35 kV and 25 mA, thermo gravimetric analysis was carried out using a Thermo Haake, Cahn VersaTherm HS with a heating ramp of 10°C/min to 800°C using air as atmosphere. The SEM images of the CN_x-MWNT are shown in Figure 2.6-(**a-c**) and the CO_x-MWNT are presented in Figure 2.6-(**d-f**). The two types of MWCNTs are different in length, diameter and composition, see Table 2.1.

Typically when the nanotubes are synthesized under the same conditions, CN_x-MWNTs are shorter and exhibit lower amount of iron. In this case both CN_x-MWNTs and CO_x-MWNTs have similar average diameter.

Table 2-1.- Carbon nanotubes characteristics.

	CN_x-MWNTs (N-doped)	CO_x-MWNTs (ethanol/toluene produced)
Lenght	81 ± 24.5 μm	451 ± 74 μm
Diameter	30 ± 9.2 nm	33 ± 14.6 nm
Aspect ratio	2 700	13 666
At% C	96.5	97.33
At% N	1.90	0
At% O	1.29	1.74
At% Fe	0.31	0.93

However, the CO_x-MWNTs present higher standard deviation in both diameter and length. The length of the CO_x-MWNTs is five times larger than the CN_x-MWNTs.

The MWCNTs X-ray diffraction patterns are shown in Figure 2.7-(**a**), the peaks of iron carbide are more intense in the CO_x-MWNTs sample due to its higher content. CO_x-MWNTs differ from the pure carbon multiwalled nanotubes (MWCNTs) due to the introduction of carbonyl, hydroxyl and other oxygen functional groups during the synthesis. Due the presence of these defects, CO_x-MWNTs exhibit higher chemical reactivity than MWCNTs, but less than the CN_x-MWNTs.

These results can be seen in Figure 2.7-(**b**) in the thermo-gravimetric analysis plots (TGA). CN_x-MWNTs exhibit higher reactivity showing a peak in the derivate at 418℃, while the CO_x-MWNTs show the peak at 471℃, MWCNTs would show the peak at ~480℃. Thus meaning that the CO_x-MWNTs are less reactive than the CN_x-MWNTs. These results are very interest because they demonstrate the different interaction capability of the nanotubes.

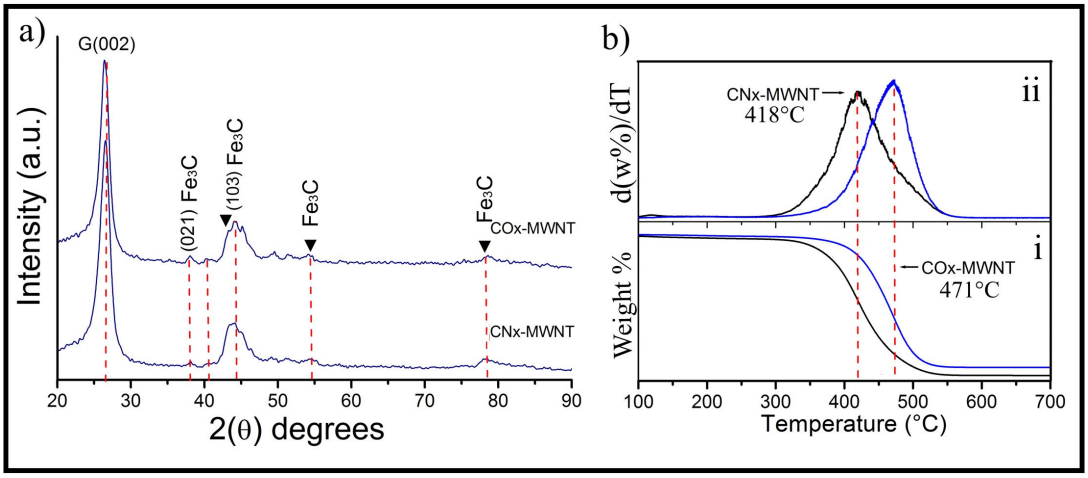

Figure 2-7.- X-ray powder diffraction pattern and TGA plot. (**a**) X-ray diffraction pattern of CO_x-MWNTs and CN_x-MWNTs, the G(002) reflection corresponds to graphite, the others come from Fe_3C. (**b**) TGA analysis of both N-doped and functionalized multiwalled nanotubes, (**i**) the weight loss vs. temperature, (**ii**) the first derivative of the weight loss.

2.3.2 Nitrogen-doped carbon nanotubes/zinc oxide composites (CN_x-MWNTs/ZnO)

The effect of thermal treatment on the particle size of ZnO clusters

This MWCNTs coating process is able to produce the MWCNTs/ZnO composite before the thermal treatment, but residual material covering the nanotubes and the nanoparticles are also present (see Figure 2.8). For this reason we decide to perform a thermal treatment in order to remove residual material, so the first analysis was carried out by varying the temperature of calcinations in order to determine the behavior of the particle size with respect to temperature. Figure 2.9-(**a**) shows the X-ray powder

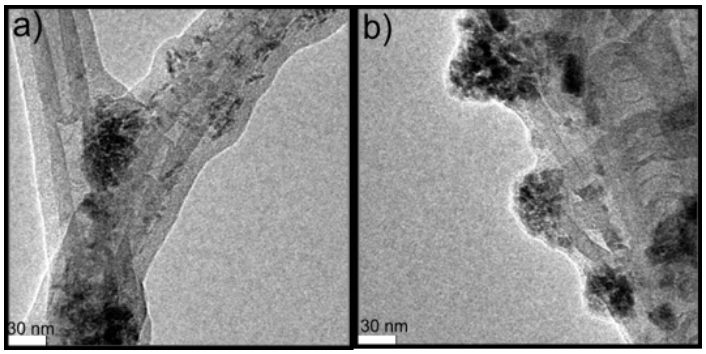

Figure 2-8.- TEM images of CN_x-MWNTs/ZnO before the thermal treatment.

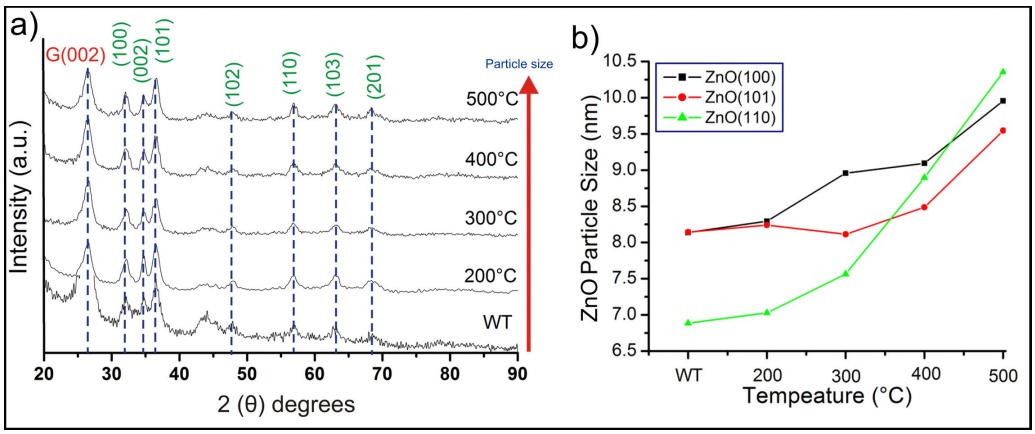

Figure 2-9.- X-ray powder diffraction pattern and particle size of CN_x-MWNTs/ZnO composite: (**a**) X-ray diffraction pattern of CN_x-MWNTs/ZnO composite heated at different temperatures (thiophene:zinc ratio 0:1); (**b**) The ZnO particle size obtained from the X-ray analysis using the Scherrer equation in three different crystalline planes.

diffraction pattern of the CN_x-MWNTs/ZnO composite obtained at different calcinations temperatures, all these experiments were completed without the addition of thiophene (thiophene:zinc ratio 0:1). The particle size was obtained from three different crystalline planes using the X-ray diffraction data and the Scherrer equation, in this case we used the (100), (101) and (110) ZnO planes. These results are presented in Figure 2.9-(**b**). All planes exhibit similar behavior, indicating an increase of approximately 2 nm in size when the samples are heated to 500℃, the minimal recorded average value was around 7.5 nm.

After this analysis, we chose 400℃ as the optimal temperature, in order to assure the complete decomposition of the residual material and avoid problems with the particle size; the effect of thiophene on the particle size is described below.

The effect of thiophene concentration on the particle size of ZnO clusters

During the experiments different concentrations of thiophene were added in order to evaluate its effect on the particle size and the load of the CNTs. We changed thiophene concentration from a molar ratio of thiophene:Zinc (thi:Zn) of 0:1 to 80:1, the particle size is determined by using SEM images and X-ray powder diffraction patterns, these results are illustrated in Figure 2.10.

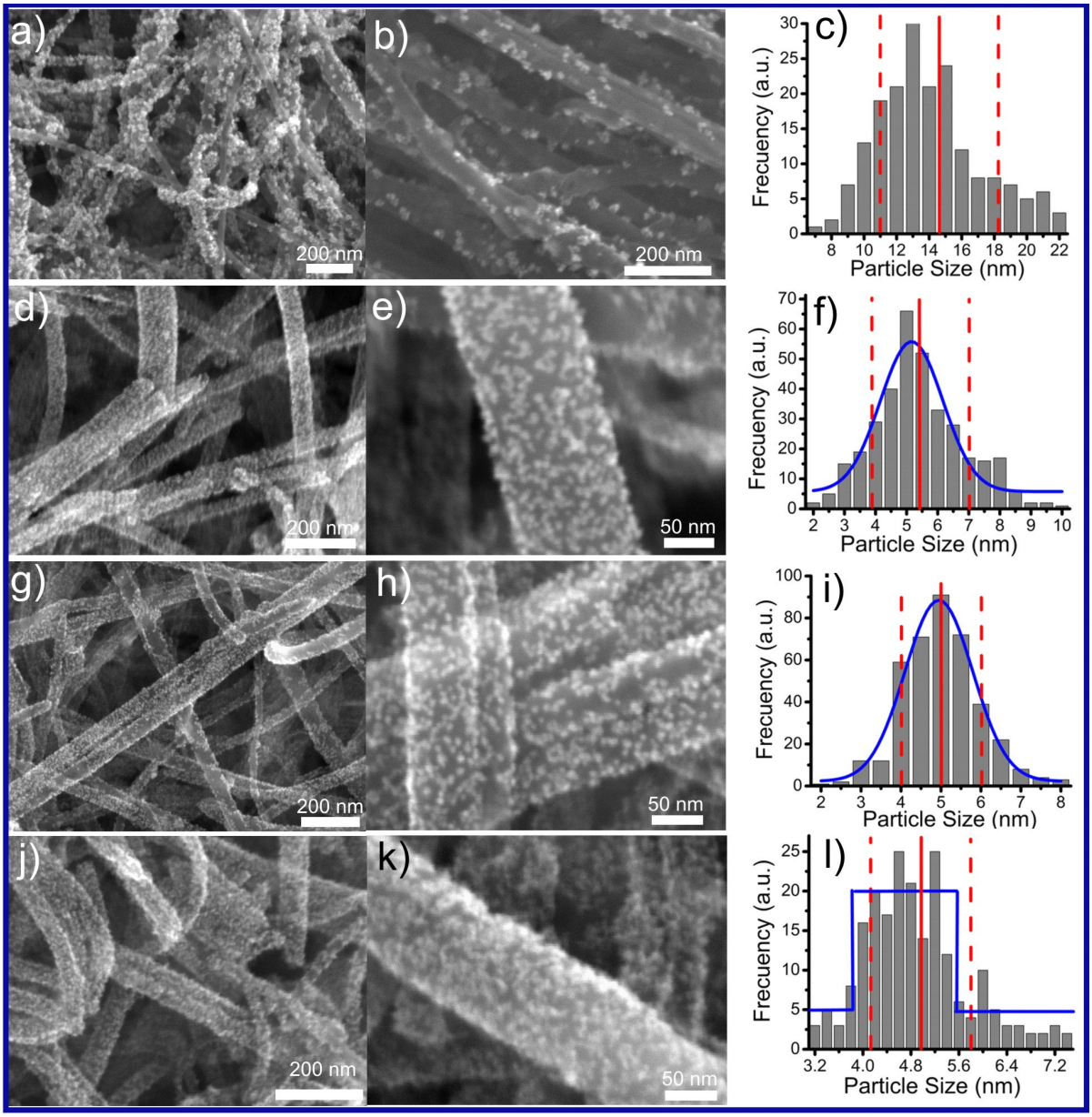

Figure 2-10.- CN_x-MWNTs/ZnO composites and their ZnO particle size distribution. (**a-c**) SEM images and the size distribution histogram of the composite with a molar ratio of thiophene:zinc (thi:Zn) 20:1; (**d-f**) SEM images of the composite obtained with a molar ratio of 40:1; (**g-i**) 60:1 and (**j-l**) 80:1. The average value is shown as a solid line (red), the dashed lines are the standard deviation and the curve line (blue) is a Gaussian fit, except in (**l**) that shows a representation of a pulse function; (**j**) A SEM image of CN_x-MWNTs/ZnO composite with a molar ratio of 80:1 (thi:Zn), and (**k**) The high spatial density of particles observed on the nanotube's wall, with an average diameter of 4.90 nm and the smallest standard deviation of ± 0.85 nm.

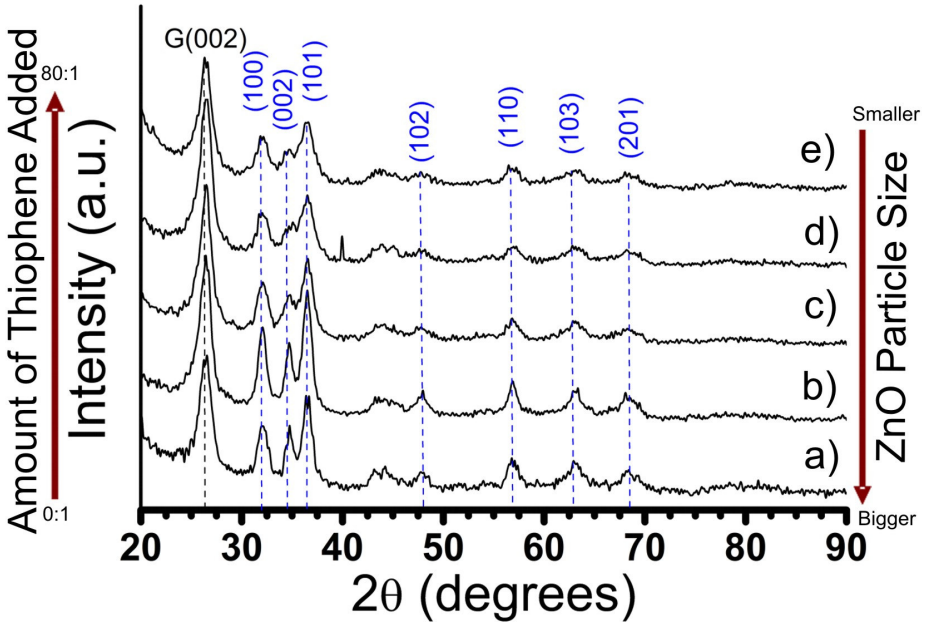

Figure 2-11.- X-ray powder diffraction pattern of ZnO/CN_x-MWNT composite. The particle size of ZnO is decreasing from (**a**) to (**e**) due to the addition of thiophene, the smallest particles are obtained with larger quantities of thiophene. The G(002) reflection corresponds to graphite (nanotubes) the other peaks to ZnO nanoparticles.

We can observe that standard deviation (SD) of the particle size decrease with high thi:Zn ratios and the particle size is centered at 5 nm. Figure 2.10-(**a-c**) shows SEM images of the composite with thi:Zn ratio equal to 20:1 and its corresponding particle size histogram; it has larger particle size distribution with a SD of ± 3.63 nm. When we increased the thiophene concentration to 13.2µl/ml (equivalent to molar ratio thi:Zn 40:1), the particle size reduced to 5.65 nm and the SD to ± 1.45 nm. This composite is depicted in Figure 2.10-(**d-f**), where the SEM images show the high load of nanoparticles and their size distribution.

If we continue adding thiophene into the systems to 26.4µl/ml (thi:Zn ratio 80:1), the particle size change slightly, but the SD displayed a continuous decrease to ± 0.85 nm with an average size ZnO particle of 4.90 nm. This SD could be the smallest standard deviation achieved with ZnO particles anchored on a carbon nanotube. The composite is shown in Figure 2.10-(**j-l**).

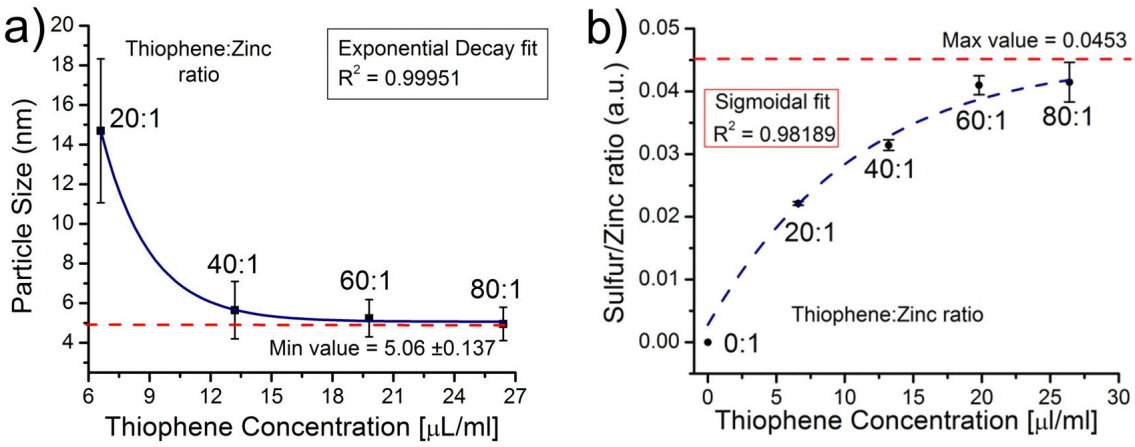

Figure 2-12.- ZnO particle size, sulfur/zinc ratio vs. thiophene concentration. In (**a**) the graph shows the correlation between the ZnO particle size and the amount of thiophene added into the system, it has a typical exponential decay behavior; it presents a minimal value (red line, dashed line) of the particle size given by the exponential fit as 5.06 nm; that corresponds to the experimental value of 4.90 nm; In (**b**) the chart shows the correlation between sulfur:zinc ratio (determined by EDX after calcinations) and the initial thiophene concentration, it presents a sigmoidal behavior giving a maximum value of 0.045 (red line).

The composite with thi:Zn ratio 80:1 exhibit the smallest ZnO particle size and standard deviation. More interestingly, it shows the highest number of ZnO nanoparticles on their surfaces.

The X-ray powder diffraction pattern of ZnO/CN_x-MWNTs composites are shown in Figure 2.11, it can be observed how the diffraction peaks of ZnO become wider with the addition of thiophene, it means the particle size is decreasing. Figure 2.11 form (**a**) to (**e**) corresponds to thi:Zn relation 0:1, 20:1, 40:1, 60:1 and 80:1 respectively, here we can notice that the intensity of the graphitic peak G(002) of the diffraction patterns change very little with the addition of thiophene, this provides indirect evidence that the anchoring process does not alter considerably the crystallinity of carbon nanotubes, thus avoiding considerably change on their mechanical properties. With the aid of Scherrer equation we determined the crystal size.

The particle size of ZnO decreases with the addition of thiophene, but the particle size does not decrease in a linear manner with the thiophene ratio; it follows a typical exponential decay behavior, illustrated in Figure 2.12-(**a**).

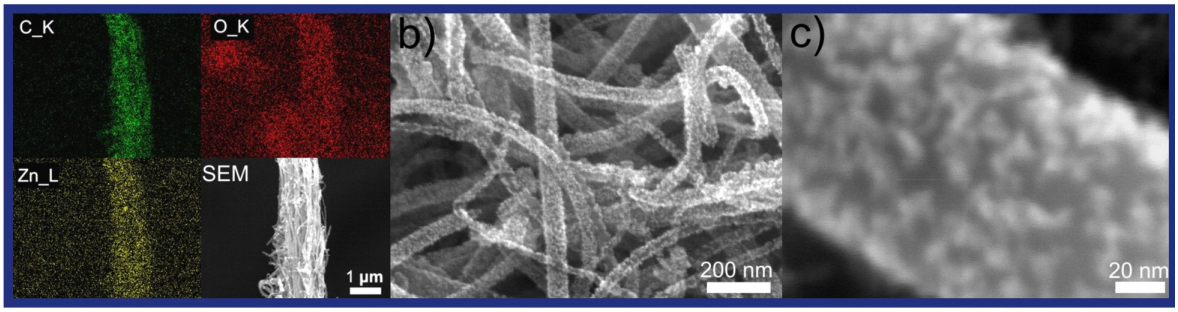

Figure 2-13.- ZnO/CN_x-MWNT composite with a thiophene:Zinc ratio of 80:1. (**a**) An EDX map showing the signals of carbon, zinc and oxygen (green, yellow and red respectively), the fourth images is a SEM micrograph. (**b**) SEM image, all the nanotubes are completely coated by ZnO nanoparticles. (**c**) A magnification of (**b**) showing the high density of nanoparticles anchored to the nanotube's wall.

The bars correspond to the standard deviation (it can see how the SD is decreasing), with data from SEM images. This particular behavior has an enormous consequence; it shows that the *particle size will not decrease* more even if we increase the thiophene concentration in the sample, only the SD will becomes smaller, and this means all the particles will exhibit very similar sizes. For this reason, we will able to achieve a minimal value on the particle size of 5.06 nm (given by the exponential fit) with the smaller standard deviation.

Due to the introduction of thiophene into the systems, we performed EDX analysis in order to evaluate the amount of sulfur contained in the samples after calcinations. However, we preferred to use the sulfur:zinc ratio (S:Zn) to determine the behavior of the sulfur in the samples. This relationship gives us information about how many sulfur atoms are presents with respect to the zinc ones. The S:Zn ratio was evaluated and correlated with the initial thiophene concentration, this information is presented in Figure 2.12-(**b**). The S:Zn ratio exhibits a sigmoidal behavior, giving a maximum value of 0.045 (determined by the sigmoidal fit), this behavior is in agreement with the behavior presented in Figure 2.12-(**a**), the addition of thiophene will not decrease the particle size further, so the amount of sulfur into the systems will not increase either. All these results suggest that the sulfur could be fixed on the surface of the nanoparticles, because the surfaces area within the cluster will not change if we add more thiophene, so the amount of sulfur fixed on the nanoparticles surface remains constant.

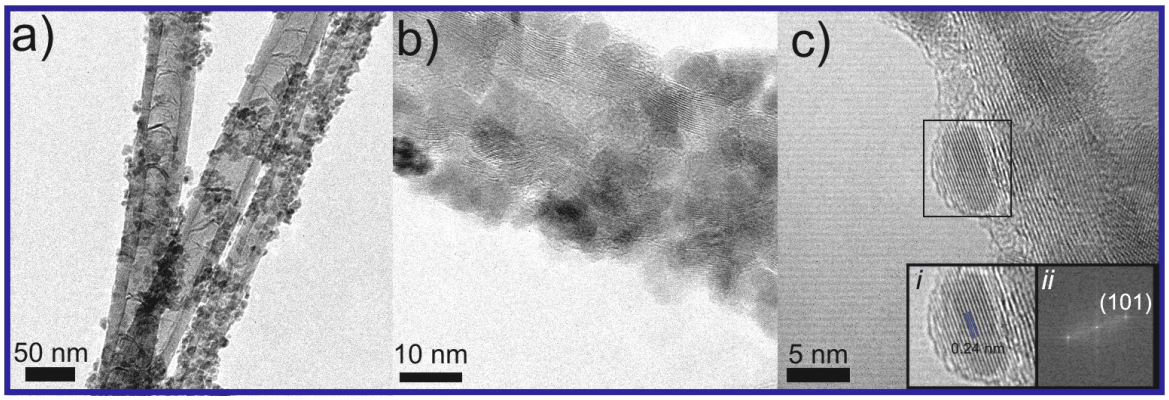

Figure 2-14.- TEM images of CN_x-MWNTs/ZnO composites. (**a**) Image shows how the ZnO nanoparticles are distributed along the nanotube; (**b**) It can be seen the high load of ZnO nanoparticles is deposited, and (**c**) HRTEM micrograph showing a typical ZnO nanoparticle and their crystalline planes with an average distance of 0.24 nm (see inset *i*), the inset (*ii*) shows the FFT (fast Fourier transformation) of inset (*i*) showing the ZnO(101) planes.

An EDX map of the CN_x-MWNT/ZnO composite with a molar ratio of 80:1 (thi:Zn) is presented in the Figure 2.13-(**a**). It shows the signals carbon, zinc and oxygen (green, yellow and red respectively), the map was taken on an alumina substrate, for this reason the oxygen signal is presented over the entire surface. These results demonstrate the presence of ZnO over the nanotubes. In Figure 2.13-(**b**) we can see the carbon nanotubes entirely coated with ZnO nanoparticles with the highest load of particles being deposited (Figure 2.13-(**c**)).

The CN_x-MWNTs/ZnO composite with a thi:Zn ratio 80:1 was analyzed with a TEM. These results are presented in Figure 2.14, low magnifications in Figure 2.14-(**a-b**) shows a CN_x-MWNT completely covered by ZnO clusters and it confirms the high number of nanoparticles anchored on the nanotube wall. Figure 2.14-(**c**) shows a high resolution TEM image of CN_x-MWNT/ZnO composite, we can see a typical ZnO nanoparticle, and the shape of the nanoparticles (low contact angle) suggests a high interaction between the CN_x-MWNTs and the ZnO clusters.

2.3.3 Functionalized-multiwalled carbon nanotubes/zinc oxide composites (CO_x-MWNTs/ZnO)

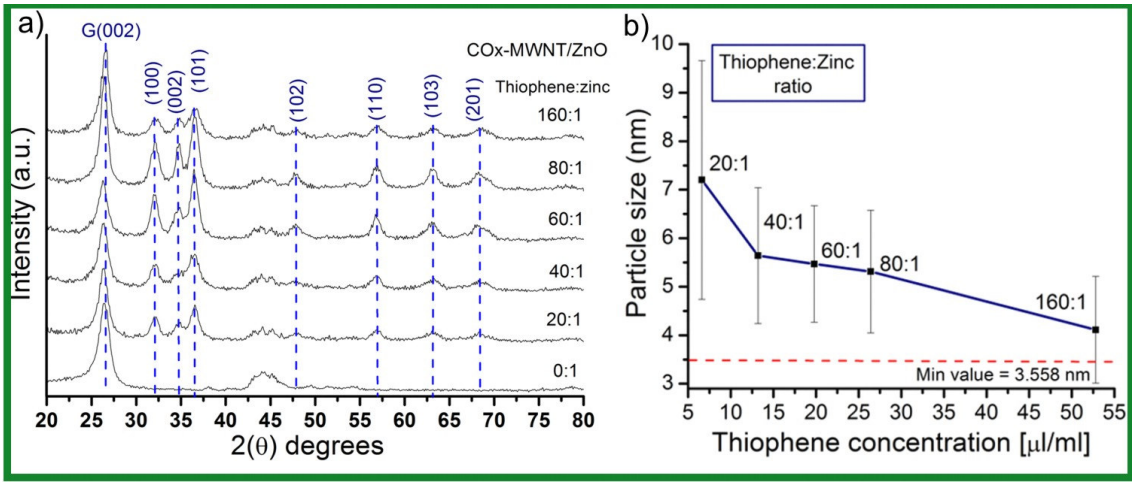

Figure 2-15.- X-ray powder diffraction data and ZnO particle size on CO_x-MWNTs/ZnO composite. (**a**) X-ray diffraction data at different thiophene:zinc molar ratios; and (**b**) Behavior of the particle size with respect to the thiophene concentration in the suspension.

We carried out the same experimental procedure to obtain CO_x-MWNTs/ZnO composites. Different concentrations of thiophene were used in order to promote the attachment of nanoparticles on the CO_x-MWNTs, we changed the thiophene concentration from a molar ratio thiophene:Zinc (thi:Zn) 0:1 to 160:1. Due to the different chemical behavior of the CO_x-MWNTs, the results differ from the CN_x-MWNTs.

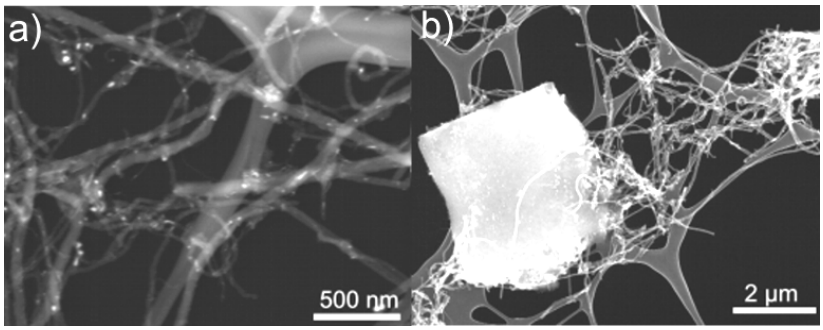

Figure 2-16.- STEM images of CO_x-MWNTs/ZnO composite without any amount of thiophene. This composite exhibit some ZnO agglomerations.

Table 2-2.- ZnO particle size determined by XRD and SEM

Thiophene:Zinc ratio	XRD-P(100)[a] (nm)	XRD-P(110)[a] (nm)	SEM[b] (nm)
0:1	-	-	-
20:1	8.28	8.59	7.20 ± 2.46
40:1	8.57	9.23	5.64 ± 1.37
60:1	9.22	9.12	5.47 ± 1.20
80:1	8.03	7.49	5.31 ± 1.26
160:1	7.05	6.51	4.11 ± 1.09[c]

(a) Obtained from X-ray diffraction data, the numbers are the Miller index from each ZnO crystalline plane.
(b) Data obtained form SEM images.
(c) Data obtained from SEM and TEM images.

The composite produced with a molar ratio of thi:Zn 0:1, it did not show *any particle* anchored on the surfaces of the nanotubes, these results are shown in Figure 2.16).

However, if we added a small amount of thiophene (such as 6.6 µl/ml) to the nanotube's suspension, we were able to promote the anchorage of ZnO clusters. The ZnO cluster size was determined by SEM images and X-ray powder diffraction data, these results are presented in Figure 2.15-(**b**). We noticed that the cluster size is decreasing with the addition of thiophene, however, the standard deviation almost keep constant; the smallest particle size was found in the composite with thi:Zn ratio equal to 160:1.

The different chemical behavior of CO_x-MWNTs has a big consequence over the anchorage of nanoparticles. Without the addition of thiophene, the nanotubes do not show any particle on their surfaces, but with thiophene we noticed many particles anchored on the nanotubes wall. When increasing the thiophene concentration, we were able to note a poor increment in the load of ZnO nanoparticles. Thus behavior differs from that observed with CN_x-MWNTs, in which these tubes increased their covered surface with high thiophene:zinc ratios. The CO_x-MWNTs do not show their surfaces totally covered, meaning that the number

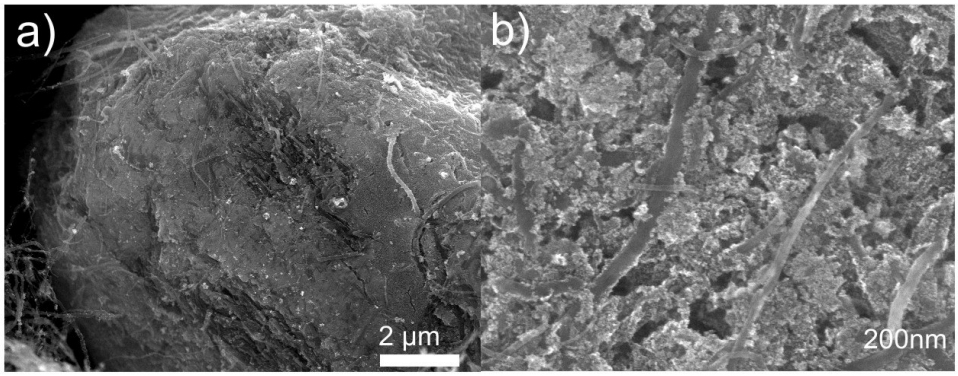

Figure 2-17.- SEM images of CO_x-MWNTs/ZnO agglomerates with a molar ratio of thi:Zn (160:1). (**a**) A large agglomerate containing carbon nanotubes and ZnO, an EDX analysis is shown in Table 2.3; these agglomerates exhibit higher quantities of zinc, oxygen and sulfur than the "normal" composite, even in the same experiment, (**b**) A higher magnification of the agglomerate, showing the nanotubes and ZnO nanoparticles.

of ZnO nanoparticles remains similar and just decreased slightly their size and standard deviation. Table 2.2 illustrates the ZnO particle size obtained from the X-ray diffraction patterns using different crystalline planes and SEM images.The XRD data corresponds to an average size of all ZnO particles produced, and the SEM images just correspond to the anchored ZnO clusters.

Another interesting observation occurred with SEM images and the XRD data, the composites produced with high thi:Zn ratio (such as 60:1-160:1) shows the formation of some agglomerations composed of nanotubes and ZnO particles. These results are shown in Figure 2.17. An EDX analysis of the agglomerate material was performed and the results are shown in Table 2.3.

Table 2-3.- EDX analysis of the agglomerates and the CO_x-MWNTs/ZnO composite with a molar ratio of thi:Zn (160:1) presented in the same sample

Element	Agglomerates (At%)	CO_x-MWNTs/ZnO (At%)
C	69.96	92.86
O	12.91	2.87
Zn	15.76	3.46
S	0.83	0.12
Fe	0.55	0.57

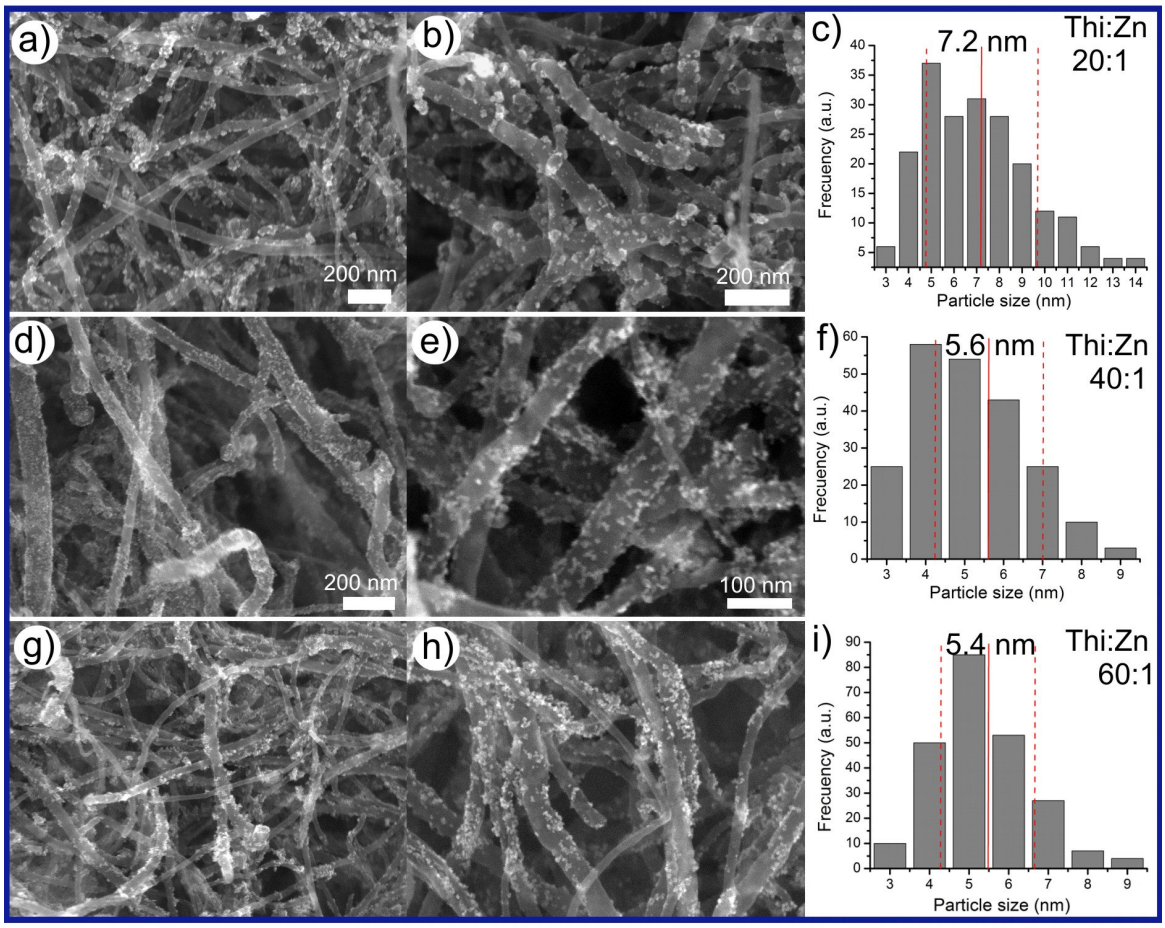

Figure 2-18.- CO_x-MWNTs/ZnO composites, SEM images and ZnO particle size distribution. (**a-c**) Composites with a thi:Zn molar ratio of 20:1. (**d-f**) 40:1, and (**g-i**) 60:1.

The agglomerations, the EDX analysis, and the X-ray diffraction pattern that exhibit wide peaks characteristic of small size ZnO crystals (crystal size ranging from 9 to 6 nm, see Table 2.2), suggest that the coating process is able to produce ZnO nanoparticles that are not fixed on the nanotube's surfaces.This material exhibit higher quantity of zinc, oxygen and sulfur when is compared with CO_x-MWNTs/ZnO composite, produced in the same experiments.

Due to the very low chemical reactivity of COx-MWNTs, during the coating process some nanoparticles appear anchored on their surfaces due to the presence of defects and functional groups. However, the lack of reactivity of the nanotubes allows the formation of other ZnO crystals in solution.

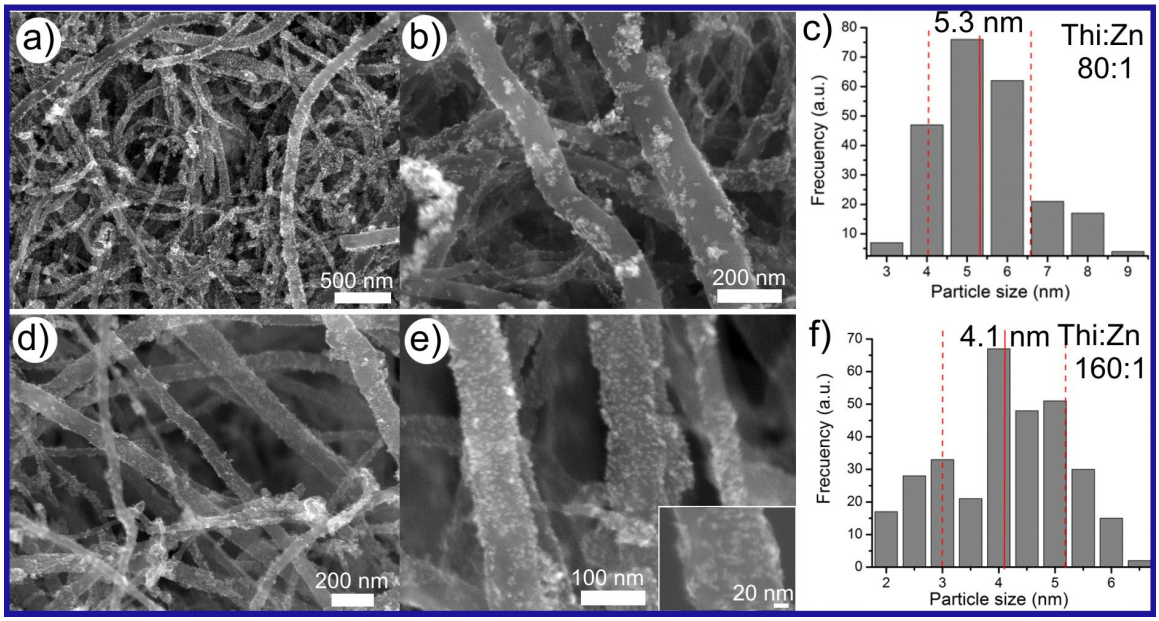

Figure 2-19.- CO_x-MWNTs/ZnO composites, SEM images and ZnO particle size distribution. (**a-c**) Composites with a thi:Zn molar ratio of 80:1, and (**d-f**) 160:1.

These ZnO crystals are passivated with sulfur atoms, and when the solvent is evaporated during the coating process the nanoparticles tend to form agglomerates. Basically, in these composites two types of nanoparticles appear, anchored and isolated. The size of the clusters attached on the nanotubes is presented in Figure 2.15-(**b**), where it can be seen how the size decreases slightly with the addition of thiophene.

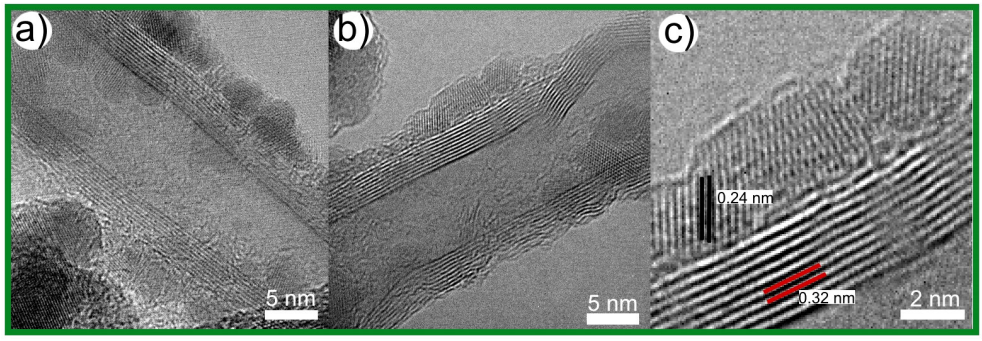

Figure 2-20.- TEM micrographs of CO_x-MWNTs/ZnO composite with a thi:Zn molar ratio equal to 160:1 (**a-b**) TEM images showing some typical nanoparticles of ZnO anchored on the nanotubes; (**c**) High magnification of (**b**) showing the plane distance of ZnO nanoparticles (marked in black, that correspond with the (101) plane), and the nanotube interlayer spacing (marked in red).

In Figure 2.18 and 2.19 SEM images and the particle size histogram of the CO_x-MWNT/ZnO composites are presented at different thi:Zn ratios.

This behavior can be related to the nanotube synthesis process, due the temperature gradient presented in the furnaces, the nanotubes exhibit a slightly change in their chemical properties. TEM analysis of the CO_x-MWNT/ZnO with highest thi:Zn molar ratio is depicted in Figure 2.20. The achieved particle size was 4.1 nm, despite of the high quantities of thiophene, we were not able to get a totally coverage of the surfaces. In Figure 2.20, we observe that the shape of some nanoparticles is spherical, suggesting less interaction between the surface and the cluster, this structure differ from the CN_x-MWNT/ZnO results, in which the nanoparticles exhibited lower contact angles. This means better interaction between both systems.

All these results demonstrate the different chemical behavior that the nanotubes can exhibit, just by changing their surfaces with different functional groups.

2.4 Conclusions

We have analyzed two systems, CN_x-MWNTs and CO_x-MWNTs, using the same coating process. We demonstrated that these systems exhibit different chemical reactivity and behavior.

We achieved high nanoparticles load on CN_x-MWNTs and a complete coverage of the surfaces without any chemical pre-treatment of the MWCNTs that could damage their mechanical properties or increase the cost in the process.

The CN_x-MWNTs due to their high reactivity constituted the material that displayed the best surface coverage, but not the smallest particles. The reactivity of the surfaces is an important factor to control the nucleation of the nanoparticles. The results suggest that the sulfur atoms could be fixed on the surfaces of the nanoparticles, these atoms could passivate the ZnO cluster, thus facilitating to decrease their size.

We were able to attach ZnO particles on the CO_x-MWNTs without any chemical pre-treatment, due to their low reactivity; only some nanoparticles were anchored, and others were created in solutions and passivated with the same mechanism that the fixed ones. Typically we can expect the systems (under the same conditions) with the smallest particles will be the CO_x-MWNTs but the systems with higher covering will be CN_x-MWNTs.

2.5 References

[1] Y. Chen, D. M. Bagnall, H. Koh, K. Park, K. Hiraga, Z. Zhu, T. Yao, "Plasma assisted molecular beam epitaxy of ZnO on c -plane sapphire: Growth and characterization", *J. Appl. Phys*. Vol. 84, 3912 (1998)

[2] L. Vayssieres, K. Keis, A. Hagfeldt, S.-E. Lindquist, "Three-Dimensional Array of Highly Oriented Crystalline ZnO Microtubes", *Chem. Mater.* Vol. 13, 4395-4398 (2001)

[3] H. Rensmo, K. Keis, H. Lindström, S. Södergren, A. Solbrand, A. Hagfeldt, S-E. Lindquist, L. Wang, M. Muhammed, "High Light-to-Energy Conversion Efficiencies for Solar Cells Based on Nanostructured ZnO Electrodes", *J. Phys. Chem. B,* Vol. 101, 2598-2601 (1997)

[4] C. J. Lee, T. J. Lee, S. C. Lyu, Y. Zhang, H. Ruh, H. J. Lee, "Field emission from well-aligned zinc oxide nanowires grown at low temperature", *Appl. Phys. Lett*., Vol. 81, 3648-3650 (2002)

[5] X. D. Bai, P. X. Gao, Z. L. Wang, E. G. Wang, "Dual-mode mechanical resonance of individual ZnO nanobelts", *Appl. Phys. Lett.,* Vol. 82, 4806-4808 (2003)

[6] Hughes, W. L., Wang, Z. L., "Nanobelts as nanocantilevers", *Appl. Phys. Lett.* Vol. 82 , 2886-2888 (2003)

[7] L. Wang, M. Muhammed, "Synthesis of zinc oxide nanoparticles with controlled morphology", *J. Mater. Chem*., Vol. 9, 2871-2878 (1999)

[8] Y. Zhang, N. Wang, S. Gao, R. He, S. Miao, J. Liu, J. Zhu, X. Zhang, "A Simple Method To Synthesize Nanowires", *Chem. Mater*. Vol. 14, 3564-3568 (2002)

[9] M. H. Huang, Y. Wu, H. Feick, N. Tran, E. Weber, P. Yang, "Catalytic Growth of Zinc Oxide Nanowires by Vapor Transport ", *Adv. Mater.* Vol. 13, 113-116 (2001)

[10] Y. B. Li, Y. Bando, T. Sato, K. Kurashima, "ZnO nanobelts grown on Si substrate", *Appl. Phys. Lett*. Vol. 81, 144(2002)

[11] Y. J. Xing, Z.H. Xi, Z.Q. Xue, X.D. Zhang, J.H. Song. "Optical properties of the ZnO nanotubes synthesized via vapor phase growth", *Appl. Phys. Lett.* Vol. 83, 1689 (2003)

[12] J. J. Wu, S. C. Liu, “Low-Temperature Growth of Well-Aligned ZnO Nanorods by Chemical Vapor Deposition”, *Adv. Mater.* Vol. 14, 215-218 (2002)

[13] S. C. Liu, J. J. Wu, “Low-temperature and catalyst-free synthesis of well-aligned ZnO nanorods on Si (100)”, *J. Mater. Chem.,* Vol. 12, 3125–3129 (2002)

[14] W. Yu, X. Li, X. Gao, “Catalytic Synthesis and Structural Characteristics of High-Quality Tetrapod-Like ZnO Nanocrystals by a Modified Vapor Transport Process”, *Crystal Growth & Design*, Vol. 5,151-155 (2005)

[15] H-W Suh, G-Y. Kim, Y-S. Jung, W-K. Choi, D. Byun, “Growth and properties of ZnO nanoblade and nanoflower prepared by ultrasonic pyrolysis”, *J. Appl. Phys.* Vol. 97 044305 (2005)

[16] J. Y. Lao, J. Y. Huang, D. Z. Wang, Z. F. Ren, “ZnO Nanobridges and Nanonails”, *Nano Letters*, Vol. 3, 235 -238 (2003)

[17] X.Y. Kong, Z. L. Wang, “Spontaneous Polarization-Induced Nanohelixes, Nanosprings, and Nanorings of Piezoelectric Nanobelts”, *Nanolett*, Vol. 3, 1625-1631 (2003)

[18] J. Y. Lao, J. G. Wen, Z. F. Ren, “Hierarchical ZnO Nanostructures”, Nano Letters, Vol. 2, 1287 -1291 (2002)

[19] J. J. Wu, S. C. Liu, C. T. Wu, K. H. Chen, L. C. Chen. “Heterostructures of ZnO–Zn coaxial nanocables and ZnO nanotubes”, *Appl. Phys. Lett.* Vol. 81, 1312 (2002)

[20]J. Y. Lao, J. G. Wen, Z. F. Ren, “Hierarchical ZnO Nanostructures” , *Nano Lett.,* Vol. 2, 1287-1291 (2002)

[21] Z. L. Wang, J. Song, “Piezoelectric Nanogenerators Based on Zinc Oxide Nanowire Arrays”, *Science*, Vol. 312, 242-246 (2006)

[22] H.-W. Suh, G.-Y. Kim, Y.-S. Jung, W.-K. Choi, D. Byun, “Growth and properties of ZnO nanoblade and nanoflower prepared by ultrasonic pyrolysis”, *J. Appl. Phys*. Vol. 97, 044305 [6 pages] (2005)

[23] A. Becheri, M.Dürr, P. Lo Nostro, P. Baglioni, *J. Nanopart. Res.* Vol 10, 679-689 (2008)

[24] H. Kim, W. Sigmund, “Zinc oxide nanowires on carbon nanotubes”, *Appl. Phys. Lett.* Vol. 81, 2085-2087 (2002)

[25] J. M. Green, L. Dong, T. Gutu, J. Jiao, J. Conley, Y. Ono, "ZnO-nanoparticle-coated carbon nanotubes demonstrating enhanced electron field-emission properties" *J. Appl. Phys.* Vol. 99, 094308 [4 pages] (2006)

[26] W. B. Choi, D. S. Chung, J. H. Kang, H. Y. Kim, Y. W. Jin, I. T. Han, Y. H. Lee, J. E. Jung, N. S. Lee, G. S. Park, J. M. Kim, "Fully sealed, high-brightness carbon-nanotube field-emission display", *Appl. Phys. Lett.* Vol. 75, 3129-3131 (1999)

[27] Ke Yu, Y. S. Zhang, F. Xu, Q. Li, Z. Q. Zhu, Q. Wan, "Significant improvement of field emission by depositing zinc oxide nanostructures on screen-printed carbon nanotube films", *Appl. Phys. Lett.*, Vol 88, 153123 (2006)

[28] Y. M. Ho, J. W. Liu, J. L. Qi, W. T. Zheng, "Spectroscopic investigation on carbon nanotubes coated with ZnO nanoparticles", *J. Phys. D: Appl. Phys*. Vol. 41, 065308 [6 pages] (2008)

[29] J. Sun, L. Gao, M. Iwasa, "Noncovalent attachment of oxide nanoparticles onto carbon nanotubes using water-in-oil microemulsions", *Chem. Commun.* Vol. 7, 832-833 (2004)

[30] C.S. Chen, X.H. Chen, B. Yi, T.G. Liu, W.H. Li, L.S. Xu, Z. Yang, H. Zhang, Y.G. Wang, "Zinc oxide nanoparticle decorated multi-walled carbon nanotubes and their optical properties", *Acta Materialia*, Vol. 54, 5401-5407 (2006)

[31] G. Guo, J. Guo, D. Tao, W.C.H. Choy, L. Zhao, W. Qian, Z. Wang, "A Simple method to prepare multi-walled carbon nanotube/ZnO nanoparticle composites", *Appl. Phys. A*, Vol. 89, 525–528 (2007)

[32]Y. S. Min, E. J. Bae, J. B. Park, U. J. Kim, W. Park, J. Song, C. S. Hwang, N. Park, "ZnO nanoparticle growth on single-walled carbon nanotubes by atomic layer deposition and a consequent lifetime elongation of nanotube field emission", *Appl. Phys. Lett.* Vol. 90, 263104 (2007)

[33] L. Huang, S.P. Lau, H. Y. Yang, E.S.P. Leong, S.F. Yu, S. Prawer, "Stable Superhydrophobic Surface via Carbon Nanotubes Coated with a ZnO Thin Film", *J. Phys. Chem. B* , Vol. 109, 7746-7748 (2005)

[34] C. Fauteux, R. Longtin, J. Pegna, D. Therriault, “Fast Synthesis of ZnO Nanostructures by Laser-Induced Decomposition of Zinc Acetylacetonate”, *Inorg. Chem.*, Vol. 46, 11036-11047, (2007)

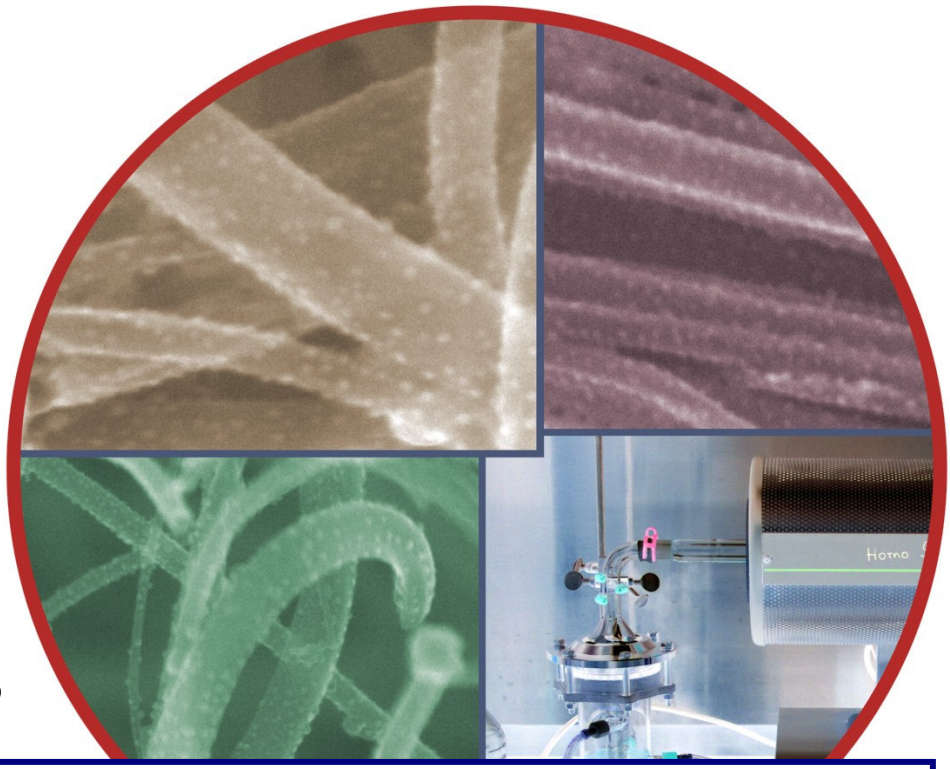

Chapter 3

Manganese Oxide (α-Mn_2O_3) Cluster Deposition on Nitrogen-Doped (CNx-MWNTs) and Functionalized (COx-MWNTs) Multiwalled Carbon Nanotubes

We have developed a novel methodology that allows us to coat efficiently carbon nanotubes with α-Mn_2O_3 nanoparticles without employing expensive chemicals, using manganese (III) acetylacetonate as a metal precursor. The results indicate that the solvent is a crucial factor for the anchorage of α-Mn_2O_3, this process is based on the adsorption properties of carbon nanotubes. We studied the effect of the solvent, the addition of sodium dodecyl sulfate (SDS) and the resting time of the solution on the quantity and size of the α-Mn_2O_3 nanoparticles.

3.1 Introduction

Manganese is a transition metal that exhibit a wide range of oxidation states (+2, +3, +4, +6 y +7), and is able to create a variety of oxide compounds. All manganese oxide materials are of considerable importance in technological applications including catalysts, electrodes, rechargeable batteries, high density magnetic data storage devices, ion-exchange materials, sensors and other electronic devices.

3.1.1 Nanostructured manganese oxide

Recently, nanocrystals have attracted great interest due to their form and size, thus determining their chemical and physical properties. It is possible that the nanostructured materials exhibit properties totally different from the bulk materials, and it has been demonstrated that MnO_2 nanoparticles could display superparamagnetic behavior, while the bulk material is antiferromagnetic [1,2]. In addition, it has been shown that Mn_3O_4 exhibit higher Curie temperature than the bulk material [3].

In recent years, the controlled synthesis of MnO_x nanomaterials has attracted considerable attention, a wide range of manganese oxide nanostructures have been produced with various morphologies, including: flowers, stars, tetrapods[4], hexapods[4], dendritic clusters[5], dumbbells[6], needles[7], etc. Some structures could exhibit negative curvature, and these types of materials could be used in various devices such as sensors, capacitors, catalysis and bio-markers.

Figure 3.1 illustrates a wide range of manganese oxides nanostructures, from simple structures such as nanorods to more complex configurations like octahedral nanostructures. All these materials display novel electrochemical and catalytic properties that could be used in a wide variety of applications.

Some manganese oxide particles have been demonstrated to be excellent materials, for the fabrication of electrochemical supercapacitors devices.

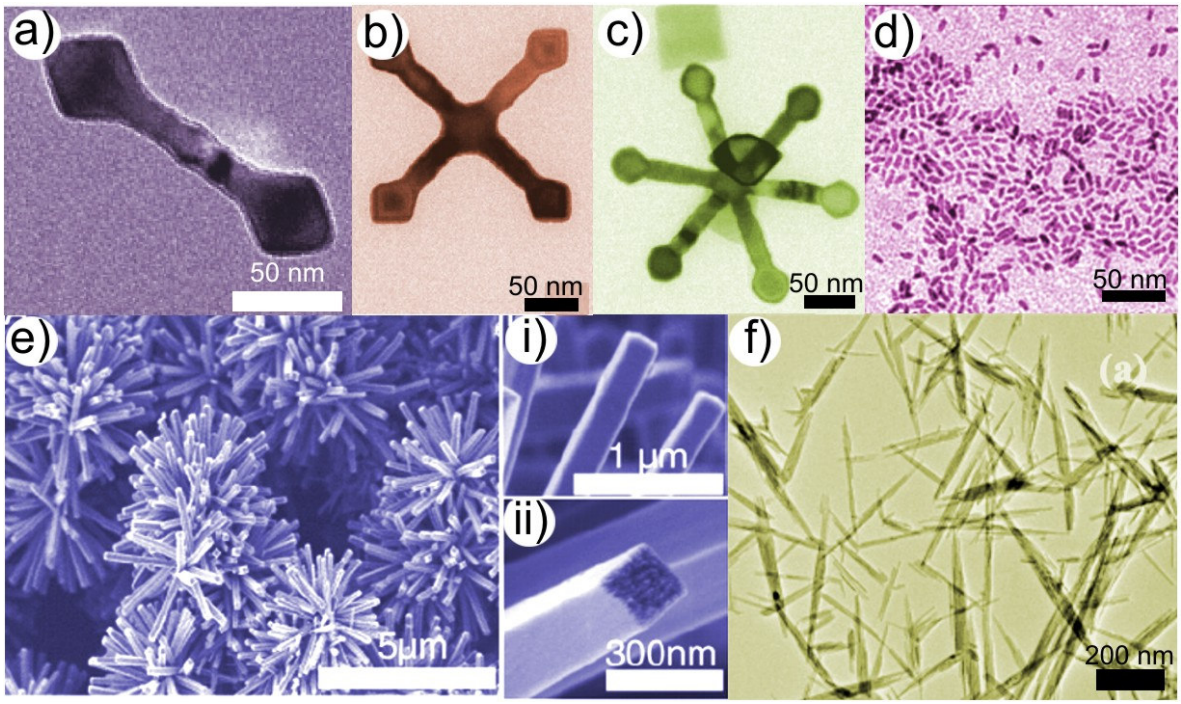

Figure 3-1.- MnO_x nanostructures with different morphologies. (**a**) Dumbbells [6], (**b**) Tetrapods and (**c**) Octahedral nanoparticles [4], (**d**) Nanorods [8], (**e**) Dendritic clusters composed of nano-tetragonal prisms with square cross-section(i-ii) [5], and (**f**) Nanoneedles [7]. All these structures exhibit different catalytic, electrochemical and physical properties.

Moreover, these materials offer low cost, high effective capacitance and they are environmentally friendly [9]. Particularly Mn_3O_4 is known as an efficient catalyst for NOx decomposition, nitrobencene reduction and methane oxidation [10]. It is widely used for fabricating Li-Mn-O electrodes in lithium rechargeable batteries and magnetic materials [11,12]. The Mn_2O_3 has also been proposed as cheap, environmental-friendly catalysts for carbon monoxide [13] and organic pollutants oxidation [14] and nitrogen oxide decomposition [15]. In addition, it has been observed that Mn_2O_3 could potentially be a highly efficient combustion catalyst at low temperatures (<527 K) for pollution control.

3.1.2 Carbon nanotubes-manganese oxide composites

It has been anticipated that the presence of manganese oxide in carbon nanotubes can significantly increase the performance of MWCNTs for many applications. The development of carbon nanomaterials, particularly nanotubes, opened possibilities for producing novel catalysts by deposition of known catalytic materials on the surface of carbon nanotubes.

A typical method for obtaining manganese oxide/CNTs composites is by a direct redox reaction between CNTs and MnO^{-4} anions, but this process generates a continuous coating of MnO_2 particles ranging from 10 to 20 nm in size [16]. If any other Mn oxide is desired, another method must be applied. This method has been widely used to produce electrochemical capacitors with materials based on CNT/MnO_2 nanocomposites [17]. Even it has been reported the filling of CNTs with MnO_2 [18].

The supercapacitor properties have been studies using different systems such as manganese oxide/MWCNTs (M/M) composite and MWCNTs as positive and negative electrodes. The energy density of the hybrid capacitor can reach 32.91 W h/kg even at a current density of 10 mA/cm^2 in 1.0 M $LiClO_4$ electrolyte, which is comparable to manganese oxide/activated carbon hybrid capacitor [19,20]. Other systems used as a substrate materials to deposit MnO_2 particles are SWCNTs, and they have been tested as supercapacitor electrode materials [21]. The authors demonstrated that a better performance for the composites is obtained by the better interconnectivity of MnO_2 particles with entangled SWCNTs. The MnO_x/CNTs composites are expected to be applied in the rechargeable lithium batteries with very high power density and specially the MnO_2/CNT composite could be explored as a supercapacitor electrode material in the future [22,23,24,25].

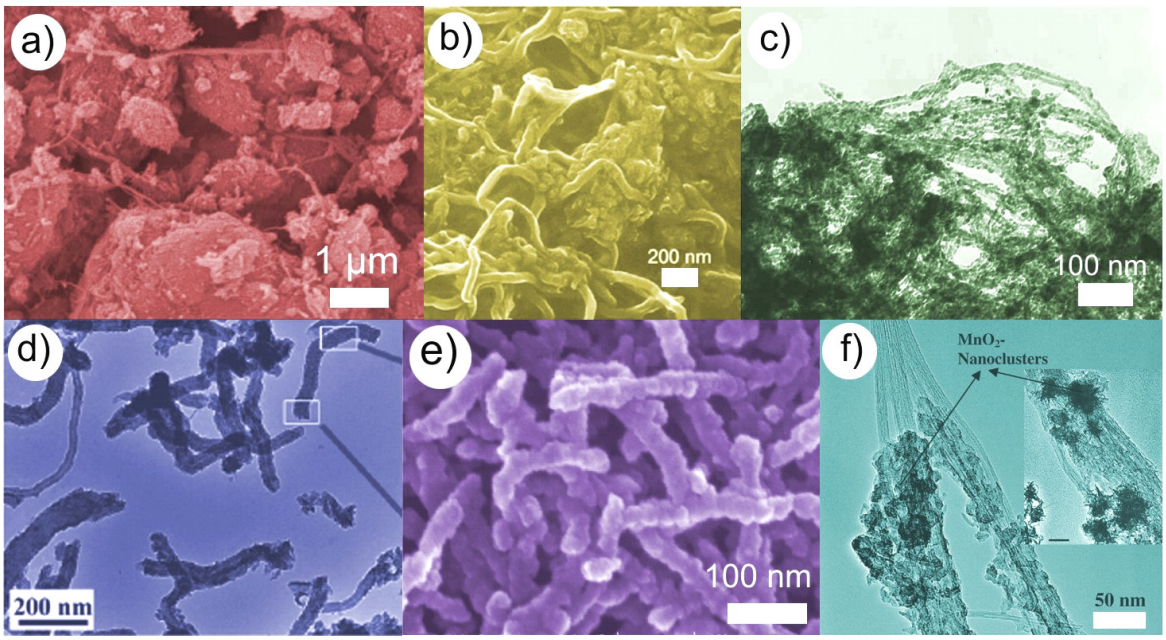

Figure 3-2.- Images of carbon nanotubes-manganese oxides composites. (**a**) Composite with crystallites of MnO_2 100–300 nm in length and 20–40 nm in diameter [19], (**b**) MWCNTs/MnO composite [20], (**c**) MWCNTs/MnO_2 nanoparticles composites [28]. (**d**) A composite with a MnO_2 coating layer of 6.2 nm [26]. (**e**) A thin MnO_2 layer which deposits spontaneously on CNT substrates [25], and (**f**) SWCNTs and MnO_2 composite for supercapacitor electrode material[21].

Other applications of manganese oxide/carbon nanotubes composite are for environmental purposes, such as the removal of Pb(II) from aqueous solution[27]. When compared with MWCNTs, the composite shows a significant improvement on the adsorption properties of Pb(II), and as efficient electrode material for fuel cells [28].

Because of the facile phase transformation of MnO_x during preparation, only multivalence mixtures of manganese oxides (MnO_2, Mn_2O_3 and Mn_3O_4) are usually obtained. Mn_2O_3 particles are prepared by heating MnO_2 or $MnCO_3$ in air at temperatures ranging from 600 to 800 ℃. Sphere- or cube-like Mn_2O_3 have been obtained at 550 ℃ through the decomposition of the $MnCO_3$ precursors synthesized via a hydrothermal reduction route [29], but this has not been used for composites elaboration. In this chapter, we describe a simple process to obtain α-Mn_2O_3 nanoparticles anchored on carbon nanotubes.

3.2 Anchorage of α-Mn_2O_3 clusters on carbon nanotubes; Experimental methodology

3.2.1 Reagents

The manganese acetylacetonate (III), $Mn(acac)_3$ was from Aldrich®, acetone was CTR scientific®, tetrahidrofurane (THF) and methyl-ethyl-ketone (MEK) were Fermont® , the ethylene glycol (>99%), sodium dodecyl sulfate (SDS, >98.5) and N,N-dimethylformamide (DMF, 99%) were form Sigma-Aldrich®. All the chemical substances were used as a received.

3.2.2 Characterization

The products were characterized by scanning electron microscopy (SEM, FEI XL30 FEG/SFEG) operated at 15 kV, the X-ray powder diffraction pattern of all samples were performed using a XRD D8 Advance – Bruker AXS, with Cu K_α radiation (λ = 1.54060 Å) the operating current and voltage were maintained at 35 kV and 25 mA.

3.2.3 Manganese oxide deposition process

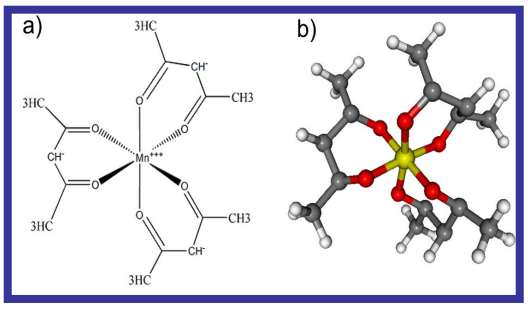

Figure 3-3.- Molecular formula and model of manganese acetylacetonate (III). In this case, (**a**) and (**b**), the manganese exhibit an oxidation state of 3, and their thermal decomposition produce Mn_2O_3.

Manganese acetylacetonate (III) was used as the manganese source due to the low decomposition temperature, easy manipulation and good solubility on a wide range of solvents. This chemical has been employed for the synthesis of manganese oxides nanostructures [30]

Anchoring process

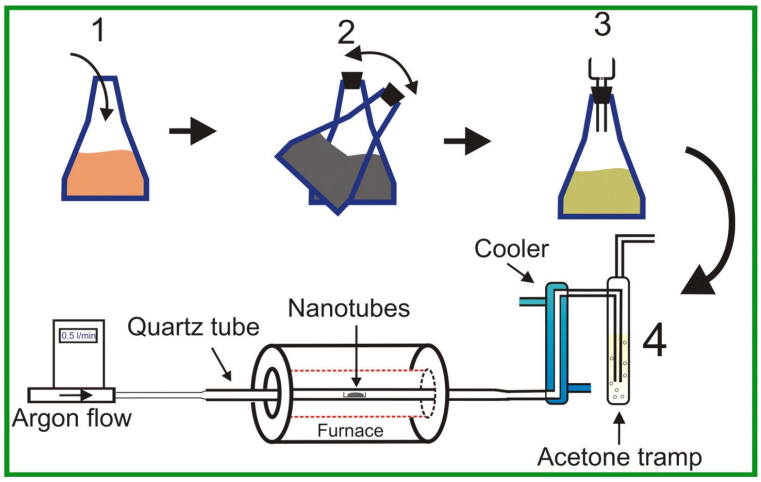

Figure 3-4.- Experimental scheme for coating carbon nanotubes; (**1**) First all the components are mixed, (**2**) The suspension is sonicated for one hour and settled for another hour, (**3**) The carbon nanotubes with $Mn(acac)_3$ are recovered by filtration. (**4**) Finally the nanoparticles are obtained by thermal decomposition of the manganese precursor.

Two types of carbon nanotubes were employed in these experiments, the nitrogen-doped carbon nanotubes (CN_x-MWNT) and the nanotubes with oxygen groups (CO_x-MWNT), were produced by the CVD process described in section 2.2.2; the nanotubes were used without further modification.

The coating process consists of adding 5 mg of carbon nanotubes to 10 ml of solution containing manganese acetylacetonate, $Mn(acac)_3$, sodium dodecyl sulfate (SDS) and solvent. The molar ratio of carbon (from the CNT) and manganese was kept at 10, during the experiments the concentration of SDS was varied using 0.1, 0.5 and 1.0 mg/ml. The nanotubes were suspended for one hour using an ultrasonic bath. After that, the solution was left to settle down for one hour. Subsequently, the suspension was filtered using PTFE membranes with a pore size of 0.2 μm. The nanotubes were collected form the membrane by scraping. The samples were then heated to 400℃ for 15 minutes in an argon atmosphere. Figure 3.4 illustrates the coating process of MWCNTs.

3.3 Results and discussion

The effect of the solvent on the particle size of α-Mn_2O_3 clusters

Table 3-1.- Solvents used in the experiments, describing the solvent type, polarity index and chemical structure (see Figure 3.5). In the last column the solvents that showed an anchorage of nanoparticles on nanotubes are indicated.

Solvent	Type of solvent	Polarity index	Anchored nanoparticles
Dimethylformamide (DMF)	**Aprotic**	6.4 (highly polar)	-
Ethylene glycol (EG)	Protic	-	-
Acetone	**Aprotic**	5.4	✓ (yes)
Ethanol	Protic	5.2	-
Methyl Ethyl Ketone (MEK)	**Aprotic**	4.5	✓ (yes)
Isopropyl alcohol	Protic	4.3	-
Tetrahydrofuran (THF)	**Aprotic**	4.2 (Lower polarity)	✓(yes)

During the experiments several solvents were used in order to improve the dispersion of the nanotubes and the anchorage of nanoparticles. We used organic solvents that vary on their polarity, and a brief description of the solvents appears in Table 3.1, and their chemical structures are shown in Figure 3.5.

We notice that the systems with low polarity and aprotic solvent were able to cover carbon nanotubes with manganese oxide nanoparticles. The aprotic solvents such as acetone tend to have large dipole moments (separation of partial positive and partial negative charges within the same molecule) and solvate positively charged species via their negative dipole. These characteristics of the solvents allow to control the interaction between the CNTs surface and molecules of $Mn(acac)_3$; we also add sodium dodecyl sulfate (SDS) in the process.

This method is based on the adsorption properties of the CNTs and further thermal decomposition of the metal precursor. The amount of $Mn(acac)_3$ adsorbed by the CNTs can be controlled by adding a surfactant that allows the interaction between

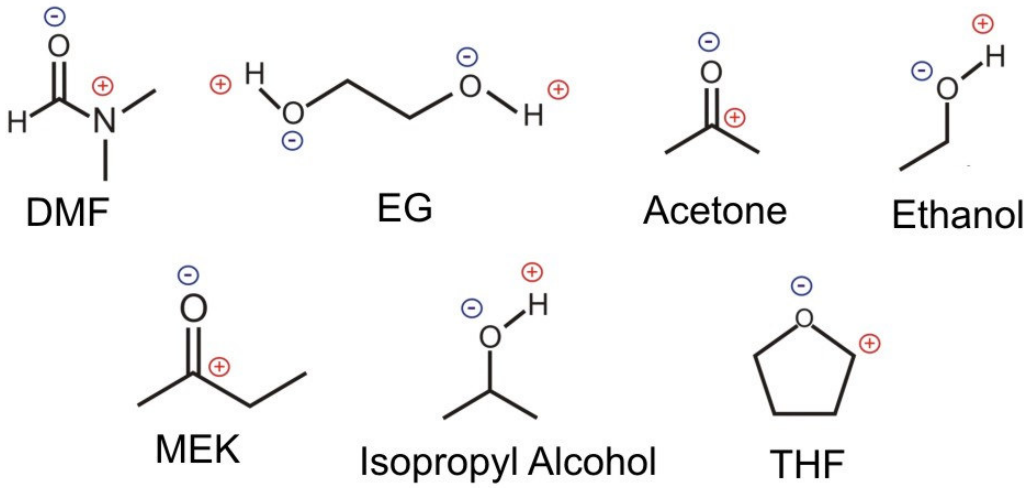

Figure 3-5.- Chemical formulas of solvents used during these experiments. In each case the dipoles are shown. These dipoles are present in each molecule due to different electronegativity between oxygen atom and the others. A brief description of the solvent is given in Table 3.1. From (**a**) to (**g**): DMF, EG, Acetone, Ethanol, MEK, Isopropyl alcohol and THF.

CNTs and the $Mn(acac)_3$, thus acting as a bridge between them. Using this property we are able to control the particle size and the number of particles anchored on the nanotubes surface.

The nanotubes that were immersed in systems with **aprotic solvents that exhibited a low polarity,** (acetone, MEK and THF) showed particles of manganese oxide on their surface. These three systems were studied in detail by varying the concentration of sodium dodecyl sulfate and the resting time, to evaluate the effect of these variables on the particle size and the number of particles on the nanotube walls.

Those only low polar and aprotic solvents were successful in coating carbon nanotubes could be due to their different chemical structures and polarity. Aprotic solvents only solvates positive ions. Here, we speculate that the $Mn(acac)_3$ in presence of this solvent is partially dissociated and easily solvated, so the interaction between CNTs and $Mn(acac)_3$ is too weak to get adsorbed, (see Figure 3.6-(**b**)).

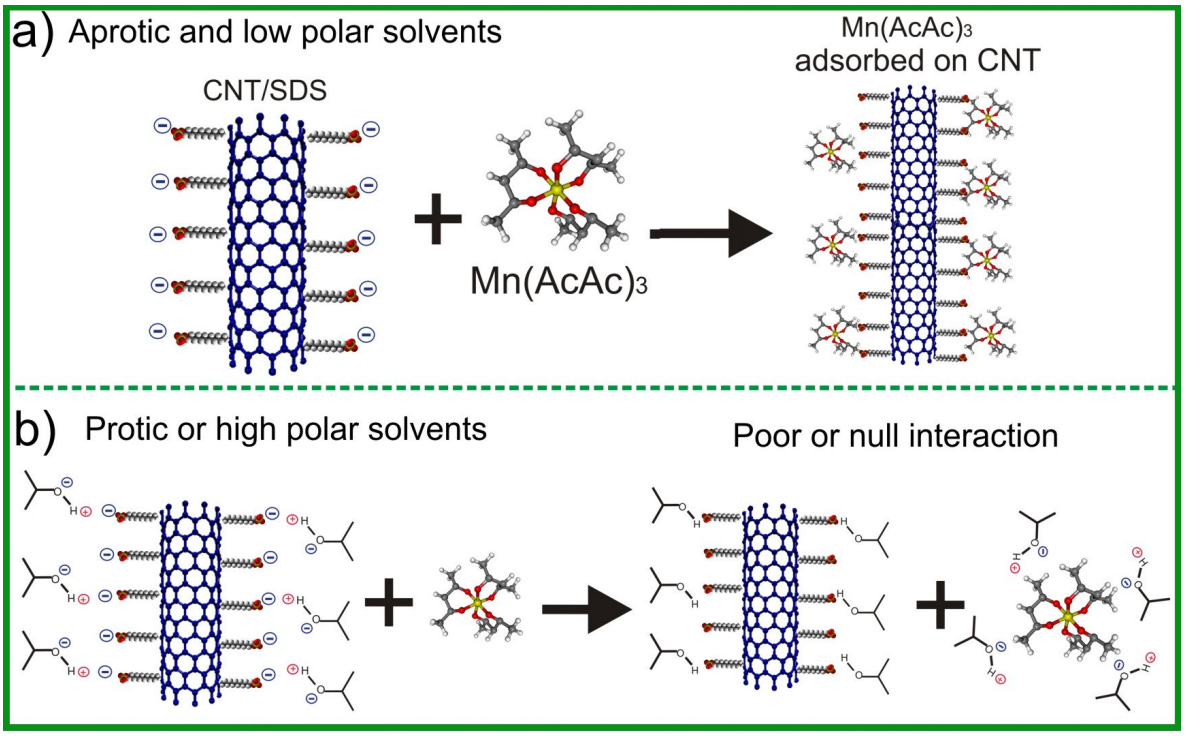

Figure 3-6.- Carbon nanotubes and Mn(acac)$_3$ interactions with different types of solvents. (**a**) CNT/SDS system and Mn(acac)$_3$ can interact directly by electrostatic forces in the presence of aprotic and low polar solvents. (**b**) In the presence of protic or high polar solvents, the CNT/SDS system is totally solvated, avoiding a direct interaction with the Mn(acac)$_3$ molecule.

On the other hand, we have the lipid chain containing the anion of the surfactant molecule that could be adsorbed on the surface of the nanotube, thus forming a monolayer [31] making the nanotubes negatively charged which enhances the forces between CNTs and the Mn(acac)$_3$; this process is illustrated in Figure 3.6-(**a**). This behavior depends on the type nanotubes, solvent and amount of SDS. In the next section we describe in detail both CN_x-MWNTs and the CO_x-MWNTs systems.

3.3.2 Functionalized carbon nanotubes/manganese oxide composites (CO_x-MWNTs/α-Mn_2O_3)

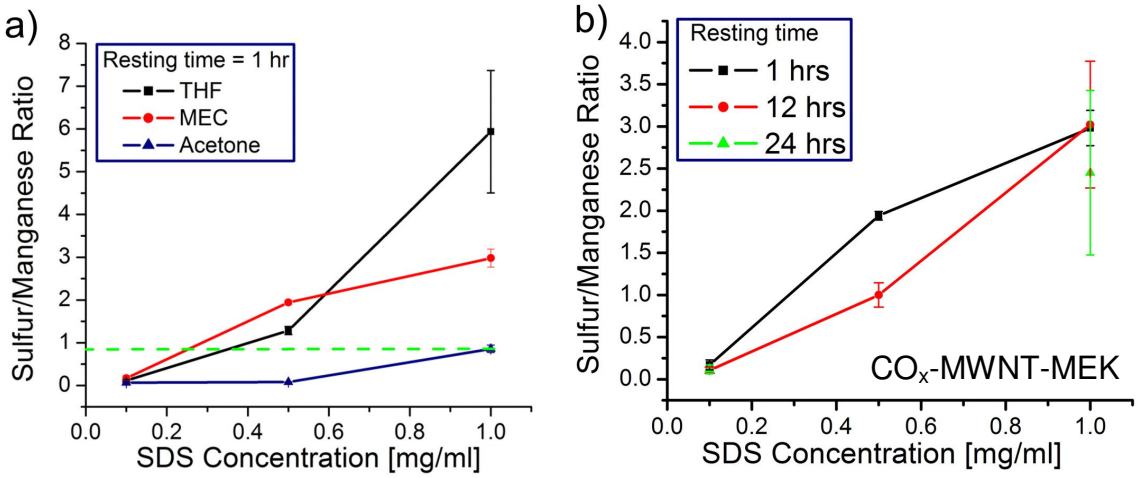

Figure 3-7.- Sulfur/Manganese ratio vs. surfactant (SDS) concentration Mn_2O_3/CO_x-MWNTs composite. In (**a**) correlation between sulfur:manganese (S:Mn) ratio and the SDS concentration in the initial solution, the quantity of sulfur (determined by EDX) present in the samples depend strongly on the type of solvent. In (**b**) the relationship between S:Mn ratio and the SDS concentration using MEK as solvent with different resting times. We observed the same behavior in all cases, the S:Mn ratio increase with the addition of SDS, but we notice that the time does not influence in the S:Mn ratio in the samples because all the points for different times are almost equal.

In order to evaluate the relationship between sulfur:manganese (S:Mn) ratio and the SDS concentration, an EDX analysis was performed. It appears that when we increase the SDS concentration, the S:Mn ratio increase too, but these behavior strongly depends on the type of solvent present in the system, because the interactions between CNTs and surfactant molecules appear to be different in all systems.

In Figure 3.7-(**a**) we can observe the effect of the SDS concentration on the S:Mn ratio using different solvents (ACE, MEK and THF). Here we note that less polar solvents (THF and MEK, black and red lines respectively) results in a larger interaction between the CNTs and the surfactant molecules. When the nanotube suspension is prepared with acetone as solvent, the nanotubes have the lower

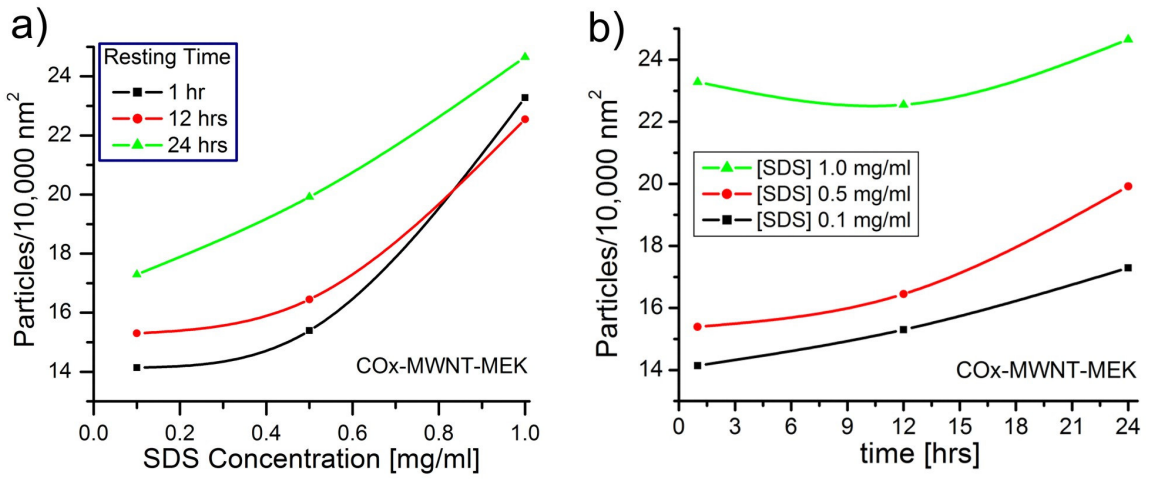

Figure 3-8.- Particles, SDS relationship observed in Mn_2O_3/CO_x-MWNT composites. In (**a**) the graph shows the particle density per 10,000 nm^2 vs SDS concentration. It can be observed that the particle density is slightly modified with the addition of surfactant. In (**b**), the chart shows the relationship between particle density and the resting time of the solution, apparently the time does not modify the particle density on the nanotubes wall.

S:Mn ratio in all cases. Other variable that can affect the adsorption properties is the resting time. We carried out some experiments and preliminary results demonstrate that the amount of SDS adsorbed by the CNT does not change but the particles size is affected.

Figure 3.7-(**b**) shows the relationship between SDS concentration and the S:Mn ratio at different resting times using MEK as a solvent. The S:Mn ratio has the same behavior in all cases, it can be seen that as the time does not modify the sulfur uptake of the nanotubes, this effect strongly depends on the type of nanotube, (different surface properties). In Figure 3.8-(**a**) we show the relationship between the number of particles per 10,000 nm^2 and SDS concentration (data obtained form SEM images; ~50 nanotubes by sample were analyzed). We note that the particles density is affected with the addition of SDS. When we increase the surfactant concentration, we increase the SDS adsorbed on the nanotubes, and these molecules will cover completely the nanotube surfaces due to the enhanced interaction between CNTs and the manganese precursor. The dependence of the time was only carried out with nanotube suspension using **methyl ethyl ketone** (MEK) as a solvent. The suspensions were settled for 1, 12

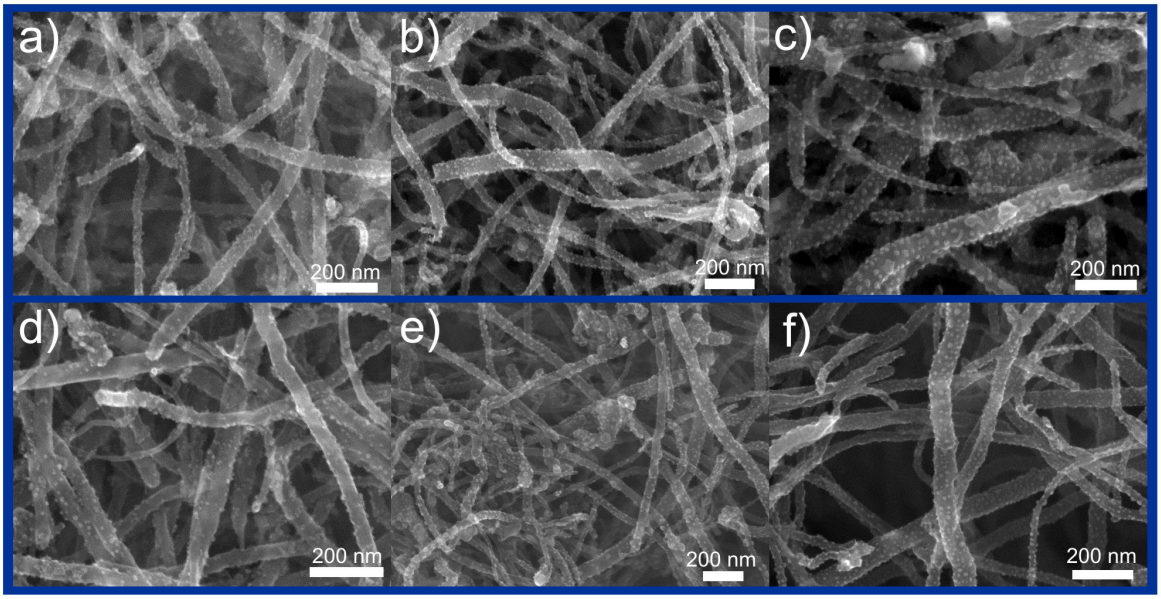

Figure 3-9.- SEM images of CO_x-MWNTs/α-Mn_2O_3 composites: α-Mn_2O_3 nanoparticles were anchored using acetone as a solvent. The images show the composite obtained using different concentration of sodium dodecyl sulfate, 0.1 mg/ml (a), 0.5 mg/ml (b) and 1.0 mg/ml (c). When we use MEK as solvent, we obtained a mixture of MnO_2 and Mn_2O_3 nanoparticles. Due to the high quantity of SDS in the system, the images (d), (e) and (f) show the composite at different SDS concentration (0.1, 0.5 and 1.0 mg/ml respectively). We can observe how the particle size can be controlled with the addition of SDS.

and 24 hours in order to study the effect of the resting time on the particle size and the spatial density of the nanoparticles. Our results demonstrate that the particle density on the nanotube wall is almost constant throughout the time.

In Figure 3.8-(**b**) we observe that the curve corresponding to 1.0 mg/ml of SDS (green line), exhibit the highest density, approximately 23 particles per 10,000 nm^2, all points throughout the time are very similar, so in this case the time almost does not modify the particle density.

Table 3-2.- Manganese oxide clusters sizes using different solvents

SDS [mg/ml]	Acetone	Methyl-ethyl-ketone	Tetrahidrofurane
0.1	6.49 ± 1.11 nm[b]	5.65 ± 1.79 nm[b]	7.37 ± 1.97 nm[b]
0.5	8.2 ± 1.71 nm[b]	8.64 nm[a]	8.81 ± 2.17 nm[b]
1.0	10.7 nm[a]	8.7 nm[a]	9.4 nm[a]

(a) Acquired from the X-ray diffraction patterns
(b) Obtained from SEM images

In Figure 3.9, SEM images of the experiments carried out with different solvents and concentrations of sodium dodecyl sulfate are presented. Figure 3.9-(**a**) has a concentration of 0.1 mg/ml, (**b**) 0.5 mg/ml and (**c**) 1.0 mg/ml. These samples were treated with acetone, and we can appreciate that the particle size is larger in Figure 3.9-(**c**), but the number of nanoparticles on the nanotubes are constant. This confirms the low interaction caused by the acetone between the surfactant and the CNTs, because only the active sites that have the nanotube play a role. When we use MEK as a solvent we obtain Mn_2O_3 nanoparticles, if we increase the SDS concentration we obtain a mixture of MnO_2 and Mn_2O_3 (see Figure 3.10). Due to the high quantity of oxygen introduced by SDS in the system, the images (**d**), (**e**) and (**f**) show these composites prepared with different SDS concentrations (0.1, 0.5 and 1.0 mg/ml respectively). We can observe how the particle size can be controlled by adding the surfactant in the system.

Table 3.2 describes the particle size of all composites using different solvents. We can appreciate that the cluster size is modified by the type of solvent used during the experiments. In all cases, we obtain the lowest particle size with the smallest SDS concentration (0.1 mg/ml), but usually the CNTs exhibit very low load of nanoparticles. When increasing the SDS concentration, we increase both particle size and load of particles on the CNTs surfaces. This suggests that we are not able to modify the load of nanoparticles without affecting the particle size. The best composites that were prepared used acetone and MEK as a solvent, due to the low quantity of sulfur presented in the system after calcination (in this case, the acetone was the best) and better cover of the surfaces.

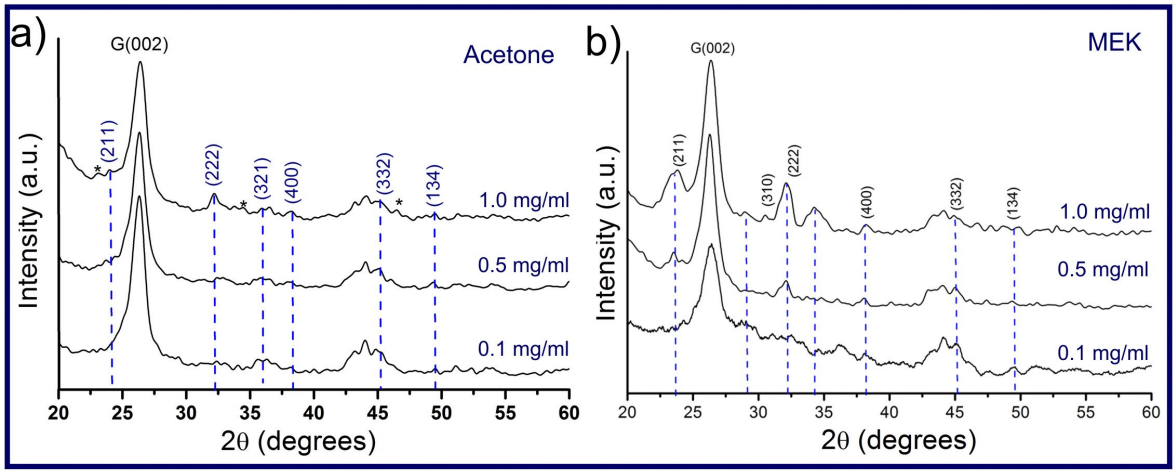

Figure 3-10.- X-ray diffraction patterns of CO_x-MWNT/MnO_x prepared with different solvents. When we use acetone as a solvent, the nanoparticles exhibit a crystalline cubic phase of Mn_2O_3. (**a**) The G(002) peak is attributed to graphite, the other belong to Mn_2O_3; (**b**) when MEK is employed as solvent we obtain Mn_2O_3 too, when the SDS concentration is 1.0 mg/ml, the nanoparticles become a mixture of MnO_2 and Mn_2O_3. This can be attributed to the high quantity of oxygen introduced by the SDS molecule.

The optimal SDS concentration was 0.5 mg/ml in both cases, due to the perfect balance between the particle size and covered surface.

When we use acetone as solvent, the nanoparticles revealed a crystalline cubic phase of α-Mn_2O_3 independent of the SDS concentration. These results can be observed in the diffraction pattern (Figure 3.10-(**a**)). These results confirm the fact that the acetone exhibits low interaction with the SDS molecules, avoiding the introduction of high concentration of oxygen (from the SDS) and further oxidation of the manganese particles. In Figure 3.10-(**b**) the X-ray powder diffraction pattern of the sample prepared with MEK, we see that Mn_2O_3 is present at low surfactant concentration, and when the SDS concentration is increased, it begins to appear another oxidation state of manganese (MnO_2). This can be attributed to the high quantity of oxygen introduced by the SDS molecules.

Similar results were obtained using THF as solvent, and at low surfactant the nanocomposite only exhibits the α-Mn_2O_3 phase, but at higher SDS concentration, both MnO_2 and Mn_2O_3 are produced. In this case, the composite showed the lowest particle load and the highest S:Mn ratio.

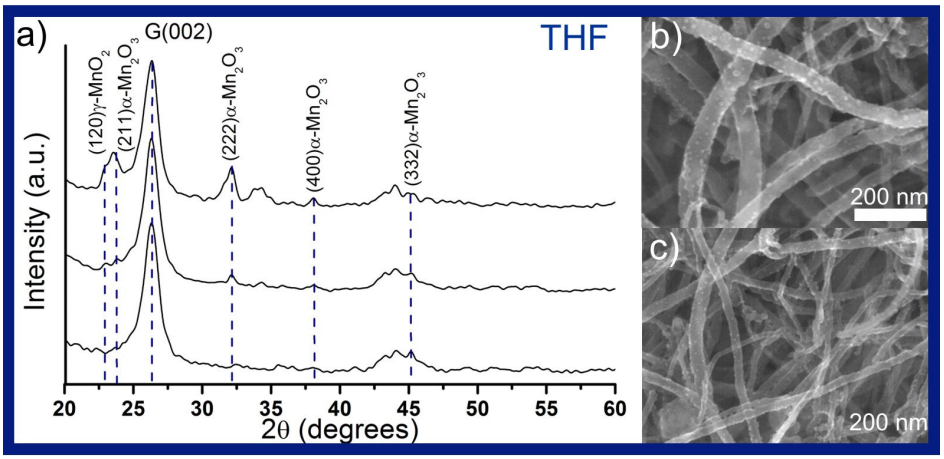

Figure 3-11.- X-ray diffraction pattern and SEM images of CO_x-MWNTs/MnO_x composite using THF as a solvent. (**a**) XRD analysis using THF as a solvent, the composite shows two oxidation states of manganese, due to the high oxygen presented in the system; (**b**) SEM image of the material produced when is used 0.5 mg/ml of SDS; (**c**) SEM image when using 1.0 mg/ml of SDS.

SEM images and XRD patterns are illustrated in Figure 3.11, the peaks from the patterns show very low intensity, reflected by the poor quantity of nanoparticles fixed on the CO_x-MWNTs. This composite exhibits the worst characteristics (high amount of sulfur and a few particles). However, the particle size reveals similar behavior when compared to other solvents. At low SDS concentration the achieved size was 7.37 ± 1.97 nm, the maximum size was recorded on composites prepared with the highest SDS concentrations (9.4 nm).

3.3.3 Nitrogen-doped carbon nanotubes/manganese oxide composites (CN_x-MWNTs/α-Mn_2O_3)

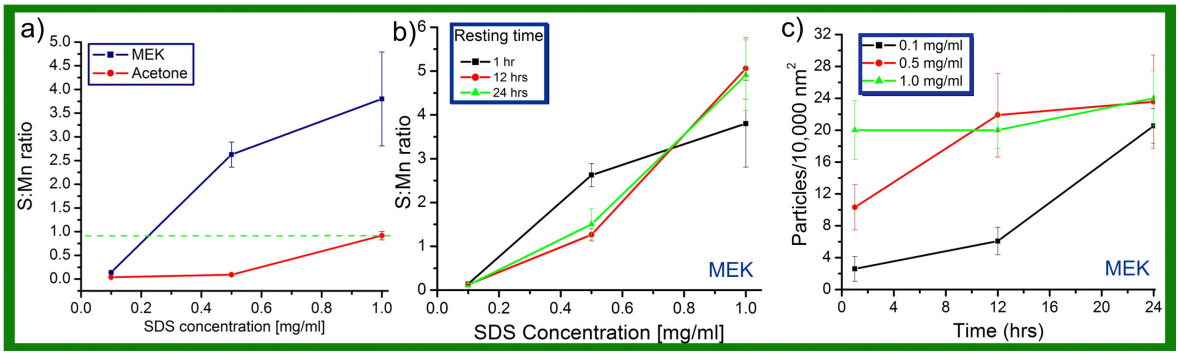

Figure 3-12.-S:Mn ratio and particle density of Mn_2O_3/CN_x-MWNTs composite. (**a**) S:Mn ratio using different solvents at various SDS concentrations. (**b**) The relationship between the S:Mn ratio and the SDS concentration at different times, and (**c**) The progress of the number of particles anchored at different times and SDS concentrations. The maximum numbers of nanoparticles achieved were obtained using 24 hours of rest.

In this section we describe the anchoring results using CN_x-MWNTs as a substrate material to deposit manganese oxide nanoparticles. We carried out the same methodology used for CO_x-MWNTs.

We use the solvents listed in Table 3.1. In this investigation only acetone and MEK were studied in detail. THF was not included due to the high amount of sulfur present in the sample. After the anchoring process, we studied the relationship between S:Mn ratio (determined by EDX analysis) and the SDS concentration. The suspensions prepared using acetone exhibited the lowest amount of sulfur; see Figure 3.12-(**a**) (red line). Even at the highest SDS concentration, the sulfur:manganese (S:Mn) ratio was maintained below 1, but using MEK, the S:Mn was increased up to ~ 4. These results are similar to CO_x-MWNTs, in which acetone exhibits a poor interaction with the surfactant molecules.

Studies considering varying the time were also carried out using MEK as a solvent. These results are illustrated in Figure 3.12-(**b**). By varying the SDS concentration, we observed that the S:Mn ratio increases approximately in a linear manner.

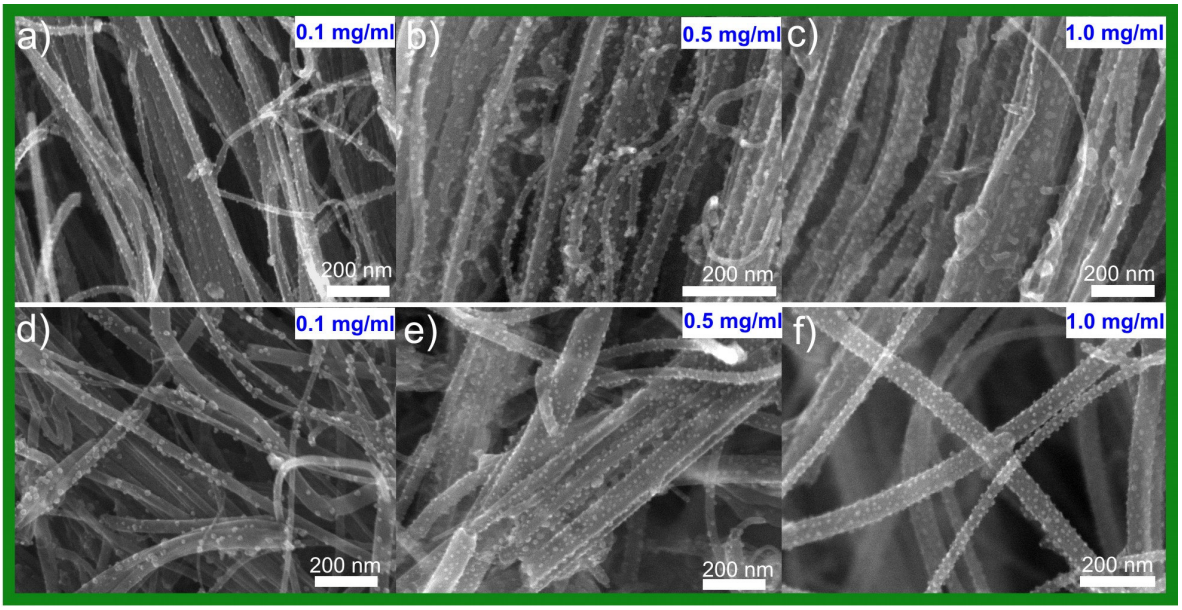

Figure 3-13.- SEM images of CN_x-MWNTS/MnOx composites with different solvents at various SDS concentrations. (**a-c**) Using acetone as a solvent, in (**a**) The lowest particle size is obtained at 0.1 mg/ml of SDS. (**b**) The particle size and the load of nanoparticles is increased at 0.5 mg/ml and 1.0 mg/ml. (**d-f**) Using MEK as a solvent, in (**d**), the composite achieved at 0.1 mg/ml of SDS. (**e**) at 0.5 mg/ml and (**f**) at 1.0 mg/ml. At concentrations of SDS greater than 0.5 mg/ml, the surfaces presented better distribution of nanoparticles.

Moreover, the S:Mn ratio can be considered constant throughout the time. This does not mean that the quantity of particles is not affected. In fact, with low amounts of SDS, the number of nanoparticles per 10,000 nm^2 increases from ~ 5 up to ~ 20 particles. This information is presented of Figure 3.12-(**c**), but with highest SDS concentration, the number of clusters can be considered constant (green line). When all the samples with different amounts of SDS were settled for 24 hrs, all of them exhibited approximately the same number of clusters per 10,000 nm^2; this is in agreement with the saturation of all reactive sites present in the nanotubes.

The results obtained from the SEM analysis of the composites prepared with acetone as solvent at various SDS concentrations are presented in Figure 3.13. It can be seen, that the particle size is increasing with the addition of SDS and apparently the number of clusters is increasing too. A similar behavior was

Table 3-3.- Size of manganese oxides clusters on CN_x-MWNTs with different types of solvents and SDS concentrations.

SDS [mg/ml]	Acetone	Methyl-ethyl-ketone
0.1	6.38 ± 1.38 nm[a]	7.34 ± 2.07 nm[a]
0.5	7.40 ± 1.51 nm[a]	7.38 nm[b]
1.0	12.1 nm[b]	13.6 nm[b] MnO_2 16.8 nm[b] Mn_2O_3

(a) Results obtained from SEM images
(b) Data obtained from XRD analysis

observed for the composites that were prepared with MEK, the cluster size increased with the addition of SDS and the quantity of clusters also increased. The particle size was determined by X-ray diffraction patterns and SEM images. The smallest particle size is obtained using acetone, these results differ from those obtained with the CO_x-MWNTs as a substrate (MEK was the solvent that showed the smallest particles).

The X-ray powder diffraction pattern using acetone as a solvent at different surfactant concentrations are illustrated in Figure 3.13-(**a**). The intense peak correspond to α-Mn_2O_3, the other ones arise from MnO_2 and the ones marked with a star (*) are related with the residual material generated by the calcinations of surfactant molecules. These types of composites below 1.0 mg/ml exhibit only Mn_2O_3 particles, but at higher concentrations they also exhibit a small amount of MnO_2 clusters. On the other hand, the composites that were prepared using MEK as a solvent revealed different behavior at higher surfactant concentrations; this composite show the higher contents of MnO_2 particles. However, at low SDS concentrations, only Mn_2O_3 are present. Due to the high amount of surfactant in the sample, it is possible to observe some peaks that belong to residual material of SDS molecules after calcinations; peaks marked with a (*). All these results demonstrate that the solvents are important to control the size of particles and the interaction with the surfactant molecules able to form a variety of manganese oxides.

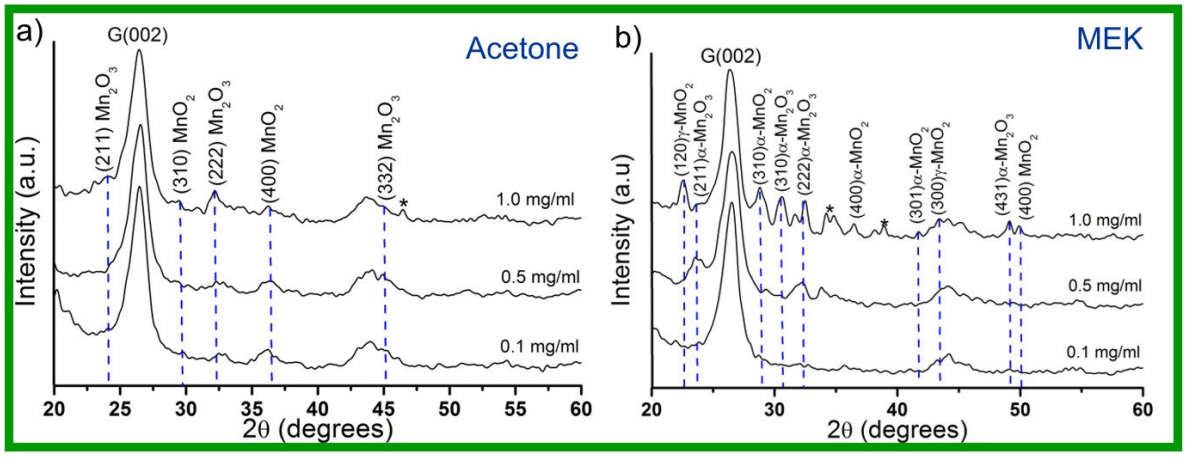

Figure 3-14.- X-ray powder diffraction patterns of MnO_x/CN_x-MWNTs composites using different solvents. (**a**) When acetone is used, the oxidation state of manganese is predominantly III (Mn_2O_3); (**b**) If MEK is used as a solvent, a mixture of MnO_2 and Mn_2O_3 is obtained, due to the large quantity of oxygen introduced by the surfactant. All peaks are indexed, the peaks marked with (*) are generated by the residual material of the surfactant.

3.4 Conclusions

We have obtained α-Mn_2O_3/CO_x-MWNT composite employing a simple process without using expensive materials or special equipment. This simple method allows the control of the particle size and permit to obtain only α-Mn_2O_3 nanoparticles anchored on the CO_x-MWNTs.

We have analyzed the effect of the solvent and the addition of surfactant on the particle. It may be that other surfactants could be used avoiding the addition of sulfur into the system. We have achieved the formation of α-Mn_2O_3/CO_x-MWNT without any chemical treatment of the carbon nanotubes, and therefore we have minimized the damage of their surfaces. We obtained similar results using CN_x-MWNT as a substrate material.

Our results suggest that this process can be easily extended to other metal oxides using acetylacetonate molecules as the metal precursor. These types of molecules are easy to manipulate and are soluble by wide range of solvents. In addition, this anchoring method could be easily adapted to produce larger quantities of metal oxides/CNTs composites.

3.5 References

[1] I. Djerdj, D. Arcon, Z. Jaglicic, M. Niederberger, "Nonaqueous Synthesis of Manganese Oxide Nanoparticles, Structural Characterization, and Magnetic Properties", *J. Phys. Chem. C,* Vol. 111, 3614-3623 (2007)

[2] I. V. Solovyev, K. Terakura, "Effective single-particle potentials for MnO in light of interatomic magnetic interactions: Existing theories and perspectives", *Phys. Rev. B*, Vol. 58, 15496- 15507 (1998)

[3] P.Z. Si, D. Li, J. W. Lee, C. J. Choi, Z.D. Zhang, D. Y. Geng, E. Brück, "Unconventional exchange bias in oxide-coated manganese nanoparticles", *Appl. Phys. Lett.* Vol. 87, 133122 (2005)

[4] T. Ould-Ely, D. Prieto-Centurion, A. Kumar, W. Guo, W. V. Knowles, S. Asokan, M.S. Wong, I. Rusakova, A. Lüttge, K.H. Whitmire, "Manganese(II) Oxide Nanohexapods: Insight into Controlling the Form of Nanocrystals", *Chem. Mater.*, Vol. 18, 1821-1829 (2006)

[5] J. Yuan, W-N. Li, S. Gomez, S. L. Suib, "Shape-Controlled Synthesis of Manganese Oxide Octahedral Molecular Sieve Three-Dimensional Nanostructures", *J. Am. Chem. Soc.* , Vol. 127, 14184-14185 (2005)

[6] X. Zhong, R. Xie, L. Sun, I. Lieberwirth W. Knoll, "Synthesis of Dumbbell-Shaped Manganese Oxide Nanocrystals", *J. Phys. Chem. B*, Vol. 110, 2-4 (2006)

[7] L. X. Yang, Y. J. Zhu, W. W. Wang, H. Tong, M.L. Ruan, "Synthesis and Formation Mechanism of Nanoneedles and Nanorods of Manganese Oxide Octahedral Molecular Sieve Using an Ionic Liquid", *J. Phys. Chem. B*, Vol. 110, 6609-6614 (2006)

[8]J.-W. Seo, Y.-W. Jun, S. J. Ko, J. Cheon, "In Situ One-Pot Synthesis of 1-Dimensional Transition Metal Oxide Nanocrystals", *J. Phys. Chem. B*, Vol. 109, 5389-5391 (2005)

[9] I. Zhitomirsky, M. Cheong, J. Wei, "The Cathodic Electrodeposition of Manganese Oxide Films for Electrochemical Supercapacitors", *J.O.M.,* Vol. 59. No. 7, 66-69, (2007)

[10] L. X. Yang, Y. J. Zhu, H. Tong,W. W. Wang, G. F. Cheng, "Low temperature synthesis of Mn_3O_4 polyhedral nanocrystals and magnetic study", *J. Solid State Chem.*, Vol. 179, 1225-1229 (2006)

[11] Y. C Zhang,T. Qiao, X. Y. Hu, "Preparation of Mn_3O_4 nanocrystallites by low-temperature solvothermal treatment of γ-MnOOH nanowires", *J. Solid State Chem.*, Vol. 177, 4093-4097(2004)

[12] T. Nakamura, A. Kajiyama, "Synthesis of Li–Mn spinel oxide using Mn_2O_3 particles", *Solid State Ionics*, Vol. 124, 45-52 (1999)

[13] S. Imamura, M. Shono, N. Okamoto, A. Hamada, S. Ishida, "Effect of cerium on the mobility of oxygen on manganese oxides", *Appl. Catal. A,* Vol. 142, 279-288 (1996).

[14] M. Baldi, V. Sanchez Escribano, J.M. Gallardo Amores, F. Milella, G. Busca, "Characterization of manganese and iron oxides as combustion catalysts for propane and propene", *Appl. Catal. B*, Vol. 17, L175 – L182 (1998)

[15] T. Yamashita, A. Vannice, "N_2O Decomposition over Manganese Oxides", *J. Catal.* Vol. 161, 254-262 (1996).

[16] S. B. Ma, K. Y. Ahn, E. S. Lee, K. H. Oh, K. B. Kim, "Synthesis and characterization of manganese dioxide spontaneously coated on carbon nanotubes", *Carbon*, Vol. 45 375-382 (2007)

[17] S. B. Ma, K. W. Nam, W. S. Yoon, X. Q. Yang, K. Y. Ahn, K. H. Oh, K. B. Kim "A novel concept of hybrid capacitor based on manganese oxide materials", *Electrochem. Commun.*, Vol. 9, 2807–2811 (2007)

[18] S. H. S. Zein, L.-C. Yeoh, S.-P. Chai, A. R. Mohamed, M. E. M. Mahayuddin, "Synthesis of manganese oxide/carbon nanotube nanocomposites using wet chemical method", *J. Mat. Pro. Tech.* Vol. 190, 402–405 (2007)

[19] G. X. Wang, B.-L. Zhang, Z.-L. Yu, M.-Z. Qu, "Manganese oxide/MWNTs composite electrodes for supercapacitors", *Solid State Ionics*, Vol. 176, 1169–1174 (2005)

[20] H. Yue, X. Huang, Y. Yang, "Preparation and electrochemical performance of manganese oxide/carbon nanotubes composite as a cathode for rechargeable lithium battery with high power density", *Mat. Lett.,* Vol. 62, 3388-3390 (2008)

[21] V. Subramanian, H. Zhu, B. Wei, "Synthesis and electrochemical characterizations of amorphous manganese oxide and single walled carbon nanotube composites as supercapacitor electrode materials", *Electrochem Commun*, Vol. 8, 827–832 (2006)

[22] X. P. Huang, C. X. Pan, "Absorbing Manganese Oxide on Multi-Walled Carbon Nanotubes", *Solid State Phenomena*, Vols. 121-123, 85-88 (2007)

[23] X. P. Huang, C. Pan, X. Huang, "Preparation and characterization of γ-MnO_2/CNTs nanocomposite", *Mat. Lett.*, Vol. 61, 934–936 (2007)

[24] G.-X. Wang, B.-L. Zhang, Z.-L. Yu, M.-Z. Qu, "Manganese oxide/MWNTs composite electrodes for supercapacitors", *Solid State Ionics*, Vol. 176, 1169–1174 (2005)

[25] S.-B. Ma, K.-W. Nam, W.-S. Yoon, X.-Q. Yang, K.-Y. Ahn, K.-H. Oh, K.-B. Kim, "Electrochemical properties of manganese oxide coated onto carbon nanotubes for energy-storage applications", *J. Power Sources*, Vol. 178, 483-489 (2008)

[26] X. Xie, L. Gao, "Characterization of a manganese dioxide/carbon nanotube composite fabricated using an in situ coating method", *Carbon*, Vol. 45, 2365-2373 (2007)

[27] S. G. Wang, W. X. Gong, X. W. Liu, Y. W. Yao, B. Y. Gao, Q. Y. Yue, "Removal of lead(II) from aqueous solution by adsorption onto manganese oxide-coated carbon nanotubes", *Separation and Purification Technology*, Vol. 58, 17–23 (2007)

[28] M.O. Danilov, A.V. Melezhyk, "Carbon nanotubes modified with catalyst-Promising material for fuel cells", *J. Power Sources*, Vol. 163, 376–381(2006)

[29] S. Lei, K. Tang, Z. Fang, Q. Liu, H. Zheng, "Preparation of α-Mn_2O_3 and MnO from thermal decomposition of $MnCO_3$ and control of morphology", *Mater. Lett*. Vol. 60, 53-56 (2006)

[30] Y. F.Han, F. Chen, Z. Zhong, K. Ramesh, L. Chen, E. Widjaja, "Controlled Synthesis, Characterization, and Catalytic Properties of Mn_2O_3 and Mn_3O_4 Nanoparticles Supported on Mesoporous Silica SBA-15", *J. Phys. Chem. B,* Vol. *110,* 24450-24456 (2006)

[31] C. Richard, F. Balavoine, P. Schultz, T.W. Ebbesen, C. Mioskowski, “Supramolecular Self-Assembly of Lipid Derivatives on Carbon Nanotubes”, *Science,* Vol. 300, 775-778 (2003)

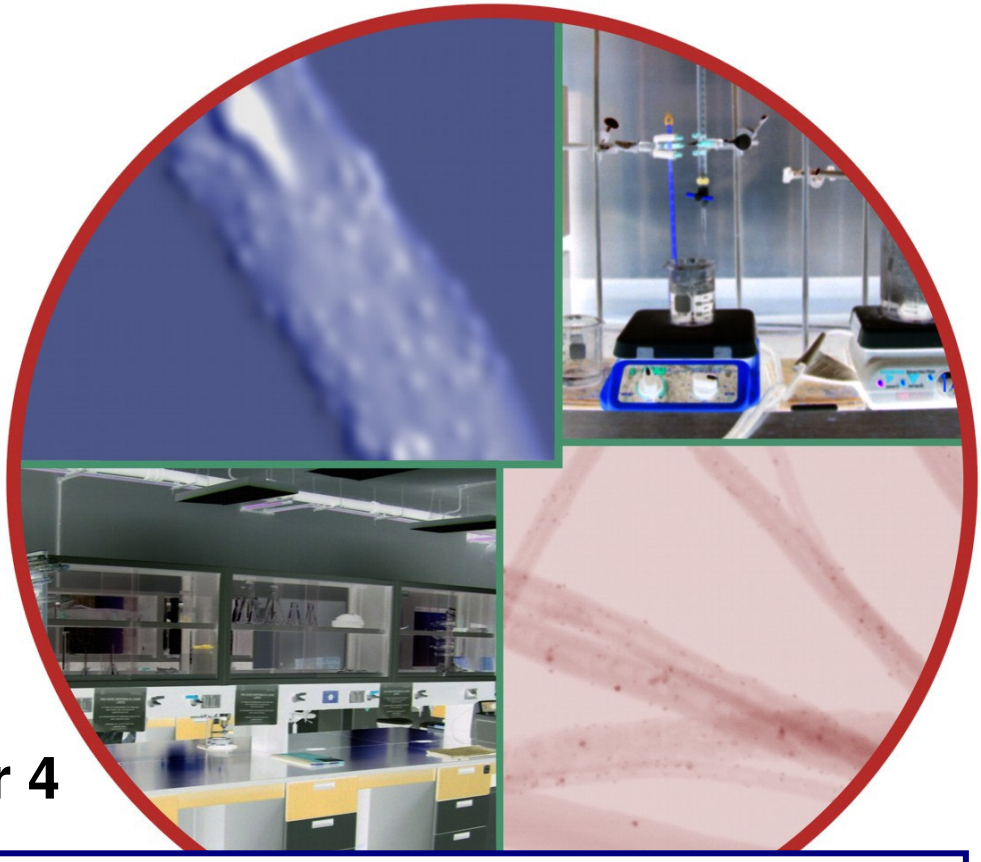

Chapter 4

Silver Cluster Attachment on Different Types of Carbon Nanotubes (CN_x-MWNTs and CO_x-MWNTs)

We report a simple process able to anchor efficiently small Ag nanoparticles (3-7 nm OD) on N-doped and functionalized multiwalled carbon nanotubes. These tubes react very differently and their surfaces chemistry is not similar. We analyze the effect of the reducing agent and the coating time on the particle size. This process is able to fix Ag particles without any external reducing agent. In this case, the CNTs could act as reducing agents for the silver ions.

4.1 Introduction

Carbon nanotubes can be coated with different species and metals in order to generate novel functional materials, a wide range of noble metals have been adhered to nanotubes, e.g. Pd[1], Pt[2], Au[1], Ag[1] and Cu[3]. When these metallic particles coat nanotubes they exhibit enhanced properties, and it is possible to modify their electron conduction [4]. Due to due their size (high surface:volume ratio), these clusters could also exhibit extremely efficient chemical activity which could be exploited in the generation of chemical and biological sensors, catalysts and hydrogen storage devices.

4.1.1 Carbon nanotubes with silver nanoparticles

In particular, Ag decorated carbon nanotubes are now gaining the attention of researchers due to their potential application as catalysts [5], conducting electrodes, high selective sensors at room temperature [6,7], bactericides useful for water treatment applications [8,9] and hydrogen storage [10]. The methods developed to anchor Ag particles on carbon nanotubes are usually complex and comparative studies using different types of tubes with different reactive groups on their surface are limited. In this context, the chemical treatments of nanotubes with acidic solutions are usually used to introduce functional groups. In 1996, Ebbesen and coworkers [11] refluxed mixtures of multiwalled carbon nanotubes and $AgNO_3$ in the presence of a small amount of formaldehyde for a couple of hours. Subsequently, Satishkumar et al. obtain coated MWCNT with Au, Pt and Ag [12], refluxing MWCNTs with $AgNO_3$ in concentrated nitric acid (HNO_3) during 48 hours. Unfortunately, these acid treatments introduce a large number of defects in the nanotube surfaces that results in lower mechanical and electronic performances. Many efforts have been made to avoid these acidic process, along this line, D. J. Guo, *et al*. [5] first modified MWNT with a 4-aminobenzene monolayer, subsequently Ag^+ was adsorbed onto the grafted MWCNT surface by electrostatic interactions and finally, Ag nanoparticles were obtained via a pulsed potentiostatic

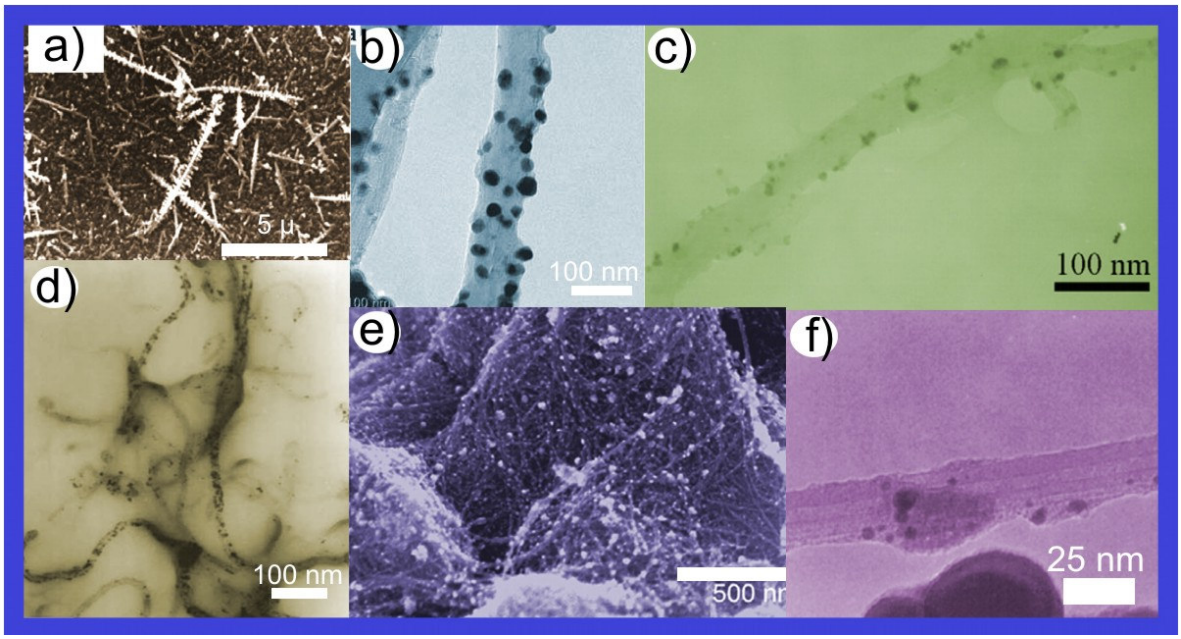

Figure 4-1.- Images of Carbon nanotubes/Silver composites. (**a**) MWCNTs/Ag obtained by electrochemical deposition, the film thickness varied between 25–30 nm [13], (**b**) MWCNTs/Ag reduced with formaldehido[11], (**c**) Acid treated MWCNTs with silver NPs [14], (**d**) MWCNTs/Ag composite for methanol oxidation [5], (**e**) SWCNTs/Ag composites [15], and (**f**) A silver layer is coated on MWCNTs by ion beam assisted deposition (IBAD) [9]

reduction. Alternative methods have reported the synthesis of Ag nanoparticles prior to their anchoring to the tube surface. In particular, Zamudio et al. [16] used CN_x-MWNTs, first synthesized Ag nanoparticles, subsequently, the authors sonicated N-doped carbon nanotubes in dimethyl sulfoxide (DMSO) with the pre-synthesized Ag nanoparticles, and the CN_x-MWNTs/Ag composite was obtained. Liu et al. [17], used Tollens reagent (a classical methodology to produce a silver coatings) to decorate MWCNTs with Ag nanoparticles. First they produce the Tollens reagent (a mixture of 1% $AgNO_3$ with 5% liquid NH_3), and then add a suspension of MWNT on 0.1% sodium dodecyl sulfate (SDS) and formaldehyde at 60ºC for 0.5h. Although these procedures are able to produce reasonable quality material, they appear to be laborious, complex or difficult to scale up.

4.2 Anchorage of Ag cluster on carbon nanotubes; Experimental methodology

In this chapter, we report a simple process able to anchor efficiently small Ag nanoparticles (3-7 nm OD) on different types of nanotubes: (**a**) N-doped multiwalled and (**b**) multiwalled carbon nanotubes with oxygen groups. We also noted that these tubes react very differently and their surfaces chemistry is not similar.

4.2.1 Characterization

The nanotubes and products were characterized by: Termogravimetric analysis (TGA, Thermo-Haake, Cahn VersaTherm Hs) heating at 10°C/min to 800°C in air, scanning electron microscopy (SEM, FEI XL30 FEG/SFEG) operated at 12 kV, X-ray powder diffraction using a XRD D8 ADVANCE – BRUKER AXS, with Cu K_α radiation (λ = 1.54060 Å), and high resolution transmission electron microscopy (HRTEM) using a JEM-2010 FEF instrument operated at 200 kV and equipped with an EDX detector and an Ω-Filter.

4.2.2 Silver anchoring process

The two different types of nanotubes tested in this work were used without any chemical modification. The tubes were synthesized following the procedure described in Section 2.2.2. The general procedure consisted of adding 10 mg of the nanotubes to a solution of acetone (20 ml) and silver nitrate (83 µl from a solution 0.1 N, J.T. Baker®) in a flask. Subsequently, the suspension was dispersed ultrasonically for one hour. The solution was then placed in a water bath to increase the temperature to 60°C, and at this point 10 ml of N,N-dimethylformamide (DMF, 99% Sigma-Aldrich®) were added as a reducing agent; the temperature of the suspension was maintained for 20 additional minutes. Subsequently, the nanotube samples were centrifuged, washed with distilled water twice and dried at 110° C in an oven.

4.3 Results and discussion

The effect of amount of DMF on the size of Ag clusters

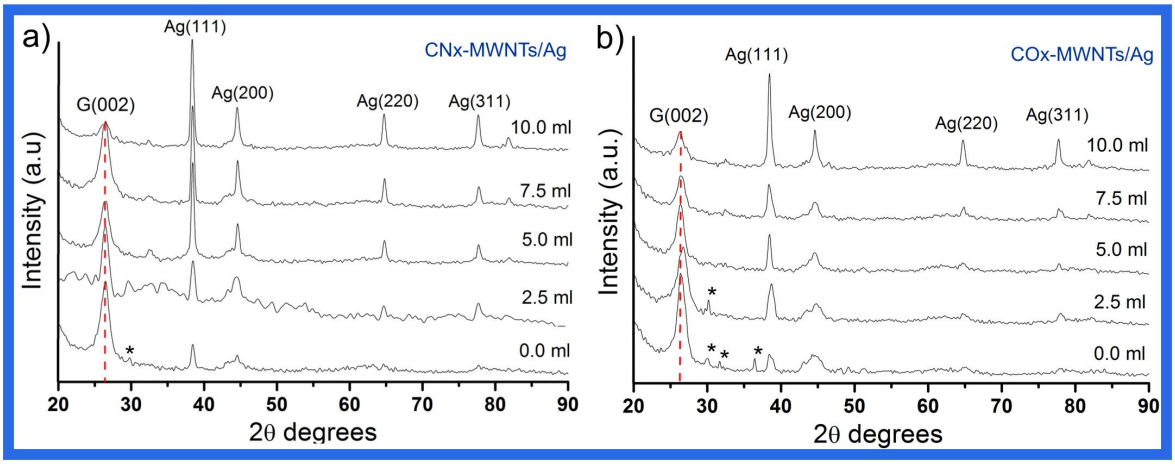

Figure 4-2.- X-ray powder diffraction patterns of CNT/Ag composites at different amounts of DMF. (**a**) The CN_x-MWNTs/Ag composite prepared using different quantities of DMF, we can appreciate the narrow peaks using high amounts of DMF, in which the particle size becomes larger. The marked peaks as (*) belong to residual $AgNO_3$, and (**b**) The CO_x-MWNTs/Ag composites obtained by varying the quantity of DMF. We can observe that the peaks are wider in all cases compared to the CN_x-MWNTs/Ag composites.

The DMF is an expensive and hazardous chemical that is usually used as a reducing agent and it is excellent to make stable CNTs suspensions. The amount of DMF used per unit mass of CNT is usually high (Zamudio *et al,* [16] utilized 10ml of DMF per 1mg of CN_x-MWNTs), making the process difficult to scale up.

During our experiments, acetone was used to prepare the suspensions and the DMF was employed as a reducing agent. The coating time was maintained for 20 minutes, but the amount of DMF was varied in order to study the effect on the silver cluster size. We added from 0 up to 10 ml of DMF. The XRD patterns of both CN_x-MWNTs and CO_x-MWNTs are illustrated in Figure 4.2-(**a-b**) respectively. We observe that the Ag peaks for the composite made with CO_x-MWNTs are wider in all cases than the peaks observed in the CN_x-MWNTs. This can be attributed to the higher reactivity of CN_x-MWNTs.

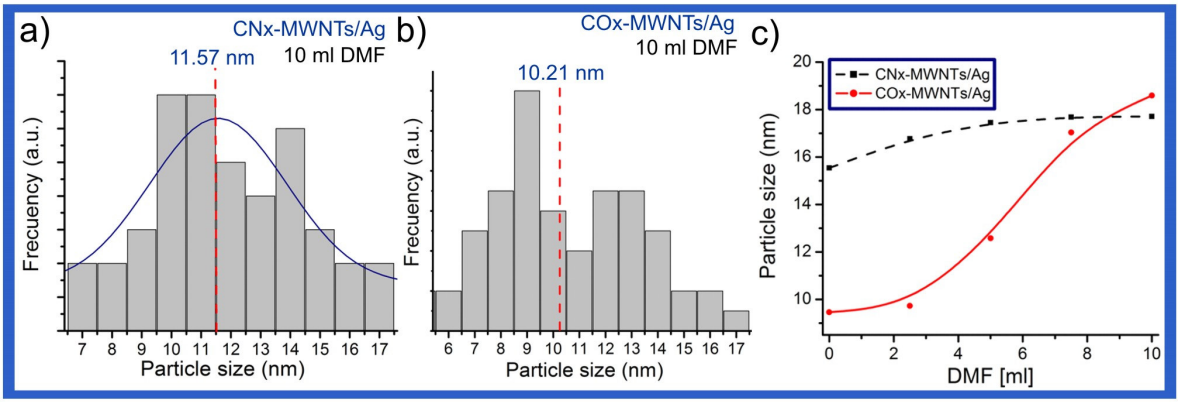

Figure 4-3.- Particle size distribution and particle size with respect to amount of DMF added to the reaction. (**a**) Ag cluster size histogram deposited on CN_x-MWNTs using 10 ml of DMF, obtained from TEM images. The red line (dashed one) is the average value, the blue one is a Gaussian fit. (**b**) Ag particle size histogram using CO_x-MWNTs at 10 ml of DMF, acquired from TEM images. The red line is the average value. (**c**) Behavior of the particle size with respect to the amount of DMF added to the system, the dashed line corresponded to CN_x-MWNTs. We notice that in all experiments, the CO_x-MWNTs exhibit the smallest particle size; Data obtained from XRD patterns.

The particle size obtained by varying the amount of DMF was determined by the XRD patterns and this information is presented in Figure 4.3-(**c**). The CN_x-MWNTs and CO_x-MWNTs exhibit dissimilar behaviors, the size of Ag clusters deposited on CN_x-MWNTs are kept constant through out the DMF range, thus increasing the size approximately in 2 nm and the CO_x-MWNTs display big changes, increasing the particle size from ~ 10 up to 20 nm. However, the Ag cluster size determined by TEM (see Figure 4.3-(**a-b**)) and XRD are not similar, possibly due the presence of some agglomerations that are produced by the high reductions rates promoted by the presence of DMF. The CNT/Ag composites at 10 ml of DMF were analyzed by TEM to obtain the particle size. These results are shown in Figure 4.3-(**a-b**), the mean size of Ag clusters for the N-doped CNTs is 11.57 nm and the functionalized CNT is 10.21 nm. Nevertheless, both types of composites exhibit high standard deviation. At low DMF concentrations, the particle size is becoming smaller. In addition, at concentrations equal to zero, the CNTs present very small Ag nanoparticles deposited on the tubes, but a low number of Ag clusters. In this case the nanotubes act as reducing agents, due to their low capacity to reduce the silver ion. The nucleation velocity is low, allowing the particle size to be controlled with

better precision. This important behavior can be used to produce smaller particles, but it is necessary to modify the surface of the nanotubes to improve the chemical reactivity and the interaction. These modifications are studied in detail in the following section.

Study on effect of coating time on the particle size of Ag on CNTs

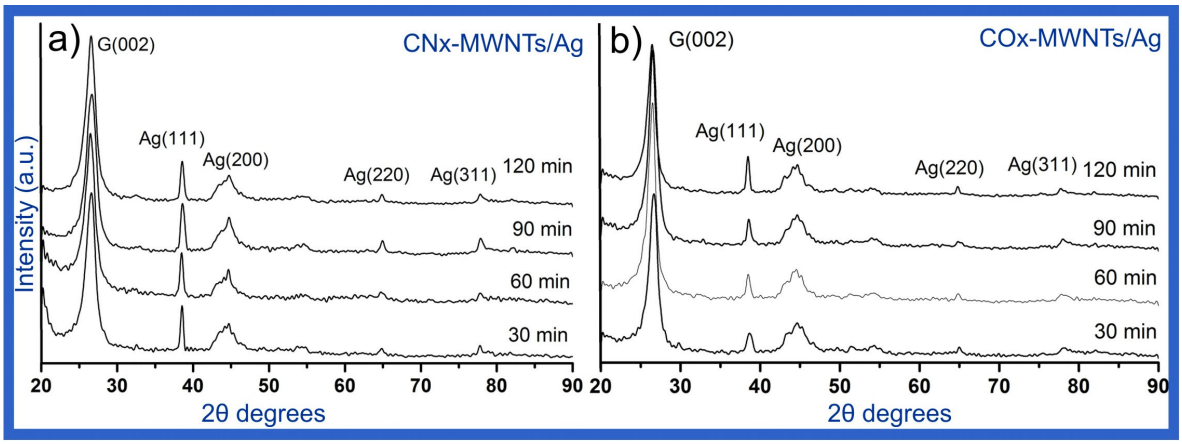

Figure 4-4.- X-ray powder diffraction patterns of CNT/Ag composites produced at different coating times without DMF. (a) CN_x-MWNTs/Ag, we can observe that we can control the Ag particle size, and due the low nucleation rates, the particle size can be controlled with better accuracy; (b) CO_x-MWNTs/Ag, it can be seen that all the peaks that correspond to Ag are less intense and wider than those showed on the CN_x-MWNTs/Ag.

In this part of the research, we noticed that MWCNT/Ag composites can be produced without the addition of any external reducing agent. We decide to modify slightly the coating process in order to enhance the chemical reactivity and the interaction with the Ag ions, thus improving the anchorage of nanoparticles. The modification involves a thermal treatment of the MWCNTs. The MWCNTs were heated at 300℃ in air for 5 minutes; in order to modify their surfaces adding some functional groups but avoiding high damage to their properties. Subsequently, the procedure described on section 4.2.2 was carried out, with the exception of no DMF was added to the systems, with these modifications we expect that the negative charge (created by the oxygen groups added by the thermal treatment) enhance the interactions with the silver ions on the surfaces of the CNTs.

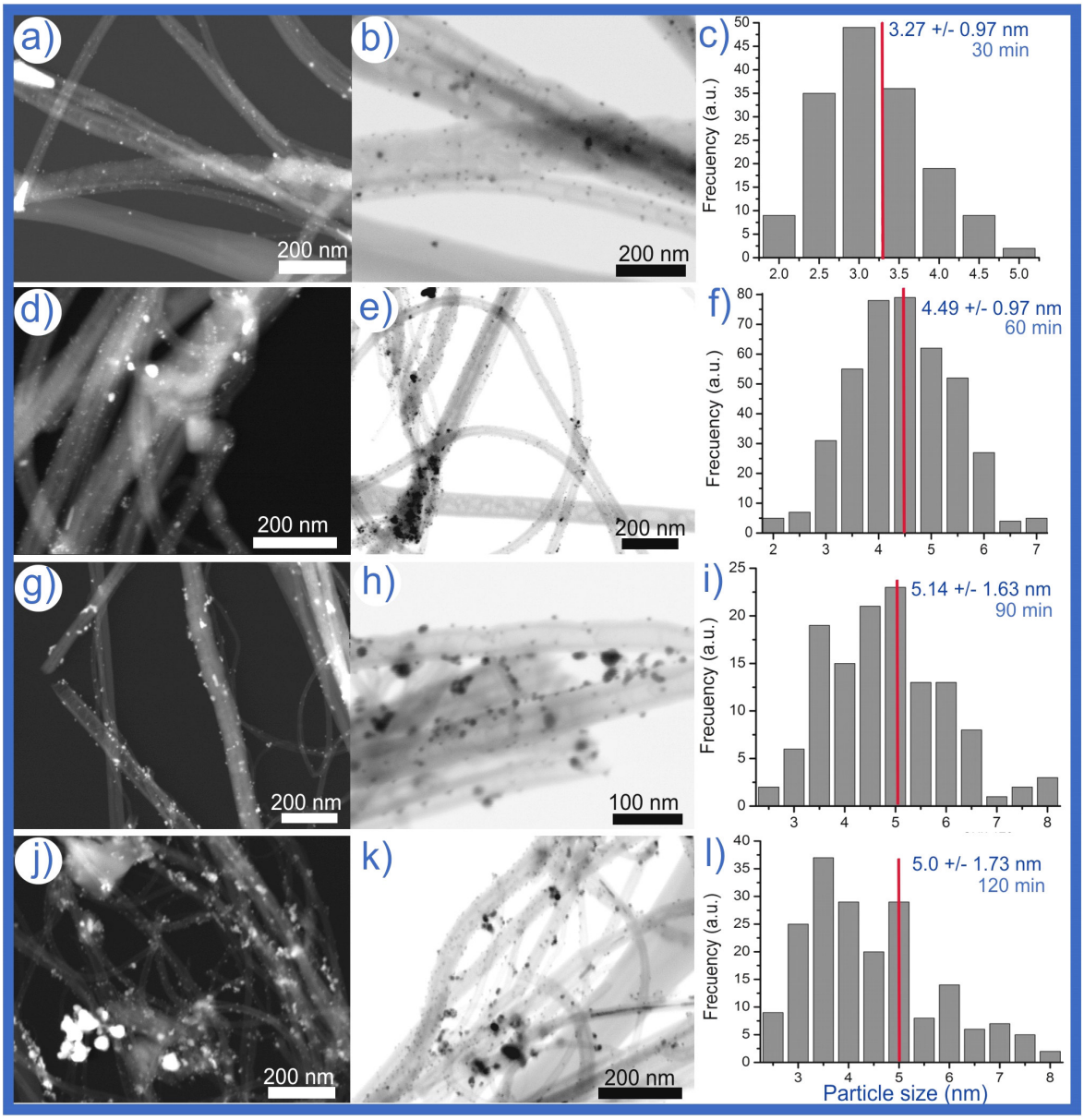

Figure 4-5.- STEM images and Ag particle size histogram of CN_x-MWNTs/Ag composites using different coating times. (**a-c**) Composite with 30 minutes process, this composite show the smallest particle size (3.27 ± 0.97 nm); (**d-f**) Composite produced after 60 minutes of coating; this material exhibit higher load of nanoparticles and a cluster size of 4.49 ± 0.97 nm; (**g-i**) When using 90 minutes, the particle size keeps constant at ~ 5 nm , but the standard deviation increase slightly, and (**j-l**) At 120 minutes, the SD increase and, it can be seen that at a high coating time the particle size histogram loss their Gaussian behavior and the standard deviation increase.

Table 4-1.- Particle size in CNT/Ag composites using different coating times.

Coating time (min)	CN_x-MWNTs/Ag (nm)		CO_x-MWNTs/Ag (nm)	
	XRD(111)	STEM	XRD (111)	STEM
30	13.71	3.27 ± 0.97	9.92	3.65 ± 1.88
60	17.17	4.49 ± 0.97	15.67	5.19 ± 1.68
90	16.00	5.14 ± 1.63	15.49	5.18 ± 3.37
120	16.31	5.00 ± 1.73	17.99	6.36 ± 2.10

We varied the coating time in order to control the size of the nanoparticles. The time range was fixed from 30 up to 120 minutes (30, 60, 90 and 120 min). The XRD patterns for both CN_x-MWNTs/Ag and the CO_x-MWNTs/Ag composites are shown in Figure 4.4-(**a-b**). In all cases, the Ag peaks are smaller and wider than the composites obtained with DMF, but we observed that the Ag peaks presented in the composite CO_x-MWNTs/Ag are wider that the CN_x-MWNTs/Ag. After the thermal procedure, we improved the number of nanoparticles anchored to the tube, and due the low nucleation rate we were able to achieve a smaller particle size of ~ 3 nm in diameter.

Scanning transmission electron microscopy (STEM) images of the composite CN_x-MWNTs/Ag are illustrated in Figure 4.5. Here we can appreciate that at large coating times, the composite reveals large particles (see Figure 4.5-(**j-k**)). The particle size histograms with different anchoring times are presented in Figure 4.5. We can notice that the standard deviation and the cluster size increases with the coating time; the smallest particle achieved was obtained using 30 minutes (size of 3.27 ± 0.97 nm). After 120 minutes, the particle size increased approximately 2 nm. This is an important observation because allow the control of the particle size with high accuracy. When the coating time is increased, the typical Gaussian behavior of the particle size distributions is lost; these results are reflected by an increase in their standard deviation.

The Ag particle size is determined by STEM images and XRD patterns using the Ag(111) plane. These results are presented in Table 4.1, we noticed again, that the

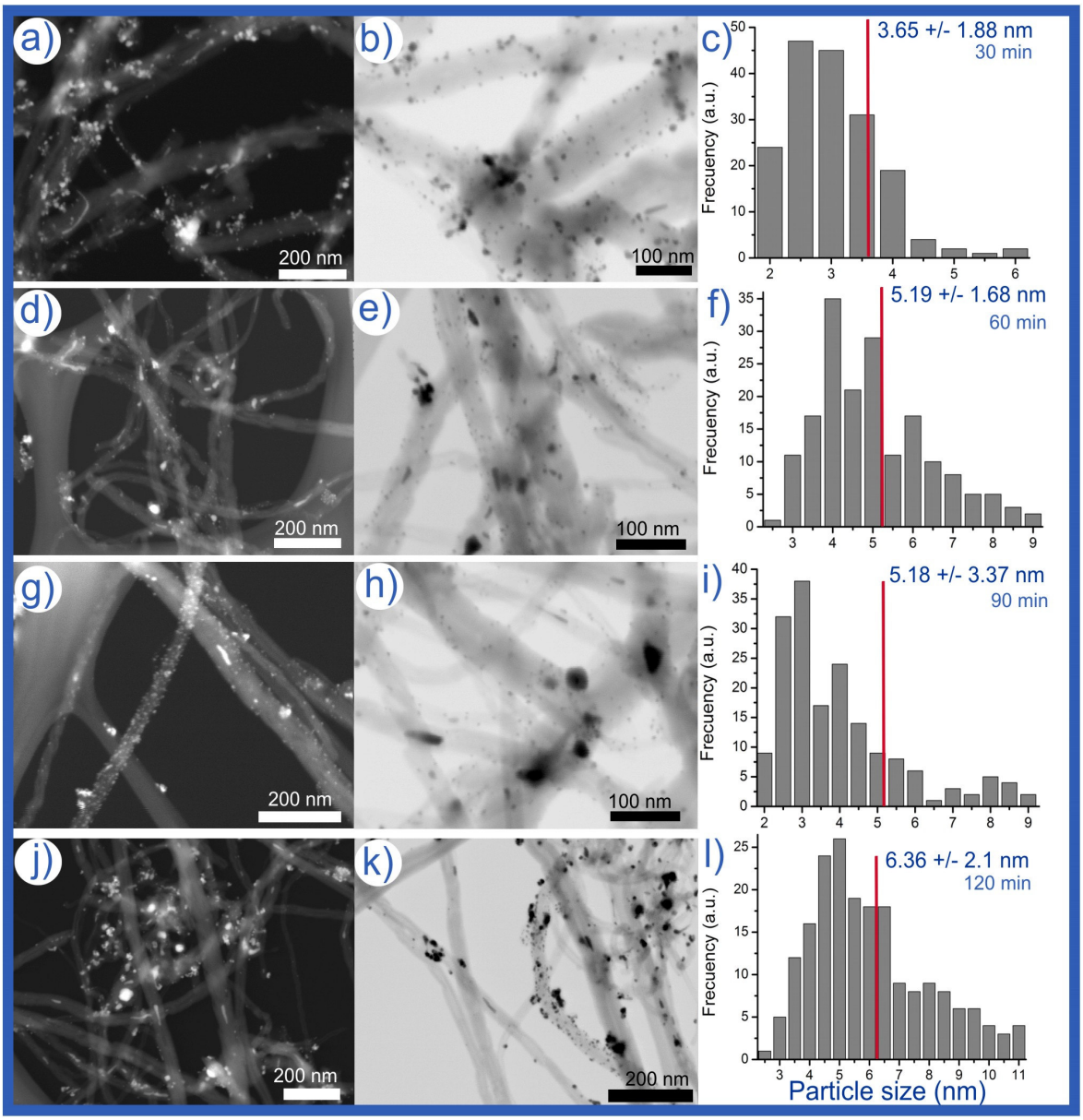

Figure 4-6.- STEM images and particle size histogram of CO_x-MWNTs/Ag composites using different coating times. (**a-c**) Composite using a 30 minute process, this composite present the smallest particle size (3.65 ± 1.88 nm) and the quantity of clusters seems to be high; (**d-f**) Composite produced after 60 minutes of coating; this material shows higher load of nanoparticles and a cluster size of 5.19 ± 1.68 nm; (**g-i**) After 90 minutes, the standard deviation of the cluster size increased drastically, due some agglomerations that are caused by the long time. (**j-l**) After 120 minutes of coating process, the particle size has grown up, reaching a maximum value of 6.36 nm.

particle size data (XRD and STEM) do not match because particle agglomerations that could be created by high reductions rates that modify the width of the XRD peaks. But the size obtained by SEM images reflects more real information, because only the anchored Ag clusters are taken into account. Similar particle size is obtained in both CN_x-MWNTs/Ag and the CO_x-MWNTs/Ag systems, but the smallest one is achieved when using CN_x-MWNTs as a substrate. Almost in all points, the standard deviation becomes larger with the increasing of the coating time.

STEM images and particle size histogram of the composite CO_x-MWNTs/Ag are illustrated in Figure 4.5. At different anchoring times, we observe that the composites show a large quantity of small nanoparticles fixed on the CNTs. After 120 minutes of coating, the composite begins to show some large particles, thus increasing the average size. We can appreciate that the standard deviation and the cluster size increase with the coating time; the smallest particle achieved was obtained using a 30 minute process with a size of 3.65 ± 1.88 nm. This value is slightly larger when compared to that obtained with CN_x-MWNTs. After 120 minutes, the particle size increases up to 6.36 ± 2.1 nm, only ~ 3 nanometers greater than the smallest ones. These composites exhibit similar behavior to CN_x-MWNTs/Ag, where they allow high accuracy in controlling the particle size.

4.4 Conclusions

We developed an easy, simple and cheap process to produce CNTs/Ag composites without the presence of any hazardous material and avoiding the addition of any external reducing agent. The MWCNTs acts as reducing agent for the silver ions, due the low nucleation rate. This process is able to anchor efficiently small Ag nanoparticles on N-doped and functionalized multiwalled carbon nanotubes. The particle size could be controlled just by varying the coating time with a high accuracy.

This low temperature process is able to anchor small Ag particles on the MWCNTs surface, it could be the smallest particle size anchored on a MWCNTs reported up to date. The smallest particle size (3.27 ± 0.97) was obtained using the CN_x-MWNTs as a substrate. However, using CO_x-MWNTs the results were similar (3.65 ± 1.88), and the load of clusters was improved by the thermal treatment. This simple and easy process could be used without difficulty and scaled up, to produce larger quantities of composites that could be used in the fabrication of biological and chemical sensors, adsorption materials, catalysts, etc.

4.5 References

[1] B. Xue, P. Chen, Q. Hong, J. Lin, K. L.Tan, "Growth of Pd, Pt, Ag and Au nanoparticles on carbon nanotubes", *J. Mater. Chem.* Vol. 11, 2378–2381 (2001)

[2] S. Hrapovic, Y. Liu, K. B. Male, J. H. T. Luong, "Electrochemical Biosensing Platforms Using Platinum Nanoparticles and Carbon Nanotubes", *Anal. Chem*. Vol. 76, 1083-1088 (2006)

[3] C. Xu, G. Wu, Z. Liu, D. Wu, T. T. Meek, Q. Han, "Preparation of copper nanoparticles on carbon nanotubes by electroless plating method", *Mater. Res. Bull.* Vol 39, 1499–1505 (2004)

[4] Q. Zhao, M. B. Nardelli, W. Lu, J. Bernholc, "Carbon Nanotube-Metal Cluster Composites: A New Road to Chemical Sensors?", *Nanolett,* Vol 5, 847-851 (2005)

[5] D. J. Guo, H. L. Li, "Highly dispersed Ag nanoparticles on functional MWNT surfaces for methanol oxidation in alkaline solution", *Carbon*, Vol. 43, 1259-1264 (2005)

[6] E.H. Espinosa, R. Ionescu, C. Bittencourt, A. Felten, R. Erni, G. Van Tendeloo, J.-J. Pireaux, E. Llobet, "Metal-decorated multi-wall carbon nanotubes for low temperature gas sensing", *Thin Solid Films,* Vol. 515, 8322–8327 (2007)

[7] R. Ionescu, E.H. Espinosa, R. Leghrib, A. Felten, J.J. Pireaux, R. Erni, G. Van Tendeloo, C. Bittencourt, N. Cañellas, E. Llobet, "Novel hybrid materials for gas sensing applications made of metal-decorated MWCNTs dispersed on nano-particle metal oxides", *Sensors and Actuators B*, Vol. 131, 174–182 (2008)

[8] J. Thiel, L. Pakstis, S. Buzby, M. Raffi, C. Ni, D. J. Pochan, S. I. Shah, "Antibacterial properties of silver-doped titania", *Small*, Vol 3, 799-803 (2007)

[9] T. Liu, H.Q. Tang, X.M. Cai, J. Zhao, D. J. Li, R. Li, X.L. Sun, "A study on bactericidal properties of Ag coated carbon nanotubes", *Nucl. Instr. and Meth. in Phys. Res. B*, Vol. 264, 282–286 (2007)

[10] B. Khoshnevisan, M. Behpour, S.M. Ghoreishi, M. Hemmati, "Absorptions of hydrogen in Ag–CNTs electrode", *Inter. J. of Hydrogen Energy,* Vol. 32, 3860-3863 (2007)

[11] T. W Ebbesen, H. Hiura, M. E. Bisher, M. M. J. Treacy, J.L. S. Keyer, R. C. Haushalter, “Decoration of carbon nanotubes”, *Adv Mat.*, Vol. 8, 155-157 (1996)

[12] B. C. Satishkumar, E. M. Vogl, A Govindaraj, C. N. R. Rao, “The decoration of carbon nanotubes by metal nanoparticles”, *J. Phys. D: Appl. Phys.* Vol. 29, 3173–3176 (1996)

[13] S. Hussain, A. K. Pal, “Incorporation of nanocrystalline silver on carbon nanotubes by electrodeposition technique”, *Mat. Lett.* Vol. 62, 1874–1877 (2008)

[14] K. Dai, L. Shi, J. Fang, Y. Zhang, “Synthesis of silver nanoparticles on functional multi-walled carbon nanotubes”, *Mat. Sci. and Eng. A*, Vol. 465, 283–286 (2007)

[15] T. Nakamura, T. Ohana, M. Ishihara, M. Hasegawa, Y. Koga, “Photochemical modification of single-walled carbon nanotubes with amino functionalities and their metal nanoparticles attachment”, *Diam. & Rel. Mat.,* Vol. 17, 559–562 (2008)

[16] A. Zamudio, A. L. Elías, J. A. Rodríguez-Manzo, F. López-Urías, G. Rodríguez-Gattorno, F. Lupo, M. Rühle, D. J. Smith, H. Terrones, D. Díaz, M. Terrones, “Efficient anchoring of silver nanoparticles on N-doped carbon nanotubes”, *Small*, Vol. 3, 346-350 (2006)

[17] Y. Liu, J. Tang, X. Chen, W. Chen , G.K.H. Pang , J.H. Xin, “A wet-chemical route for the decoration of CNTs with silver nanoparticles”, *Carbon,* Vol. 44, 381-392 (2006)

Chapter 5

Conclusions and Perspectives

5.1 Conclusions

The purpose of this research was to develop coating methods that allow efficient control of the particle size, oxidation state, and spatial density of nanoparticles. Without previous chemical treatment or any modification that could damage the mechanical and electronic properties of the substrate materials.

We were able to develop a method that permit to cover carbon nanotubes with ZnO nanoparticles, using no hazardous chemicals, with a precursor that is easy to manipulate, soluble in a wide range of solvents and exhibits low decomposition temperatures. Moreover, we avoid procedures that could damage the mechanical properties of the carbon nanotubes. Additionally, we were able to obtain very small clusters of ~ 5 nm with the small standard deviation and high density of nanoparticles.

In addition, we compared two types of nanotubes that exhibit different capabilities of interaction due to the difference in their surfaces. These studies are important because we analyzed the effect of different types of surfaces, even if we used the same nanostructure, with different surfaces, we expect different results and behavior.

Another method developed was designed to attach nanoparticles of manganese oxides on carbon nanotubes. We were able to control the size of the clusters and improve the quantity of particles on the nanotubes wall. Moreover, we controlled the oxidation state of the manganese which is challenging, due their facile transition between oxides, usually a mixture of manganese oxides are obtained by other methods. This method allows controlling the oxidation state of the manganese just varying the acetylacetonate metal precursor. We were able to obtain a Mn_2O_3 particle size ~ 5 nm, and a small SD. In the same way, we compare two types of nanostructures with the same morphology but different surfaces, obtaining different results and behaviors.

The final study was carried out to fix silver clusters on carbon nanotubes. Nowadays, many researches in this aspect have been done; the problems are the diversity in the particle size and the small amounts produced of the composites,

making difficult their application. We reported a coating method that avoids process that could damage the properties of the nanotube substrate, but allow us to obtain a very small Ag particle size of 3.27 nm. Moreover, this coating process could be scale up to produce bigger quantities of composite, boosting the applications of these composites as chemical and biological sensors, bactericides, catalyst, etc.

All these studies were carried out using two types of structures with similar morphologies but very different capabilities of interact with their surrounding media, due the different properties on their surfaces. In addition, all the processes were optimized to obtain the smallest particle size and the lowest standard deviation, maintaining their simplicity and feasible to produce larger quantities of composites preserving their characteristics.

5.2 Perspectives

All inorganic nanomaterials exhibit better and new interesting properties that differ from the bulk. These materials can be used in wide range of applications, such as sensors, gas adsorbers, field emission devices, etc. All these properties and applications can be extended to other materials, creating new composites that could exhibit better properties.

The ZnO/CNTs composites that were created during this research could be applied for the protection of the body against solar radiation [1], in field emission displays and other applications. High numbers of studies have reported that these types of composites improve the field emission [2] properties of the carbon nanotubes and extend their life time [3,4]. Usually, these composite have big particles size and low density of clusters, making possible that our designed composite could be an excellent candidate for these applications.

The manganese oxide/MWCNTs composites produced could be used to manufacture electrochemical capacitors [5] or for environmental purposes, such as the removal of Pb(II) from aqueous solution[6], and as efficient electrode material for fuel cells [7]. An advantage of this process is to control the oxidation state of

manganese oxides and could be easily scale up to produce larger quantities of composite material.

The Ag/MWCNTs composite prepared in this research exhibit small Ag particle size and high surface coverage. In addition, the coating process does not require hazardous materials and it could be easy to scale up. These composites could be used in a wide range of applications such as, bactericidal agent in biomedical and water treatment applications [8,9], in the fabrication of chemical sensors and electronics devices [10,11], catalysts [12], conducting electrodes, bactericides useful for and hydrogen storage [13].

5.3 References

[1] A. Becheri, M.Dürr, P. Lo Nostro, P. Baglioni, “Photochemical synthesis of polygonal gold nanoparticles”, *J. Nanopart. Res.* Vol. 10, 679-689 (2008)

[2] W. B. Choi, D. S. Chung, J. H. Kang, H. Y. Kim, Y. W. Jin, I. T. Han, Y. H. Lee, J. E. Jung, N. S. Lee, G. S. Park, J. M. Kim, “Fully sealed, high-brightness carbon-nanotube field-emission display”, *Appl. Phys. Lett.* Vol. 75, 3129-3131(1999)

[3] Ke Yu, Y. S. Zhang, F. Xu, Q. Li, Z. Q. Zhu, Q. Wan, “Significant improvement of field emission by depositing zinc oxide nanostructures on screen-printed carbon nanotube films”, *Appl. Phys. Lett*., Vol. 88, 153123 (2006)

[4] J. M. Green, L. Dong, T. Gutu, J. Jiao, J. Conley, Y. Ono, “ZnO-nanoparticle-coated carbon nanotubes demonstrating enhanced electron field-emission properties”, *J. Appl. Phys.* Vol. 99, 094308 (2006)

[5] S. B. Ma, K. W. Nam, W. S. Yoon, X. Q. Yang, K. Y. Ahn, K. H. Oh, K. B. Kim “A novel concept of hybrid capacitor based on manganese oxide materials”, *Electrochem Commun*, Vol. 9, 2807–2811 (2007)

[6] S. G. Wang, W. X. Gong, X. W. Liu, Y. W. Yao, B. Y. Gao, Q. Y. Yue, “Removal of lead(II) from aqueous solution by adsorption onto manganese oxide-coated carbon nanotubes” , *Separation and Purification Technology*, Vol. 58, 17–23 (2007)

[7] M.O. Danilov, A.V. Melezhyk, “Carbon nanotubes modified with catalyst—Promising material for fuel cells”, *J. Power Sources*, Vol. 163, 376–381(2006)

[8] J. Thiel, L. Pakstis, S. Buzby, M. Raffi, C. Ni, D. J. Pochan, S. I. Shah, “Antibacterial properties of silver-doped titania”, *Small*, Vol. 3, 799-803 (2007)

[9] T. Liu, H.Q. Tang, X.M. Cai, J. Zhao, D. J. Li, R. Li, X.L. Sun, “A study on bactericidal properties of Ag coated carbon nanotubes”, *Nucl. Instr. and Meth. in Phys. Res. B*, Vol. 264, 282–286(2007)

[10] E.H. Espinosa, R. Ionescu, C. Bittencourt, A. Felten, R. Erni, G. Van Tendeloo, J.-J. Pireaux, E. Llobet, “Metal-decorated multi-wall carbon nanotubes for low temperature gas sensing”, *Thin Solid Films,* Vol 515, 8322–8327 (2007)

[11] R. Ionescu, E.H. Espinosa, R. Leghrib, A. Felten, J.J. Pireaux, R. Erni, G. Van Tendeloo, C. Bittencourt, N. Cañellas, E. Llobet, “Novel hybrid materials for gas

sensing applications made of metal-decorated MWCNTs dispersed on nano-particle metal oxides", *Sensors and Actuators B*, Vol 131, 174–182 (2008)

[12] D. J. Guo, H. L. Li, "Highly dispersed Ag nanoparticles on functional MWNT surfaces for methanol oxidation in alkaline solution", *Carbon*, Vol. 43, 1259-1264 (2005)

[13] B. Khoshnevisan, M. Behpour, S.M. Ghoreishi, M. Hemmati, "Absorptions of hydrogen in Ag–CNTs electrode", *Inter. J. of Hydrogen Energy,* Vol. 32, 3860 – 3863 (2007)